BEHAVIOR OF CHITOSAN IMMOBILIZED CdS NANOCRYSTALS WITH VARIOUS CROSSLINKING AND DRYING TREATMENTS IN TEXTILE DYE PHOTODEGRADATION

SZETO WAI

M.Phil

The Hong Kong Polytechnic University

2014

The Hong Kong Polytechnic University

Institute of Textiles and Clothing

Behavior of chitosan immobilized CdS nanocrystals with various crosslinking and drying treatments in textile dye photodegradation

SZETO Wai

A thesis submitted in partial fulfillment of the requirements for the degree of Master of Philosophy

August, 2013

CERTIFICATE OF ORIGINALITY

I hereby declare that this thesis is my own work and that, to the best of my knowledge and belief , it reproduces no material previously published or written, nor material that has been accepted for the award of any other degree or diploma, except where due acknowledgement has been made in the text.

Szeto Wai

Abstract

Chitosan based photocatalyst composites containing semiconducting CdS nanocyrstals with and without glutaraldehyde and epichlorohydrin crosslinking treatments were studied for the photodegradation of Methyl Orange and Acid Blue 25. The photocatalysts dried using oven and freeze dryer were investigated. Studies of the effects of crosslinking and various drying methods on photodegradation characteristics of the chitosan-based catalyst composites were rare, although these studies were not uncommon for the studies using chitosan as an adsorbent. The chitosan polymer embedded CdS nanocrystal photocatalyst composites were characterized by using X-ray diffraction (XRD), transmission electron microscopy (TEM), scanning electron microscope (SEM), Fourier transform infrared (FT-IR) and visible reflectance spectroscopy. The degradation kinetics was investigated under the effects of catalyst dosage, initial dye concentration, initial pH of dye solution, on adsorption and photodegradation of dyes (Methyl Orange and Acid Blue 25) were investigated. The dye removal mechanism involved an initial sorption process following the photo-degradation. The sorption kinetics revealed that the sorption process undergo the pseudo second order adsorption kinetics. Photodegradation of Methyl Orange was pseudo first order kinetics. Unlike Methyl Orange, degradation profiles of CI Acid Blue 25 followed the rare second order kinetics. Nevertheless, degradation of CI Acid Blue 25 can be the first order kinetics if the reaction was commenced with high pH dye solution. Efficient colour removal was observed. The catalyst composite can remove 99% Methyl Orange at pH 4 and 98% Acid Blue 25 dye at pH10 with 75 minutes of illumination. The present study mainly carried out with the catalyst composites prepared without special shape forming technique and in form of flakes. Moreover, two innovative chitosan-based encapsulation systems,

namely (1) chitosan micro-particles and (2) chitosan mini-particles with loaded CdS catalyst aiming at facilitating the practical application have been developed and preliminary tests were conducted.

Acknowledgements

First, I would like to express my sincerest thanks to my chief-supervisor Prof. Chun Wah Yuen for his resourcefulness, guidance, and encouragement throughout the whole period of the research work.

I would also like to express my deepest gratitude to my co-supervisors, Dr. Chi Wai Kan and Dr. Kim Hung Lam. They provided me with valuable professional knowledge. Their advice and support always help me to solve the problems in my research work. Without them this project cannot possibly be accomplished.

Sincere appreciation is due to Dr. Shun Wan Chan for his help for his suggestions and encouragement.

I gratefully acknowledge the financial support from the Hong Kong Polytechnic University and the technical support provided by the Materials Research Centre, Institute of Textiles and Clothing and Department of Applied Biology & Chemical Technology of the Hong Kong Polytechnic University.

Finally, I would like to thank my family and friends for their encouragement and love throughout this research.

Contents

List of Figures

List of Tables

List of Abbreviations

A	A constant that different for different transitions
B	Full width at half maximum
C	Contaminant or dye concentration
C_0	Initial contaminant or dye concentration
C_t	Contaminant concentration at time t
D	Average size of the crystals
E_g	Band gap
hν	Light energy
K	Constant of Langmuir isotherm
k	Intrinsic reaction rate constant
K_{0p}	Rate constant of pseudo zero order kinetics of photodegradation
k_1	Rate constant of pseudo first order adsorption
k_{1p}	Rate constant of pseudo first order kinetics of photodegradation
k_2	Rate constant of pseudo second order adsorption
k_{2p}	Rate constant of pseudo second order kinetics of photodegradation
k_{app}	Apparent rate constant
m	Mass of adsorbent
M_s	Mass of solution
Q_e	Equilibrium adsorption capacity
Q_t	Adsorption capacity at time t
R	The reflectance at a given photon energy (hν)
R_{max}	Maximum value of reflectance
R_{min}	Minimum value of reflectance
t	Duration of the corresponding experiment

Greek Symbols

α	Absorption coefficient
Θ	Surface coverage
θ	Corresponding diffraction angle
λ	Wavelength of electromagnetic wave

Chapter 1 Introduction

1.1. Background

Human civilisation discharges a huge amount of complex organic pollutants to environment. For example: plastic industry discharges plasticisers[1] as well as toxic monomers[2] and textile industry discharges dyes[3]. These pollutants are potential threats to the ecosystem. Removal of these pollutants from waste streams is highly encouraged.

Due to the high variability in compositions of textile wastewater and the increasing stability of dye materials against biodegradation, most of the conventional physicochemical methods such as flocculation and adsorption as well as biological treatment are ineffective for their removal[4, 5].

Moreover, biodegradation requires nutrients[6, 7] and its products could be more toxic than the original contaminants[8].Recently, much attention has been placed on photodegradation induced by semiconductor photocatalysts. Excitation of semiconductor generates holes and electrons which may act as oxidising agent and reducing agent and then trigger various reactions that degrade the dye[5, 9-11]. In the past, most of the literatures were concerning about the strength of the semiconductor catalysts which are usually in the form of free nano-particles. However, this will discourage the catalyst recovery and practical applications as the post-treatment separation of catalysts will be difficult[12-19] and also the retrieval of these particles will be costly and time consuming[12]. Moreover, nano-catalysts will be prone to aggregate and reduce catalytic efficiency as this will impede the transfer of light-generated charge carriers to surface and increase the probability of recombination[4, 14, 16, 19-21]. Furthermore, some semiconductors such as

Cu_2O[21] and CdS[15, 22] are vulnerable to photocorrosion and the release of heavy metals is a secondary pollution. The polymers such as alginate[12, 23], cellulose acetate[13], chitosan[4, 5, 20, 24-27] and poly(diallyl dimethylammonium) chloride[22] were reported as immobilisation matrixs, which could stabilise the catalysts. Some recent publications reported the semiconductors immobilised in various polymers to improve the practical value of their photocatalysts. They suggested that polymers could enhance usability as well as stability and provide synergistic effect on dye removal[26, 28, 29]. The immobilisation of the nano-particles into polymer films or spheres of suitable size facilitates the stabilisation of unstable catalysts as well as their recollection and reusability after treatment of wastewater. Some reseachers proposed that the high adsorption ability of chitosan could bring more dye molecules into close proximity with the active sites of catalyst and then let them react with the generated active species[26]. In the close proximity with semiconductor, dye could act as photosensitiser. The excited dye molecules inject high energy electrons into the conduction band of semiconductor and provides an alternative route for degradation[5]. Chitosan (β-(1–4)-2-amino-2-deoxy-d-glucose) is the second most abundant biopolymer on earth. Chitosan is not only non-toxic but also acts as a polymeric material for biomedical engineering and pharmaceutical application. Moreover, chitosan can be slowly degraded and is generally regarded as green material. The chitosan precursor is chitin which can be obtained easily and economically from the crustacean shells. The low cost of crustacean shell waste can be easily available from the seafood processing industry.

This work was also focused on the chitosan encapsulated CdS catalyst with its

potential application suitable for colour degradation. Chitosan is the preferred polymer material since it is a neutral occurring polymer with low strength and it is water soluble. Hence, chemical crosslinking to improve its strength is common in research. Many methods of modifications were reported in the studies mainly focused on the adsorption properties of chitosan only[30-55]. Effects of various crosslinking methods on adsorption characteristics the by chitosan-based adsorbents were frequently reported[30-41]. In the field of encapsulated photocatalysts, researchers reported the use of glutaraldehyde[4, 27, 29, 56], epichlorohydrin[17, 28] and tri-polyphosphate[28] for crosslinking the natural chitosan polymer to improve its strength. However, the publications reporting the effects of crosslinking and various drying methods on photodegradation characteristics of the chitosan-based catalyst composites are rare. Jawad[17] reported that the crosslinking by epichlorohydrin improved the catalytic activity of the TiO_2/chitosan film and the photodegradation rate of phenol because the crosslinking could enhance the chemical stability of TiO_2/chitosan film against photodegradation. In contrast, Li[28] found that the catalytic activity of degrading Methyl Orange of chitosan-TiO_2 adsorbent with tri-polyphosphate crosslinking was much lower than that of its non-crosslinked counterpart.

In the present study, (1) the optimum working conditions and properties of photocatalyst CdS, (2) effects of various treatments of crosslinking chemical agents and drying methods on the chitosan-encapsulated photocatalyst composites, and (3) effects of various reaction conditions on dye degradation efficiency were investigated and reported. Chitosan, with or without crosslinking, encapsulating the

CdS nanoparticles with various drying post treatments were synthesised and used as the catalyst composites for this study. Methyl Orange (MO) and C.I. Acid Blue 25 (AB25) dyes as shown in Figure 1-1 were selected as the target models for the present study.

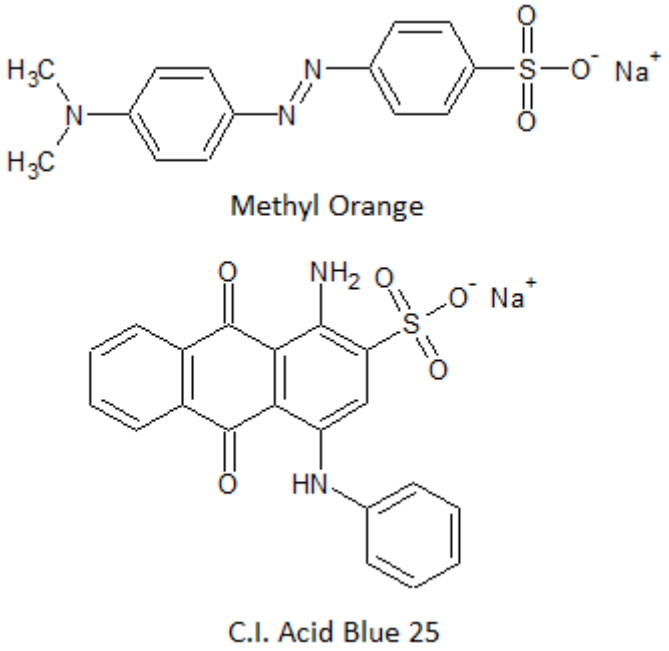

Figure 1-1 The dye structure of Methyl Orange and C.I. Acid Blue 25

The kinetics of photodegradation were also investigated. The adsorption and degradation data were collected and fitted with different kinetic models, namely the pseudo first and the pseudo second order kinetics. The catalyst composites were synthesised, retrieved and reused to assess its reusability. Moreover, two innovative chitosan-based encapsulation systems, namely (1) chitosan micro-particles and (2) chitosan mini-particles with loaded CdS catalyst have been developed and tested aiming at facilitating the practical application. Li and coworkers[28] reported a

TiO_2-based catalyst system similar which was to the chitosan mini-particles developed in the present work. To my knowledge, there have been no reports on the catalyst system similar to the crosslinked chitosan micro-particles.

1.2. Research objectives

1. To investigate the effects of crosslinking method, drying method, reuse, catalyst dosage, pH and initial dye concentration on the dye adsorption, photodegradation characteristics.
2. To investigate the adsorption and photodegradation characteristics of chitosan-based encapsulation systems.
3. To develop some innovative chitosan-based encapsulation systems that aim to improve stability, lifetime, degradation efficiency and mechanical strength

1.3. Significance of research

The chitosan-based catalyst composites for dye photodegradation was synthesised and investigated for their dye sorption and degradation. The kinetic models were employed for studying the sorption and degradation processes of the dyes using the synthesised chitosan immobilised photocatalysts.

Dye photodegradation experiments were carried out with the chitosan-encapsulated photocatalyst composite in order to determine the optimum synthesis process, optimum working condition and nature of the catalyst. Effects of various chemical crosslinking agents and physical treatments on dye removal were also studied. Some innovative chitosan-based encapsulation systems in the form of spherical particles were developed and tested aiming at facilitating the practical application. After two

decades of research of organic pollutant photodegradation, this technology still cannot be commercialised. The achievement of this research can let the technology one step forward.

1.4. Outline of thesis

Chapter 1 provides a general introduction, background, objectives and significance of this research work.

Chapter 2 reviews the necessary knowledge, methodology and the related studies presented in other publications.

Chapter 3 describes the design and synthesis of catalyst composites as well as the experimental procedures for the study of adsorption and photodegradation kinetics by means of catalyst composites. Mathematical models of adsorption and photodegradation kinetics as well as instrumental analysis of catalyst composites were examined and reported.

Chapter 4 presents the results of adsorption and photodegradation experiments. The effects of crosslinking method, drying method, reuse, catalyst dosage, pH and initial dye concentration on the dye adsorption and photodegradation characteristics were investigated. The findings of instrumentation characterisations on the catalyst composites also summarised.

Chapter 5 provides general conclusion and suggestion for future work.

Chapter 2 Literature review

2.1. Mechanism of photodegradation by various types of photocatalysts

2.1.1. Mechanisms of photodegradation involving intrinsic semiconductor

Photodegradation requires the absorption of light energy. There are two reported routes for photon uptake namely the direct excitation of semiconductor and dye photosensitisation. For direct excitation of semiconductor (**Scheme 2-1**), the first step is the promotion of electron from low lying valance band to high energy conduction band. Positive hold and extra electron are occurred at valance band and conduction band respectively.

$$VB+CB + h\nu \rightarrow VB\ h^+ + CB\ e^-$$

Scheme 2-1 The excitation of semiconductor

where VB, CB, h^+ and e^- denote valance band, conduction band and positive hole and electron respectively.

Actually, valance band and conduction band do not exist in reality. For example, conduction band electron of TiO_2 corresponds to the reduced form of Ti^{4+}, i.e. Ti^{3+} and valence band hole refers the oxidised form of O^{2-}, i.e. O^-. Excitation, of electron transfer from VB to CB, of TiO_2 where electron transfer from O^{2-} to Ti^{4+} is assisted by light energy[9].

After excitation, recombination of h^+ and e^- may occur and the energy is wasted or the h^+ and e^- may act as oxidising agent and reducing agent, and then trigger various reactions that degrade the dye.

The reported possible fates of h^+ (**Scheme 2-2**) are reacting with aqueous species or

direct oxidation of dye molecule.

$$H_2O + h^+ \rightarrow \bullet OH + H^+$$

$$OH^- + h^+ \rightarrow \bullet OH$$

$$Dye + h^+ \rightarrow Dye^{\bullet +} \text{ (oxidised dye)}$$

Scheme 2-2 The possible fates of valence band hole

The reported possible fates (**Scheme 2-3**) of e^- are reacting with dissolved oxygen or directly reducing the dye molecule.

$$O_2 + e^- \rightarrow O_2^{\bullet -}$$

$$O_2^{\bullet -} + H^+ \rightarrow \bullet HO_2$$

$$2\ HO_2^{\bullet} \rightarrow H_2O_2 + O_2$$

$$H_2O_2 + e^- \rightarrow OH^- + \bullet OH$$

$$Dye + e^- \rightarrow Dye^{\bullet -} \text{ (reduced dye)}$$

Scheme 2-3 The possible fates of conduction band electron

The hydroxyl radical generated (•OH) is a powerful oxidant for dye. Both reduction and oxidation of dye are capable of activating the dye towards degradation[10, 11].

The first step of dye photosensitisation is absorption of photon by the dye molecule. This involves the promotion of electron to a high energy orbital (**Scheme 2-4**).

$$Dye + h\nu \rightarrow Dye^*$$

Scheme 2-4 The excitation of dye molecule

If the energy of electron is high enough, the electron may transfer from the dye molecule to CB of semiconductor (**Scheme 2-5**). The excited dye molecule is oxidised by the CB.

$$Dye^* + CB \rightarrow Dye^{\bullet+} + CB\ e^-$$

Scheme 2-5 The electron transfer from dye molecule to CB of semiconductor

The CB e^- and $Dye^{\bullet+}$ can perform reactions as discussed above resulting in degradation of dye[5].

Photosensitisation predominates when the band gap of semiconductor is high and the energy of photon is not enough to induce excitation. For example, dye photodegradation is using both visible light and TiO_2. Photosensitisation is not possible for contaminants and degradation intermediates that do not absorb incident light.

2.1.2. Increasing efficiency of photocatalyst

Intrinsic semiconductors suffer from short electron-hole pair recombination lifetime[29]. Coupling two semiconductors together, introduction of precious metals and rare earth metals as well as inducing crystal defects are methods reported for increasing recombination of lifetime and charge separation.

2.1.2.1. Introduction of precious metal

Introduction of precious metal nanoparticles, e.g. Pt, Pd, Au and Ag, for improving charge separation was frequently reported in the past. Chen et al.[57] tested methyl orange degradation using Ag/ZnO. The mechanism is that ZnO is first excited (**Scheme 2-6**).

$$ZnO + h\nu \rightarrow VB\ h^+ + CB\ e^-$$

Scheme 2-6 The excitation of ZnO

Oxidation by O_2 can occur on Ag or CB e^- (**Scheme 2-7**).

$$O_2 + CB\ e^- \rightarrow O_2^{\bullet-} + CB$$

$$Ag + O_2 \rightarrow O_2^{\bullet-} + Ag^+$$

Scheme 2-7 The oxidations by O_2

If oxidation occurrs on Ag, the Ag will act as sink for electron in CB and prevent charge recombination (**Scheme 2-8**).

$$Ag^+ + CB\ e^- \rightarrow Ag + CB$$

Scheme 2-8 Ag acts as sink for electron

The remaining steps toward degradation are the same as those of intrinsic semiconductors. It is interesting to notice that the metal should be more anodic than the CB of semiconductor for thermal dynamically favourable charge transfer to

occur.

2.1.2.2. Coupling of 2 semiconductors

Coupling of 2 semiconductors is now under intense investigation. The mechanism of this method is similar to the introduction of precious metal nanoparticle. If conduction band of the excited semiconductor is more cathodic (reducing) than that of another semiconductor in contact, electron transfer from excited semiconductor to another semiconductor can occur. On the other hand, if valance band with the hole of excited semiconductor is more anodic (oxidising) than that of another semiconductor in contact, the hole transfer from the excited semiconductor to another semiconductor can occur. These can improve charge separation and catalytic activity. He and coworkers[58] reported the $GdVO_4$ / V_2O_5 system that allowed both hole and electron transfer as shown in Figure 2-1. Their valence and conduction band potentials are suitably disposed.

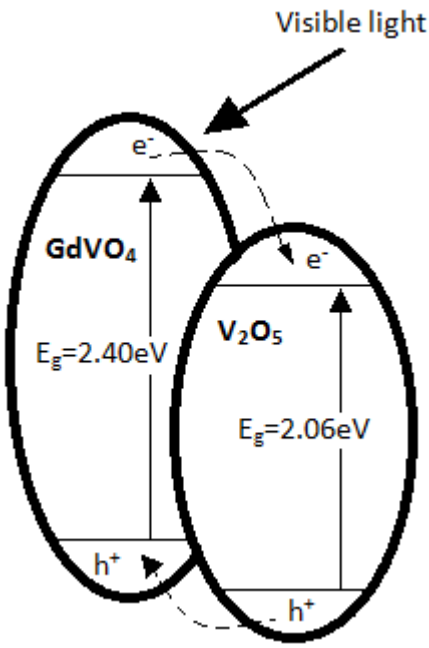

Figure 2-1 $GdVO_4/V_2O_5$

CB of the low band gap V_2O_5 is less cathodic than that of Gd_2O_3. This system does not allow electron transfer from CB of V_2O_5 to CB of Gd_2O_3. The potential difference between VBs is not large. Efficiency of charge separation by hole transfer is low. Their valence and conduction band potentials are not suitably disposed. This coupling will not enhance charge separation and degradation if energy of incident photon is not high enough to excite the Gd_2O_3 as shown in Figure 2-2.

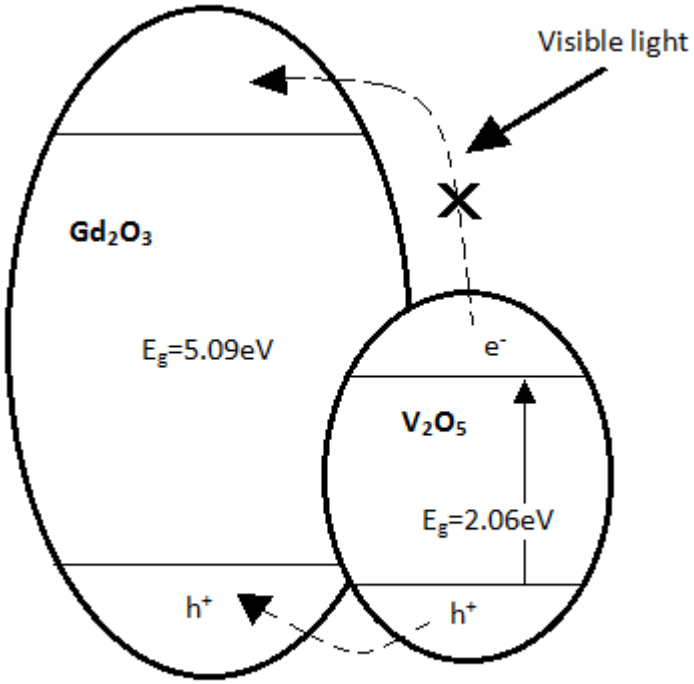

Figure 2-2 Gd_2O_3/V_2O_5

A couple of semiconductor frequently reported similar to Gd_2O_3/V_2O_5 is CdS/TiO_2 as shown in Figure 2-3. This couple consists a high band gap semiconductor, TiO_2; and a low band gap semiconductor, CdS, and it works well for enhancing degradation. Wu and coworkers[59] showed that methylene blue degradation with CdS/TiO_2 was much faster than that of CdS or TiO_2 alone under visible light. Different from Gd_2O_3/V_2O_5, CB of the low band gap CdS is more cathodic than that of TiO_2. If the energy of incident photon is high enough to excite CdS, this will allow electron transfer from CB of the activated CdS to CB of TiO_2, thereby making the charge separation occur.

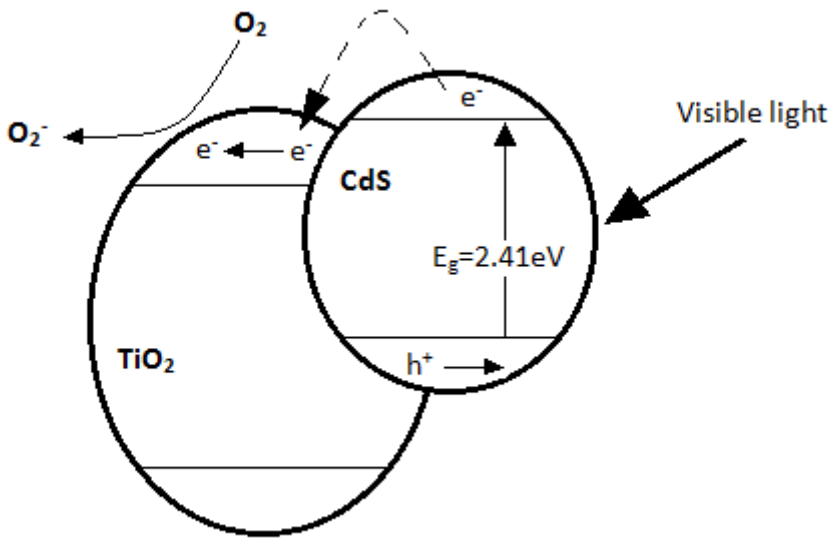

Figure 2-3 CdS/TiO_2

Hence if energy of incident photon can also excite TiO_2 the hole transfer from TiO_2 to CdS will occur and improve charge separation.

2.1.2.3. Doping rare earth or transition metal into semiconductor

Charge separation of excited semiconductor can also be achieved by doping of rare earth metals. The role of rare earth is just similar to precious metals and can act as a sink for CB electrons. Song et al.[60] reported the selenium-doped bismuth sulfide when comparing with bismuth sulfide, photodegradation rate of methylene blue using the selenium-doped bismuth sulfide under visible light was doubled. Mokhtar et al.[61] reported that the vanadium(V) doped in TiO_2 could act as electron acceptor.

2.1.2.4. Inducing defects

Some authors suggested that defects of crystal structure of semiconductors could enhance charge separation[57, 62]. Chen et al.[57] prepared Ag/ZnO and proposed that apart from the Ag, oxygen defects of ZnO also played an important role in improving charge separation. Oxygen vacancy defects are also less cathodic than CB of ZnO so that CB e^- can migrate to the defect like Ag.

2.1.3. Enhancing photodegradation rate under solar radiation by extending range of utilisable light

Most traditional photocatalysts, e.g. anatase TiO_2, are only able to utilise UV light due to the high band gap but UV light is just 3-5 % of solar radiation. Photocatalyst which is capable of utilising visible light is now under intense study as it can fully utilise the free solar radiation. In order to achieve the purpose of utilisation of the band width of solar radiation, some studies using (i) low band gap semiconductors; (ii) coupling low band gap semiconductors to other semiconductors; (iii) doping and (iv) dye photosensitisation can be the possible methods.

1. Using low band gap semiconductors: The use of low band gap semiconductors, e.g. CdS[4, 10, 22, 29, 63], Bi_2S_3[60] and rutile TiO_2[64], can achieve photodegradation under visible light.

2. Coupling low band gap semiconductors to other semiconductors: Coupling low band gap semiconductors to other semiconductors was frequently reported. Usually, the low band gap semiconductor

capturing the light energy. The high band gap semiconductor acting as merely a sink for charge. CdS/TiO_2 use frequently reported[59, 63, 65]. In addition Bi_2S_3/TiO_2 was also investigated[63].

3. Doping of non-metal elements: Doping of non-metal elements is important in electronic industry as it needs P and N type semiconductors. Liu et al.[66], Subagio et al.[67] and Wang et al.[68] reported the N or N-C doped TiO_2 for photodegradation of organic contaminants under visible light. Originally, TiO_2 only absorbs light with $\lambda<390$ nm. With the aid of those dopants, new orbital with energy lower than CB and higher than VB of TiO_2 is formed. The new orbital acts as a step for those electrons located between CB and VB. Hence, the energy required for excitation is reduced and visible light can be utilised as shown in Figure 2-4.
4. Dye photosensitisation: Dye photosensitisation is widely used for making solar cell. Usually, dye molecules capture the light energy and high band gap semiconductor acts merely as a sink for charge. Light causes transition of electrons from HOMO to LUMO of dye molecule. If HOMO is more cathodic than CB of semiconductor, charge transfer will occur and the dye molecule is oxidised. This mechanism does not occur on the colourless fragments of the partially degraded dye molecules.

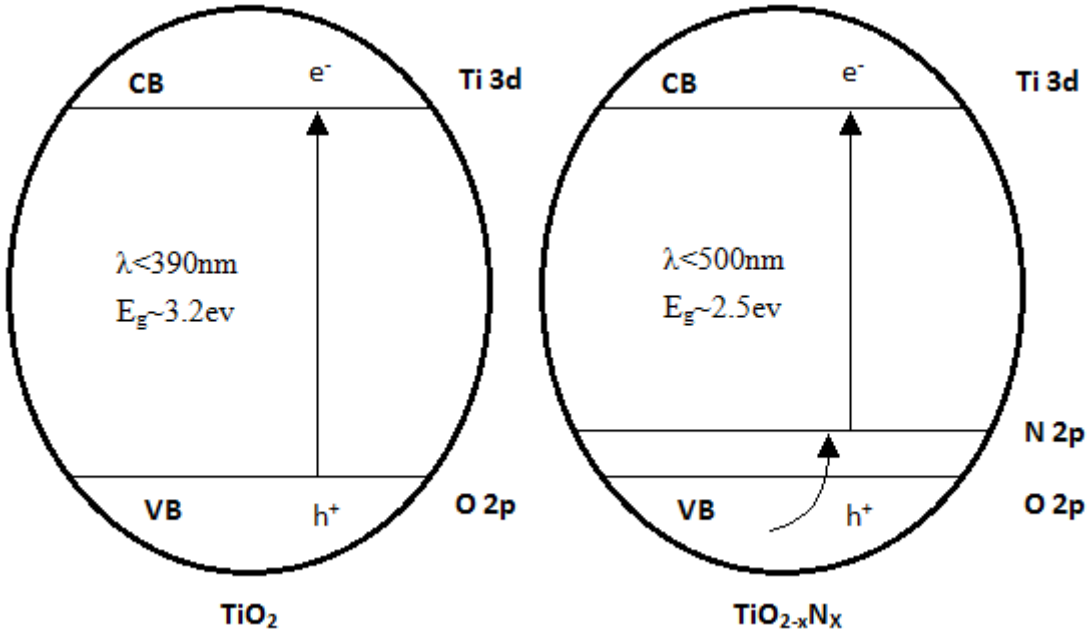

Figure 2-4 TiO_2 and N doped TiO_2

2.1.4. Steps involved in degradation of complex organic contamination

Some researchers analysed the solution taken from photodegradation after different times of illumination using the mass spectrum techniques. Their results showed that the molecules undergo multiple step reactions. Demethylation, hydroxylation, group oxidation, carbon oxidation and bond cleavage are possible to occur. Song et al.[69] attempted to assign intermediates in the photodegradation of Direct Red 23. Fragments formed periphery structures i.e. phenol, hydroquinone, *N*-(4-hydroxyphenyl) and acetamide, of Direct Red 23 and its derivatives were first observed. Later, fragments formed from the central structure, i.e. (4-hydroxynaphthalene-2-sulfonato-k*O*)sodium and 1-naphthol, were also observed. At final stage of the degradation, the highly oxidised and relatively simple fragments, urea, phthalic acid, maleic acid and acetic acid were observed.

Chen et al.[57] attempted to assign intermediates in photodegradation of a simple dye e.g. methyl orange. They found out that the periphery group modifications like *N*-demethylation and hydroxylation of aromatic ring could occur without breaking the conjugated system at the early stage. Those modified dye molecules could shift the absorption peak of UV-visible spectrum of the reaction solution.

2.2. Kinetic model of photodegradation

Some researchers attempted to fit their photodegradation data with various kinetic models where the pseudo first and pseudo second order kinetics were commonly reported. The reaction rate depends on (i) contaminant concentration; (ii) light intensity and (iii) amount of catalyst, adsorption and other chemical species, yet the models are only the relationship between the rate and contaminant concentration.

The basic expression of linear plot for pseudo first order kinetics of photodegradation is:

$$\ln \frac{C_0}{C_t} = k_{1p} t \qquad (2\text{-}1)$$

If the data follow the pseudo first order kinetics of photodegradation, the lnC_t against t plot should yield linear line.

The basic expression of linear plot for pseudo second order kinetics of photodegradation is:

$$\frac{1}{C_t} = \frac{1}{C_0} + k_{2p} t \qquad (2\text{-}2)$$

If the data follow the pseudo second order kinetics of photodegradation, the $1/C_t$ against t plot should yield linear line.

where:

C_0 = initial contaminant concentration

C_t = contaminant concentration at time t

k_{1p} = rate constant of pseudo first order kinetics of photodegradation

k_{2p} = rate constant of pseudo second order kinetics of photodegradation

t = time of illumination

Almost all of the reviewed literatures reported the high fitness with the pseudo first order kinetics of photodegradation[4, 5, 10, 26, 27, 29, 57, 70-72]. This implied that the reactions followed the common Langmuir–Hinshelwood kinetic model simplified with the approximation that the concentration of contaminant was low[29]. Details of the model and approximation are provided below: [68]

$$-\frac{\mathrm{d}C}{\mathrm{d}t} = k\Theta = k\left(\frac{KC}{1+KC}\right) \quad (2\text{-}3)$$

where:

C = contaminant concentration

t = time of illumination

Θ = surface coverage

k = intrinsic reaction rate constant

K = Constant of Langmuir isotherm

One can see that it is a combination of Langmuir isotherm and the first order chemical kinetics.

When the concentration of contaminant is low:

$k(\frac{KC}{1+KC})$ can be approximated to kKC and

$$-\frac{\mathrm{d}C}{\mathrm{d}t} = kKC = k_{\mathrm{app}}C \qquad (2\text{-}4)$$

Where k_{app} is apparent rate constant

This is an analog of the first order chemical kinetics is usually referred to the pseudo first order kinetics of photodegradation.

Nevertheless, one of the reviewed literature reported the high fitness with the pseudo second order kinetics of photodegradation[73]. The author suggested that methylene blue formed dimmers at high concentration. If the rate determining step does not involve the original contaminant molecule, the linear C_t against t plot and constant rate of photodegradation will occur. The reaction follows the pseudo zero order kinetics with respect to the contaminant[74]. The slope of C_t against t plot is the rate constant.

The equation of pseudo zero order kinetics is:

$$C_t = C_0 - k_{0p}t \quad (2\text{-}5)$$

where k_{0p} is rate constant of the pseudo zero order kinetics of photodegradation

2.3. Heat treatment, crystal structure and their effects on photodegradation

Some semiconductors require heat treatment before it can be photoactive. It was commonly reported that heat treatments such as calcination and hydrothermal synthesis could induce crystalline structure. Calcination and hydrothermal synthesis could affect crystal structure[75], crystallinity[68], band gap[64, 76], surface area[62, 76], crystal defect[62, 68] and other properties which in turn could affect the catalytic activity. Jamalluddin et al.[75] showed that the crystal structure of TiO_2 could be the controlled by temperature of calcination. 2 hours of calcination at 500 °C and 900 °C resulted in anatase and rutile respectively. Calcination at 700 °C resulted in a mixture of both phases. Paez et al.[64] reported the H_2-reduced TiO_2 xerogel. Rutile structure was observed for calcination at 700 °C for 12 hours. Anatase structure was observed for calcination at 400 or 500 °C for 12 hours. Under UV illumination, anatase material outperformed rutile material in methylene blue degradation. Reverse was also observed under visible light. It was noticed that the band gaps of anatase and rutile materials were 3.16 ev and 3.04 ev respectively. Non-calcinated material was less active when comparing with the calcinated materials. Wang[68] tested the CN doped TiO_4 catalysts for bisphenol A degradation under various heat treatment combinations of heat treatment using the hydrothermal synthesis for 4 hours followed by another 4 hours of calcinations. Their research

group employed various temperatures for the hydrothermal synthesis at 90-160 °C and calcination at300-600 °C. They found out that the hydrothermal synthesis at 120 °C and calcination at 300 °C resulted in distinctively better catalyst that showed the degradation rate at least 2 times higher than that of those processed at other temperatures. They explained that the temperatures could affect impurity and lattice defects which may inhibit recombination. At the same time, Kale[76] prepared $ZnBiVO_4$ via two different methods. The first method of using solid-state calcinations to produce the product of ZnO, Bi_2O_3 and V_2O_3 at about 700 °C was employed. Another solution approach was conducted by dissolving $Zn(NO_3)_2$, $Bi_2(NO_3)_3$ and NH_4VO_3 together and then later the solution mixture was evaporated at 70 °C. The dried material was then crushed and calcinated at 180 °C. The catalyst obtained from the solution route showed a higher band gap, larger BET surface area and higher activity in H_2S spitting. Solarska et al.[62] reported the nanoscale calcium bismuth mixed oxide formed by the spray flame synthesis in O_2/C_2H_2 torch. Methylene blue photodegradation of the catalyst was compared with that of the similar catalyst formed by the traditional hydrothermal synthesis. Spray flame synthesis showed 6 times of enhancement in the rate of degradation. The authors suggested that high performance could be resulted in an increased surface area, number of defects, and absorbance of light. These special characteristics could be caused by extreme thermal stock during spray flame synthesis.

2.4. Optimising coupled semiconductor system

For the coupled semiconductors, some authors attempted to work out the optimum ratio and method of mixing two semiconductors. Two methods namely, (1)

(co-)precipitation and (2) simple mechanical mixing for mixing were reported[63]. In both cases, electron and hole transfer between the catalyst occur to enhance charge separation and degradation. For the (co-)precipitated composite catalysts, intra-particle charge transfer occurs. For the mechanically mixed coupled catalyst systems, inter-particle charge transfer occurs after the agglomeration of discrete semiconductor particles[9]. Wu[59] tested the effect of CdS to TiO_2 ratio on the rate of degradation of Methylene Blue. Samples of co-precipitation of CdS and TiO_2 containing 1, 3 and 5 mol% of CdS were tested. The rate of samples with 3 and 5 mol% of CdS was about 2 times higher than that of the sample with 1 mol% CdS. Karunakaran et al.[9] tested the photodegradation of phenol by mechanically mixing the couples of 7 semiconductors, TiO_2, ZnO, ZnS, CdO, Fe_2O_3, CuO and Nb_2O_5. The mass ratios of mixing were 1:3, 1:1 and 3:1. Generally, the rates of degradation of 1:3 and 3:1 mixtures were 1-2 times higher than that of the 1:1 mixtures, and 2-4 times higher than that of the uncoupled separate individual semiconductors. Among the semiconductors, Nb_2O_5 showed exceptional observations with CdO and CuO. The 1:1 ratio mixtures showed optimal degradation results, and about 3 times of rates of the uncoupled separate individual semiconductors were shown. The authors suggested that variation in the rate of degradation was related to density, particle size and agglomeration after ground mixing the semiconductors together. Bessekhouad[63] reported Orange II degradation by means of Bi_2S_3 / TiO_2 and CdS/TiO_2. Simple mixing of TiO_2 and precipitation of TiO_2 were reported. They had tested various mass percentages of Bi_2S_3 or CdS with respect to TiO_2 of 10, 30 and 50 %. For Bi_2S_3, the precipitation on TiO_2 and the photocatalyst composite outperformed those by simple mixing. They investigated the reaction carried out

under both UV-visible light and visible light alone. The results obtained from only the visible light condition using simply mixture catalyst showed that photodegradation rate decreased with increasing amount of Bi_2S_3. For the precipitation step, only the sample with 10 % Bi_2S_3 showed good results while the other portion seemed inactive. CdS precipitations were almost inactive. As for the mixtures, the reaction rate increased with respect to the amount of CdS. The authors proposed that too much CdS or Bi_2S_3 could trap the TiO_2. The electrons present in the conduction band of TiO_2 and also in the conduction band of CdS or Bi_2S_3 generated from the excitation caused by light could not reach the catalyst surface to produce reactive radicals for degradation.

2.5. Encapsulation by polymer

Some recent publications reported that semiconductors immobilised in various polymers could improve the practical value of their photocatalysts. The authors suggested that polymers could (1) enhance usability and stability and (2) provide synergistic effect on dye removal.

1. Usability and stability: photocatalysts are usually semiconductor of nanoparticles and so recollection of catalysts is difficult. Immobilising the nanoparticles into polymer films or spheres of suitable size facilitates recollection after applications, thereby improving usability. The polymer films should allow penetration and adsorption of contaminants. alginate[12, 23], cellulose acetate[13], chitosan[4, 5, 20, 24-27] and poly(diallyl dimethylammonium) chloride (PDDA)[22] were reported in the journals papers. Since some catalysts are relatively unstable thus, immobilisation

of the catalysts into polymer can stabilise the catalysts. Chelating ability of chitosan with transition metals is good[27]. Lee et al.[24] reported Fe(II) immobilised in chitosan for fenton degradation. Fe(II) was chelated with chitosan to prevente Fe(II) precipitation and so working pH range was widened. Ru et al.[29] reported that chitosan could provide fixation and preventing aggregation of CdS nanoparticles. Yang et al.[22] prepared the PDDA protected by the nanosized CdS pre-incorporated with the hexagonal mesoporous silica (HMS) spheres. The PDDA-protected catalyst was much more stabile against the prolonged use and showed less Cd^{2+} leakage when comparing with the unprotected counterpart.

2.Synergistic effect: some authors[60] proposed that the high adsorption ability of chitosan could bring more dye molecules into the close proximity with catalytic sites and then let them react with the generated active species. In the close proximity with semiconductor, dye could act as photosensitiser. This provided an alternative route for degradation.

Some researchers reported that biopolymers like chitosan were not very stable, especially under strong illumination. Polysaccharides are sensitive to photooxidation under UV light, and the cleavage of glycosidic bond and formation of carbonyl groups are common reactions[26]. Therefore, chemical modification is required to improve its stability. Lee et al.[24] suggested that the stability of chitosan could be improved by crosslinking. Zhu et al.[27] reported the use of glutaraldehyde for crosslinking the chitosan polymer where mechanical properties and water resistance could be improved.

2.6. Stability in repeated use

Heterogeneous catalysts with economic value should be capable for the prolonged use as well as the changes in catalytic activity and the ability for recycle use. Publications showed that some catalysts were highly re-usable[22, 72] while some did not[22, 65]. Deactivation of photocatalyst could be caused by the adsorption of insensitive species on the photocatalyst surface[69] or the supporting matrix[27]. For recycle purposes, various methods used for regeneration were reported[22, 27, 69]. A group of researchers reported that sulfides were vulnerable to photocorrosion and so extreme stability could be achieved by their immobilisation in matrix where leakage could be prevented[22].

Yin[72] reported that the monoclinic $BiVO_4$ photocatalyst for nearly complete rhodamine B (1×10^{-5} M) degradation was 60 minutes in each run. The authors demonstrated 5 runs without any significant loss of activity. Song[69] tested Direct Red 23 (100 mg/l) degradation by $SrTiO_3/CeO_2$, and the duration of each run was 240 minutes. After 4 cycles, the percentage of COD removed was dropped from 70 % to 62 %. Regeneration could be done by rinsing with distilled water and drying at 110 °C. Deactivation of photocatalyst could also be caused by the deposition of photo-insensitive hydroxides on the photocatalyst surface, which might block its active sites. Zyoud et al.[65] reported the phenazopyridine (10 ppm) degradation on the CdS/TiO_2 coupled semiconductor. The duration of each degradation run was 60 minutes, and the phenazopyridine removal was almost halved within 3 runs. They suggested that the loss in catalytic activity might be due to the significant leakage of cadmium. Yang[22] prepared the poly(diallyl dimethylammonium) chloride (PDDA)

coated nanosized CdS in the pre-incorporated hexagonal mesoporous silica (HMS) spheres. HMS provided the spatial confinement of mesopores while PDDA provided the protection for CdS nanoparticles. They attempted the repetitive use of the composite catalyst in the photodegradation of Eosin B(1×10^{-4} M), and the complete degradation could be achieved in 250 minutes. The catalyst could be reused for 22 runs without significant drop in activity. Their catalyst could be completely regenerated with H_2S treatment. After 150 runs and 6 regenerations, no significant activity drop was observed when comparing with the newly generated catalyst. In contrast, their nanosized CdS (without PDDA protection) in the pre-incorporated HMS showed a decrease in catalyst activity in 3 cycles and displayed severe cadmium leakage. Zhu[27] reported the methyl orange (10 mg/l) degradation by SnO_2/ZnO catalyst which was immobilised in the crosslinked chitosan. The authors demonstrated 4 runs and 4 hours of treatment at 100 °C, and the duration of each run was 210 minutes for a nearly complete degradation if new catalyst was used. Dye removal dropped to 80 % at 4^{th} run. They also reported the degradation of Congo Red, Acid Red 66 and Methyl Orange by CdS which was immobilised in the crosslinked chitosan[4, 29, 56]. The authors demonstrated the experiment in 5 runs and the duration of each run was 80 minutes which allowed almost the complete degradation if new catalyst was used. Interestingly, photocatalytic activity loss in the repeated use of catalyst on the testing experiments of methyl orange removal was much severer than that of the testing experiments conducted on other dyes. Their experiments demonstrated that the reusability of catalyst was dye dependent. Nawi[26] reported the photodegradation of Reactive Red 4 (30 mg/l) by the immobilised TiO_2/chitosan on glass plates. They carried out the degradation reaction

in 3 runs with a reaction time of 120 minutes. Again, a significant drop in the first order reaction rate constant was observed after the first run. After the second run, a smaller drop in the constant occurred when comparing with the first run. They suggested that the drop in the rates of degradation or adsorption should be due to the result of saturation of chitosan adsorption site.

2.7. Effect of contaminant concentration

The rate of photodegradation is significantly affected by the types of contaminant and their concentration. Hence, optimum operation conditions should be employed for practical applications. Literatures showed that the rate dropped with respect to increasing contaminant concentration[4, 27, 29, 69, 71] but only few opposite trends[9, 65] were reported.

Zhu et al.[4, 27, 29] reported that the increase of concentration of Congo Red and Acid Red 66 would lead to a decrease in degradation by CdS immobilised in crosslinked chitosan. They observed the similar trend for the degradation of Methyl Orange induced by SnO_2/ZnO immobilised in the crosslinked chitosan. Song et al.[69] reported a similar observation for the degradation of Direct Red 23 induced by $SrTiO_3$ / CeO_2. Hayat and co-workers[71] reported that the degradation rate of safranin-O on WO_3 dropped with increasing concentration of the target contaminant. The researchers proposed two reasons. Firstly, the increase of dye concentration reduced the optical path length and light that reached the photocatalyst. Secondly, adsorption of dye molecules on the photocatalyst surface increased with dye concentration, and prevented the adsorption of OH^- and O_2 which were the important chemical species responsible for degradation. In contrast, Zyoud[65] reported the use

of CdS/TiO_2 catalyst for the degradation of phenazopyridine with the concentration of 5, 7.5, 10 and 15 ppm. They found out that the drop in quantum yield was not observed for the increase of concentration from 5 to 7.5 ppm but 7.5 to 15 ppm. At low concentration, quantum yield did not have contaminant concentration dependency. Karunakaran et al.[9] reported that the photodegradation rate of phenol on their photocatalysts, TiO_2, ZnO, ZnS, CdO, Fe_2O_3, CuO and Nb_2O_5, increased with phenol concentration. They suggested that at low substrate concentration, its adsorption on semiconductor surface was low. Langmuir-Hinshelwood model exhibits saturation kinetics and rate which increase linearly with substrate concentration.

2.8. Effect of catalyst dosage

The study of optimum dosage of photocatalyst used for photodegradation is important for practical application. This allows the maximum rate of contaminant removal without the waste of catalyst. Researchers reported that if the dosage was higher than a certain value, the drop in degradation rate was observed. Yan[10] tested the degradation of Malachite Green (0.2-1.0 g/l) induceded by CdS nanoparticles. Maximum rate of degradation occurred when the dosage was 0.6 g/l. Song et al.[69] reported the degradation of Direct Red 23 induced by $SrTiO_3/CeO_2$ (0.5-2.0 g/l) and the maximum rate of degradation was observed when the dosage was 1.5 g/l. Hayat[71] reported the degradation of Safranin-O induced by WO_3 and the range of dosage was 1.0-8.0 g/l. The rate of degradation increased rapidly with the dosage of the first 4 g/l. For 4-8 g/l, the rate of degradation decreased with increasing dosage. Zhu[27, 29] reported the degradation of Acid Red 66 induced by CdS immobilised in

the crosslinked chitosan, and the degradation of Methyl Orange induced by SnO_2/ZnO immobilised in the crosslinked chitosan (0.1-1 g/l). The reaction rate of pseudo first order kinetics increased with dosage but the difference for the dosages of 0.7 and 1 g/l was quite small. Zyoud[65] reported the degradation of phenazopyridine induced on CdS/TiO_2 and the tested dosages were 1, 2 and 3 g/l, and the reaction rate increased with dosage. Nevertheless, quantum yield only increased slightly while the quantum yield per mole catalyst dropped. They proposed that the increased dosage of catalyst could increase the availability of active sites for reaction. In addition, the number of adsorbed dye molecules and illuminated area of semiconductor was also increased for helping the reaction. In summary, the rate of photodegradation generally increases with dosage until a maximum point is reached. At high dosage, the penetration of light could also be reduced by absorption, scattering and screening.

2.9. Effect of light intensity

In general, literatures reviewed that degradation rate increased with light intensity. Karunakaran et al.[9] reported that the photodegradation rate of phenol induced by 7 semiconductors, TiO_2, ZnO, ZnS, CdO, Fe_2O_3, CuO and Nb_2O_5 increased linearly with the amount of photons (0-50 μeinstein $L^{-1}s^{-1}$). Song[69] tested the degradation of anionic Direct Red 23 induced by $SrTiO_3$ / CeO_2 with arc lamps of different powers. Complete degradation required about 80 minutes when the using lamp power of 175 W. For 400 W lamp, the degradation was reduced to about 20 minutes. Hayat[71] reported safranin-O degradation on WO_3 with laser light source. The tested energies and duration were 40-200 mJ and 10 minutes respectively. The

removal percentage increased linearly with laser energy. They proposed that the increased photon flux could excite more semiconductor particles and then generate more hole – electron pairs[69, 71]. This could degrade more dye molecules or generate more active species, e.g. OH•, which could degrade the dye.

2.10. Effect of pH

Optimum pH for efficient degradation of organic substrates seems dependent on both choice of catalyst and nature of the organic substrates. Generally, there are two obvious trends; Low pH facilitates photodegradation of anionic dyes while the reverse facilitates photodegradation of cationic dyes and dye with protonatable amino groups and TiO_2 with inorganic immobilization such as silica and activated carbon usually demonstrate best degradation efficiency in slightly acidic environment. Nevertheless, some exceptions were observed with non-immobilized catalysts. Two research groups[10, 69] reported that high degradation rate of cationic or anionic dye was observed at extreme pH, both acidic and basic and Caliman et al.[77] reported that optimum pH for photodegradation of the cationic Alcian blue 8 GX is 5.6. The researchers provided some explainations based on their results.

Those reported that better removal efficiency occurred in basic environment attributed the observation to two reasons. First, availability of OH^- is higher in basic environment and this also increases availability of the oxidative OH• because the photo-generated hole abstract a single electron from OH^- to form the OH•. [65, 71, 78, 79] Second, with pH above the point of zero charge (PZC) of the catalyst, the negatively charged catalyst surface can enhance the adsorption of cationic molecules

and this is beneficial for the photodegradation. [71, 79] Caliman et al.[77] also suggested that adsorption of the cationic dye increase with increasing pH. However, too much adsorbed dye could block the UV light and the excitation of catalyst is precluded. This resulted in slow photodegradation. Thus, maximum rate occurred at pH around the PZC. Generally, those reported that better removal efficiency occurred in acidic environment attributed the response to the pH dependent adsorption and the adsorption is beneficial for the photodegradation. Karunakaran[9] proposed that there is a repulsion between negatively charged semiconductor surface and the negative pole of phenolic -OH at high pH and this reduced the photodegradation rate. Pelaez[80] suggested that Microcystin-LR is negatively charged in pH above 2.1 and attraction between TiO_2 particles and the microcystin increased with decreasing pH because of the increasing protonation of TiO_2 surface. Shahrezaei[81] expressed that protonation of TiO_2 surface increase with decreasing pH and this also increase the attraction between TiO_2 particles and the ionized phenolic derivatives presented in refinery wastewater. They also think that the radicals essential for photodegradation are rapidly scavenged at high pH and this is detrimental to the photodegradation. The researchers studied anionic azo dye photodegradation using photocatalysts with chitosan encapsulation suggested that the negative charge of sulfonate groups on dye molecules were unaffected in the pH range but protonation of residual amino groups on chitosan only occurs at low pH. The increased adsorption of anionic dyes on chitosan occurred due to electrostatic attraction. The dyes could be oxidized more directly by OH• on semiconductor surface[4, 14, 21, 29] and dye photosensitization could also occurred[82].

Three authors reported that high degradation rate was observed at extreme pH, both acidic and basic. Yan[10] tested the cationic malachite green degradation by CdS nanoparticles at pH 3, 5, 7 and 9. Slowest degradation occurred at pH 5 while other pH showed similar results. Song[69] demonstrated the anionic direct red 23 degradation by $SrTiO_3$ / CeO_2 at pH 2, 6, 8, 10 and 12. The pH ranked by rate with descending order were: 12>2~8>10>6. Chen[83] reported that glyphosate photodegradation by TiO_2 was most efficient at pH2 while at pH12 the efficiency was slightly lower and lowest efficiency recorded at pH6. Yan believed that at weakly acidic condition, the protons interfere with surface groups of CdS to form structures like –SH and then prevent the reaction. However, at pH lower than isoelectric point of CdS, changes preventing formation of structures like –SH occurs. Song expressed that the trendless results is difficult to be explained since the reaction is governed by multiple factors. First, pH could affect adsorption of dye on semiconductor. Second, pH could affect the route of reaction after generation of hole and electron by absorbed light. At high pH, repulsion between OH^-, anionic dye and surface of the semiconductor increase as negative charge on the surface increase with pH. However, high pH also make conversion of OH^- to OH• easier. At low pH, oxidation of dye should be mainly the direct oxidation by positive holds on semiconductor but not the OH•. Moreover, the reductive cleavage of azo bond by e^- at conduction band of semiconductor also plays an important role. Agglomeration of semiconductor particles occurs under acidic condition and then reduces surface area for adsorption of dye as well as absorption of light, and leads to a lower reaction rate. Chen also suggested that high pH and high availability of OH^- could facilitate formation of OH• since single electron abstraction by photo-generated hole from

OH^- can supply OH•, notwithstanding, they proposed that the high availability of H^+ could also facilitate formation of OH• because the superoxide $\bullet O_2^-$, generated from single electron reduction of oxygen by photo-generated conduction electron, can react with H^+ and this could eventually lead to formation of OH• after a series of radical reactions. Adsorption of glyphosate on TiO_2 and photodegradation rate was stronger in acidic environment.

Both the influences of pH on photodegradation efficiency of cationic and anionic substrates using TiO_2 with inorganic immobilization were studied. Mahmoodi[84] think that the pH response of the degradation rate of cationic dyes was associated with increase in adsorption of the dyes onto TiO_2 with higher pH caused by attraction between negatively charged TiO_2 and the cationic dyes while Nam[85] suggested that TiO_2 is protonated in acidic environment and this facilitated adsorption and photodegradation of the anionic sodium lauryl sulfate. Tseng[19] also proposed that protonation of TiO_2 in low pH could improve the adsorption of anionic dye on to it, whereas too much dye could masked the photocatalyst from light and the generation of reactive radicals is precluded. That's why highest degradation efficiency occurred at pH5 rather than pH3 or pH7. Table 2-1 and Table 2-2 summarize the pH of photodegradation rate or efficiency in the selected publications.

Table 2-1: Summary of pH responses of photodegradation rate or efficiency in the selected publications

Publication	Catalyst	Substrate	Tested pH	Result
Zyoud[65]	CdS/TiO_2	Azo dye / drug: Phenazopyridine	4-9.5	Higher the pH, the higher is the removal efficiency
Hayat[71]	WO_3	Cationic dye: Safranin-O	5-11.6	Higher the pH, the higher is the removal efficiency
Qourzal[78]	TiO_2 (p25)	2-Naphthol	3-11	Higher the pH, the higher is the rate of degradation
Pouretedal[79]	CeO_2	Cationic dye: Methylene blue	2-12	Highest removal efficiency occurred at pH11
Cao, Ru and Zhu[4, 14, 21, 29]	CdS, TiO_2/ZnO or Cu_2O with chitosan encapsulation	Anionic azo dyes: Acid red 66, Congo red, Methyl orange or reactive brilliant red X-3B	2-12	Lower the pH, the higher is the removal efficiency
Nawi[82]	TiO_2 with chitosan encapsulation	Anionic azo dye: Reactive Red 4	4-10	Lower the pH, the higher is the removal efficiency
Karunakaran[9]	TiO_2, ZnO, ZnS, CdO, Fe_2O_3, CuO	Phenol	3-9	Lower the pH, the higher is the removal efficiency
Shahrezaei[81]	TiO_2 (p25)	Petroleum refinery wastewater: Rich in phenolic derivatives	4-8	Lower the pH, the higher is the removal efficiency

Chong[86]	TiO_2 impregnated kaolinite	Anionic azo dye: Congo red	4-8	Lower the pH, the higher is the removal efficiency
Pelaez[80]	TiO_2	Microcystin-LR	3-8	Lower the pH, the higher is the removal efficiency

Table 2-2: Summary of pH responses of photodegradation rate or efficiency in the selected publications (cont'd)

Publication	Catalyst	Substrate	Tested pH	Result
Yan[10]	CdS	Cationic dye: Malachite green	3-9	High degradation rate occurred with extreme pH; Slowest degradation at pH5
Song[69]	$SrTiO_3/CeO_2$	Anionic azo dye: Direct red 23	2-12	High degradation rate occurred with extreme pH; Slowest degradation at pH6
Chen[83]	TiO_2	Glyphosate	2-12	High degradation rate occurred with extreme pH; Fastest and slowest degradation occurred at pH2 and 6, respectively
Nam[85]	TiO_2 immobilized on silica	Anionic surfactant: Sodium lauryl sulfate	2-8	Highest degradation rate occurred at pH4
Tseng[19]	TiO_2 immobilized on silica	Anionic azo dye: Acid red 1	3-7	Highest degradation rate occurred at pH5

Mahmoodi[84]	TiO_2 immobilized on activated carbon	Cationic azo dye: Basic red 18 and 46	2.5-8	Highest degradation rate occurred at pH5.6 Slightly lower rate occurred at pH8 while much slower degradation was observed at pH2.5
Caliman[77]	TiO_2 (p25)	Cationic dye: Alcian blue 8 GX	4.2-7.4	Optimum pH for the photodegradation is 5.26

2.11. Effect of aeration

Oxidant is important for photodegradation since conduction band electrons need a scavenger to remove and complete the flow of electron. Other steps of the mechanisms may also need oxidant. The most common oxidant reported in the literatures is atmospheric oxygen. For instance, Karunakaran and Zhu reported the effect of dissolved oxygen level on the rate of photodegradation. Karunakaran[9] studied the photodegradation rate of phenol on semiconductors e.g. TiO_2, ZnO, ZnS, CdO, Fe_2O_3, CuO and Nb_2O_5. The dissolved oxygen level was controlled by purging nitrogen or air into the system and the tested dissolved oxygen levels (DO) was 2 and 12.6 mg/l. The reaction rate of experiments with 12.6 mg/l of DO was ranged from 0.4 to 0.8 μM/s. If the DO level of 2 mg/l or below, the reaction was essentially stopped. Zhu[27] reported that the degradation of Methyl Orange induced by the crosslinked chitosan immobilised SnO_2/ZnO . They found out that the photodegradation was a pseudo first order reaction with the reaction rate being doubled when the purging rate was increased from 0 to 100 ml/min. Small increase in photodegradation rate and pseudo first order rate constant occurred when the

purging rate was further increased to 200 ml/min. The authors suggested that bubbling could enhance mass transfer and hence increase degradation.

2.12. Effect of interfering species

In order to simulate the actual industrial application and the possibility to provide some information on the degradation mechanism, research works were reported for the effect of interfering species on the photodegradation catalysis. Common interfering species, such as the presence of anions, usually suppress photodegradation. Various common species present in wastewater, namely Cl^-, Br^-, I^-, NO_3^-, SO_4^{2-}, CO_3^-, silica, PO_4^{3-} and surfactants as well as some rarely found chemical species in wastewater were tested. The researchers suggested that these anions competed with target contaminant for the adsorption sites on semiconductor surface, and acted as scavenger of OH• and positive holes by converting itself into the relatively inactive radicals[4, 27, 68, 69].

Halogen ions

Zhu et al.[4, 27] tested the degradation of both Congo Red (20 mg/l) induced by CdS immobilised in the crosslinked chitosan and Methyl Orange (10 mg/l) induced by SnO_2/ZnO immobilised in the crosslinked chitosan. Halide ions tested were Cl^- and Br^- with the concentration of 10 mM. They found out that the concentration of halide would decrease the pseudo first order constant to half. Song et al.[69] reported the degradation of Direct Red 23 (100 mg/l) induced by $SrTiO_3$, and tested the halide ion for the presence of iodide ions (I^-) with the concentration of 0 to 50 mM. Their results showed that without interfering species, decolorisation could be completed in

60 minutes. The decolorization was reduced to 75 % and 70 % when I^- concentration was 10 mM and 50 mM, respectively.

Sulfate

Zhu et al.[27] also tested the inhibiting effect of SO_4^{2-} which was slightly weaker than that of halide ions. Wang et al.[68] tested the degradation of bisphenol A (5 ppm) induced by $SrTiO_3$ and found that the presence of 5 mM of SO_4^{2-} reduced the apparent degradation rate constant to 68 %.

Carbonate

Wang et al.[68] and Zhu et al.[27] tested the effect of CO_3^- under the above-mentioned condition. Zhu et al. reported that the presence of CO_3^- caused the rate constant decreased to half, similar to the effect of halide ions. Wang et al. showed that the inhibiting effect of CO_3^- was much higher than that of SO_4^{2-}. Systems containing SO_4^{2-} or no interfering species attained the complete removal within 300 minutes while that containing CO_3^- only attained 70 % removal. They suggested that CO_3^- could irreversibly be adsorbed on semiconductor surface by generation of the negatively charged layer. The inhibiting effect on the adsorption of bisphenol A on the catalyst of CO_3^- was also much higher than SO_4^{2-}. The effect of CO_3^- was similar to that of Cl^-, i.e. halved the rate of reaction.

Silica

Wang et al.[68] showed that the inhibiting effect of silica was much higher than that of CO_3^- and SO_4^{2-}. Only 50 % degradation was observed in the same condition. At

low pH, silica was present in the form of neutral molecular acid form. The affinity between the semiconductor surface groups and the neutral specie was low. At high pH and concentration, polymerization of silica occured. The process could associate with the surface hydroxyl groups and silica multilayer could be formed on the surface.

Phosphate

Zhu et al.[27] reported that the inhibiting effect of PO_4^{3-} was higher than that of Cl^-, $SO_4^{2-}$and CO_3^-.

Nitrate

Both inhibiting and enhancing effects were observed for nitrate. Wang[68] and Zhu[27] tested the effect of NO_3^- under the above-mentioned condition and observed the inhibiting effect. Zhu reported that the inhibiting effect of NO_3^- was weaker than the other reported ions. Wang showed that the inhibiting effect of NO_3^- was almost the same as SO_4^{2-}. However, Zhu[4] observed a strong enhancement. Under the above-mentioned condition, 7 fold increase in the rate constant was recorded. They suggested that NO_3^- yielded O• under light. O• reacted with H_2O and formed OH• that speeded up degradation.

Surfactants

Karunakaran[9] reported the photodegradation of phenol on TiO_2, ZnO, ZnS, CdO, Fe_2O_3, CuO and Nb_2O_5 under the interference of anionic micelles as well as cationic micelles such as sodium bis(2-ethylhexyl) sulfosuccinate, sodium lauryl sulfate and

cetyltrimethylammonium bromide (5 mM). No rate suppression was observed. They suggested that the reaction mechanism did not involve species in solution phase.

Oxidant other than Nitrate

Karunakaran investigated the experiments under the interference of H_2O_2, Na_2BO_3, $K_2S_2O_8$, $KBrO_3$, KIO_3 and KIO_4 (5 mM). Generally, 2-4 folds of enhancement were observed. The authors proposed that these oxidants were faster electron scavengers than O_2. This reduced electron-hold combination.

Reducing agents

Karunakaran investigated the experiments under the interference of $NaNO_2$, Na_2SO_3 (5 mM) and ethanol (5 %). The reaction rate was increased slightly for $NaNO_2$ and Na_2SO_3. Ethanol enhanced the rate by a factor of 5. They proposed that reducing agents were positive hole scavengers and could reduce electron-hold combination.

Sacrificial electron donors

Karunakaran also investigated the experiments under the interference of hydroquinone, diphenyl amine and triethyl amine(5 mM). Generally, 2-4 folds of enhancement were observed and they played a similar role as reducing agents.

Studies related to the effects of different types crosslinking and various drying methods on photodegradation characteristics of biopolymers with immobilized photocatalysts composites are still rare. There is no in-depth analysis of the fate of the dye adsorbed onto these composites under different pH although many

researchers studying similar composites reported that high dye removal rate occurred in acidic environment. One of the objectives of this work is to clarify these issues. Moreover, the studies related to the composites with spherical shape are uncommon and this work demonstrated the dye photodegradation of two innovative chitosan-based encapsulation systems in spherical shape.

Chapter 3 Methodology

3.1. Preparation of chitosan encapsulated photocatalysts

3.1.1. Preparation of CdS encapsulated in chitosan flakes

The stock chitosan solution (2 % w/w) was prepared by dissolving the commercial chitosan into 1 % w/w HNO_3 solution which was centrifuged to remove the non-dissolved matters. 100 ml of the stock chitosan solution was mixed with 3.07 g of $Cd(NO_3)_2 \cdot 4H_2O$ solution (62 % w/w), and stirred over 3 hours to ensure that the mixing process was complete. 300 ml of DDI water and 60 ml of 1 M NaOH solution were then added to the above solution mixture in a stepwise manner. Further stirring and sonication allowed the solidification of all chitosan. The liquor was discarded and the remaining chitosan lump was kept and then chopped into smaller pieces. DDI water was subsequently added and the pH of resultant mixture was lowered to 10 by adding 10 % w/w HNO_3 solution under magnetic stirring. The mixture was heated to 60 °C, and 10 ml of the thiourea solution (40 mg/ml) was added dropwisely within 45 minutes. 0.3 M NaOH was added to keep the pH of reaction mixture at 10. After the complete addition of thiourea solution, the solution was then stirred for another 1 hour. The resultant solid was washed with Mill-Q water twice before oven drying and freeze-drying.

3.1.1.1. Drying post treatments

In order to study the effect of drying process on catalyst composite, 2 different drying treatments were attempted independently. Firstly, the catalyst composite was washed with methanol twice and then oven dried at 50 °C, and the product was denoted as OC. Secondly, the catalyst composite was freeze dried, washed with

methanol twice and then oven dried at 50 °C and the product was denoted as FOC. The catalyst composite without freeze drying was much denser than the other one.

3.1.1.2. Crosslinked flakes

In the present study, the effect of crosslink was also investigated by using glutaraldehyde or epichlorohydrin as crosslinking agents. For the preparation of glutaraldehyde crosslinked composites, 1.50 g of composite was stirred in 120 ml of DDI water. 1 ml of 50 % w/w glutaraldehyde was then added the pH of the solution mixture was adjusted to 8.0 by using 0.3 M NaOH. In order to ensure a complete reaction, the mixture was continued to stir overnight. As for the preparation of epichlorohydrin crosslinked composites, 3 g of catalyst composite in 300 ml of DDI water at 50 °C. The solution pH was adjusted to 10.5 by adding 0.3 M NaOH before 1 ml of epichlorohydrin was added with further stirring for another 3 hours. The crosslinked catalyst composites were washed with DDI water for twice and methanol twice and finally dried in oven at 50 °C.

3.1.2. Preparation of CdS encapsulated in chitosan mini-particles

Firstly, 50 g of 2 % w/w chitosan in 1 % w/w HNO_3 solution was mixed with 4 g of cadmium solution containing 0.958 g of $Cd(NO_3)_2 \cdot 4H_2O$ so that the molar ratio between the amino groups and Cd^{2+} was 2:1. The solution was stirred over night. Secondly, 40 ml of 1 M NaOH solution was mixed with 20 ml of methanol in a 100 ml tall beaker. 40 ml of the chitosan solution was added dropwisely into the beaker containing NaOH solution and methanol. Intermittent and gentle stirring was applied for every 6 droplets of chitosan solution. Syringe with a modified 200 µl pipette tip

was used to produce the droplets. After the addition of chitosan solution, the beads were allowed to be hardened in the NaOH solution containing methanol for 30 minutes and then the beads were then collected by a sieve. The beads were transferred into 1 M NaOH solution and allowed to harden overnight. After the overnight hardening, the beads were washed with dilute NaOH solution at pH 10. The beads, 75 ml of the dilute NaOH solution and 22 g of 1 % thiourea solution were added and stirred in 250 ml beaker. The reaction mixture was heated and then kept at 60 °C for 4 hours. The beads started to become yellow in colour after several minutes of heating. Finally, chitosan mini-particles with the encapsulated CdS were collected by the use of sieve.

3.1.3. Preparation of crosslinked chitosan micro-particles with encapsulated CdS

3.1.3.1. Preparation of blank chitosan micro-particles by emulsion techniques

Two emulsions were prepared. The first emulsion solution (1) was prepared by adding 20 g of 3 % chitosan solution dropwise into the oil phase containing 16.6 g mineral oil, 2.25 g span 80 and 0.8 g tween 20 under stirring. 660 µl of glutaraldehyde was then dropped into the system. The system was further stirred for 3 minutes at the speed of 10 and then the speed was then reduced to 4. 4 minutes of extra stirring was applied in order to allow a good distribution of the added glutaraldehyde. The stirring speed was reduced before 6 ml of another emulsion was added. The second emulsion solution (2) was prepared by adding 5 ml of 1 M NaOH dropwisely into oil phase containing 4.15 g of mineral oil and 1 g of span 80 under stirring. All stirrings were conducted with BIBBY CB162 stirrer hot plate and three

3x10 mm stirrer bars. The system was further stirred for 2 minutes and the precipitate was allowed to form overnight. The solid formed was then collected from the liquid phase by centrifuge at 1500 rpm for 5 minutes. The liquid phase was discarded and cyclohexane was added to wash the precipitate. Subsequently, DDI water was applied to wash the precipitate. The gel beads were then collected from the DDI water by using the sieves with mesh size of 500 μm, 250 μm and125 μm and finally stored for further use.

3.1.3.2. Loading Cd^{2+} into chitosan micro-particles via adsorption

69 g of the synthesised beads were mixed with 69 g of cadmium nitrate solution containing 2 % w/w of Cd^{2+}. The system was allowed to stand overnight and the beads were collected by filtration.

3.1.3.3. In situ conversion of Cd^{2+} to CdS

234 ml of 5×10^{-3} $(NH_4)_2S$ solution was added to the beaker containing chitosan micro-particles loaded with Cd^{2+}. Gentle magnetic stirring was applied and the system was kept overnight. Afterwards, the crosslinked chitosan micro-particles encapsulated with CdS were collected by filtration. The filter papers were used to collect the chitosan micro-particles, and the filtrate was yellow in color and subjected to centrifugation.

3.2. Evaluation of photocatalysts: adsorption kinetics of dye removal

3.2.1. Experimental procedure

The adsorption tests were conducted in a 600 ml beaker under magnetic stirring.

Samples taken were analysed by PerkinElmer Lambda 25 spectrophotometer. A pair of matched quartz cuvettes (Hellma® 115F-QS 10.00 mm) was used. A given quantity of catalyst composite was mixed with the given mass of dye solution under gentle stirring. 2 ml sample was taken for each point of time as shown in the relevant figures. UV-visible absorption characteristics of initial and various treated dye solutions were analysed by the spectrophotometer. UV-visible absorption characteristics ranging from 210 to 700 nm of the samples related to MO were recorded. The absorbance at 464 nm was served as a basis for the estimation of MO concentration and quantitative analysis. UV-visible absorption characteristics ranging from 200 to 800 nm of the samples related to AB25 were recorded. The absorbance at 600 nm was served as a basis for the estimation of AB25 concentration and quantitative analysis.

3.2.2. Mathematical modeling of adsorption kinetics

Concentration can be determined by the Beer's Law plot and the data estimated from absorbance at the stated wavelengths were fitted with some kinetic models to find the possible mechanisms of adsorption, if any.

The above adsorption data were analysed with different adsorption kinetic models, the pseudo first order and pseudo second order.

The basic expression of the pseudo first order adsorption kinetics is:

$$\frac{\mathrm{d}Q_\mathrm{t}}{\mathrm{d}t} = k_1(Q_\mathrm{e} - Q_\mathrm{t}) \qquad (3\text{-}1)$$

For linearisation, the integrated form of the above expression was generated:[87]

$$\log\frac{Q_e}{Q_e-Q_t}=\frac{k_1}{2.303}t \quad (3\text{-}2)$$

If the data follow the pseudo first order adsorption kinetics, the log (Q_e-Q_t) against t plot should yield a linear line.

The basic expression of the pseudo second order adsorption kinetics is:

$$\frac{dQ_t}{dt}=k_2(Q_e-Q_t)^2 \quad (3\text{-}3)$$

For linearisation, the integrated form of the above expression was generated:

$$Q_t=\frac{k_2Q_e^2t}{1+k_2Q_et} \quad (3\text{-}4)$$

At least 4 routes for linearisation of the above expression have been proposed. The most popular one is showed below[88].

$$\frac{t}{Q_t}=\frac{1}{k_2Q_e^2}+\frac{t}{Q_e} \quad (3\text{-}5)$$

If the data follow the pseudo second order adsorption kinetics, the t/Q_t against t plot should yield a linear line.

Adsorption capacity can be determined from the concentration of dye (contaminant) solution by the below expression:

$$Q_t = \frac{(C_0 - C_t)M_s}{m} \quad (3\text{-}6)$$

where:

Q_t = adsorption capacity at time t

Q_e = equilibrium adsorption capacity

C_0 = initial contaminant concentration

C_t = contaminant concentration at time t

M_s = mass of solution

m = mass of adsorbent

k_1 = rate constant of the pseudo first order adsorption

k_2 = rate constant of the pseudo second order adsorption

t = time for adsorption

3.3. Evaluation of photocatalysts: photodegradation kinetics of dye removal

3.3.1. Experimental procedure

During the initial stage of study, an improvised photoreactor consisting of a 500 W tungsten halogen projector lamp (Philips brand), a magnetic stirrer plate, an air sparger connected to the central compressed air system, a 2 L reagent bottle filled with deionised water and a TLC glass cylinder was constructed. Air sparger, stirring bar, photocatalyst and dye solution were placed into the TLC cylinder during

reaction. Magnetic stirrer plate provided agitation in the cylinder. 2 L reagent bottle filled with deionised water acted as a lens to focus the light to the cylinder as well as IR blocker to reduce heat reaching the cylinder. Air sparger provided oxygen for the degradation as shown in Figure 3-1.

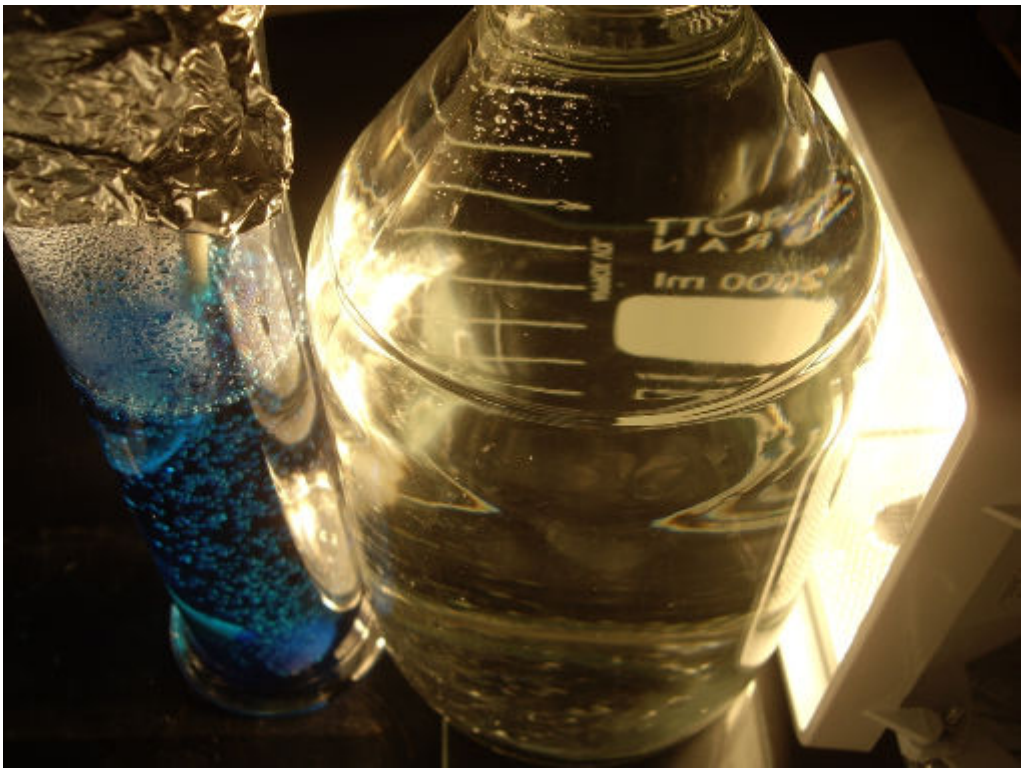

Figure 3-1 Primitive photoreactor during operation

Since excessive reaction time was required for using the improvised photoreactor, a tailor made photoreactor consisting of an immersed lamp tube containing 150 W UV blocked (broadband emission mainly at 400-600 nm with UV leakage < 26 mW) metal halide lamp (OSRAM POWERSTAR HQI-TS 150W/D), and a reaction vessel partially trapped with aluminum foil with an inverted conical bottom welded to a glass tube for air introduction was designed and constructed. The air supply also

functioned as agitation. A plastic jar with ice and water under magnetic stirring was used as a cooling jacket to keep the temperature inside the reactor at 25 °C as shown in Figure 3-2.

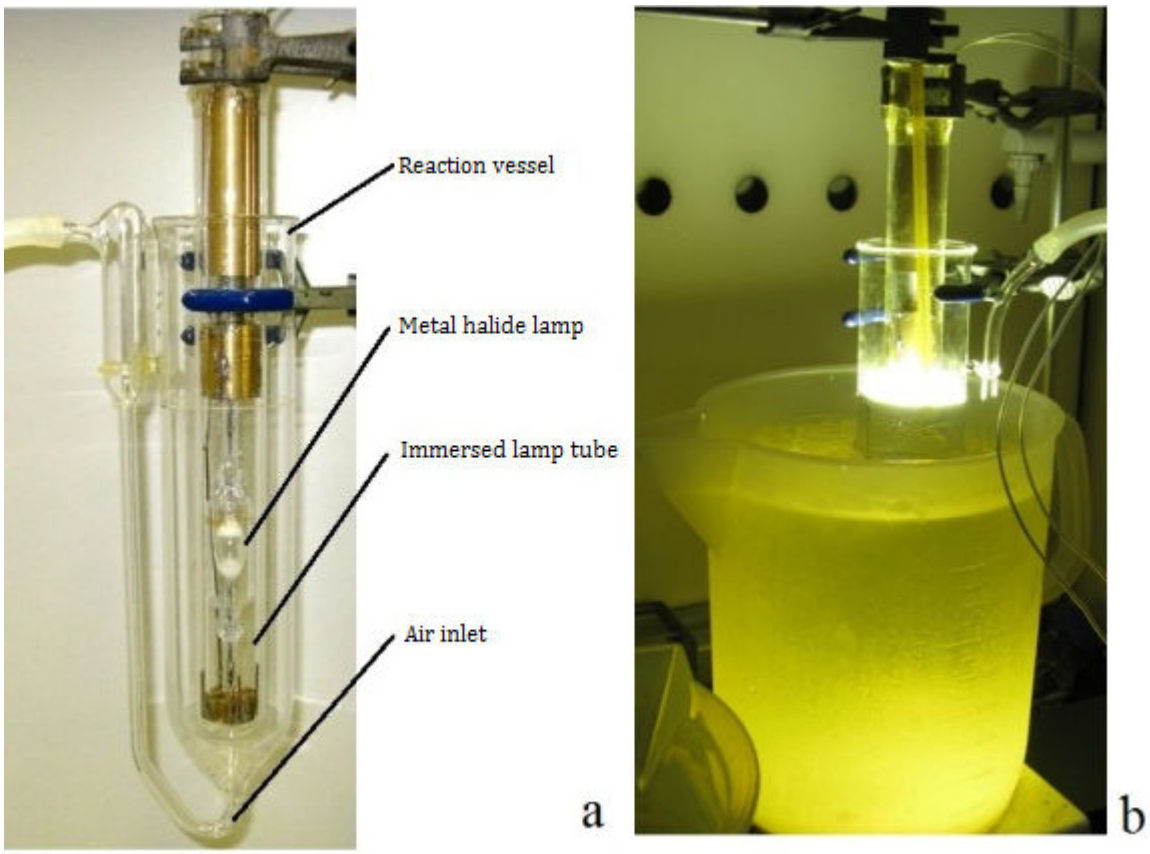

Figure 3-2 The tailor made photoreactor: (a) structure, (b) during operation

Samples taken were analysed by PerkinElmer Lambda 25 spectrometer. A pair of matched quartz cuvettes was used. The detail of analysis of samples was the same as that of the adsorption experiments.

After the 1 hour of adsorption kinetic test, the mixture was transferred to the photoreactor. 1 hour of air purging and agitation in dark were applied before

photodegradation test to allow adsorption equilibrium. Afterwards, illumination commenced with 2 ml of sample being taken for each point of time as shown in the relevant figures.

3.3.2. Mathematical modeling of photodegradation kinetics

The above degradation data were analysed with the two kinetic models as discussed in Section 2.2

3.3.3. Dye desorption test of the used photocatalyst composites

An optional test was developed to investigate the amount of residual dyes that were adsorbed onto the photocatalyst composite after photodegradation experiment. The used photocatalyst composite was rinsed twice with water and then allowed to settle. The rinsed photocatalyst composite was soaked into 40 ml of 0.05 M NaOH. The mixture was agitated in an orbital shaker for 1 week. Final dye concentration was analysed by the UV-visible absorption spectrometry.

3.4. Characterisation of catalyst composites

3.4.1. X-ray diffraction (XRD)

XRD patterns were taken to characterize the crystal structures present inside the samples using a Rigaku SmartLab X-ray diffractometer. Bragg-Brentano focusing mode was used. Measurement was performed with Cu Kα radiation (λ = 1.54 Å) in the range of 2θ = 10-80 °. The scanning speed, tube voltage and anode current were 5 °/min, 45 kV and 200 mA respectively.

3.4.2. Transmission Electron Microscopy (TEM)

The TEM images were obtained by using the JEOL JEM-2100 LaB_6 transmission electron microscope at an acceleration voltage of 200 kV.

3.4.3. Scanning electron microscopy (SEM)

The surface morphology of the photocatalysts was examined by SEM using a JEOL JSM-6490 machine.

3.4.4. Fourier transform infrared spectroscopy (FT-IR)

Infrared spectroscopy (IR) is a powerful tool for characterizing the chemical functional groups present in the samples. In the present work, IR spectra of pure chitosan, OC composite, glutaraldehyde-crosslinked OC and epichlorohydrin-crosslinked OC between 4000 cm^{-1} and 450 cm^{-1} with resolution of 4 cm^{-1}, were recorded. Samples were analysed by the PerkinElmer Spectrum100 FTIR spectrometer. About 1 mg of raw sample and 90 mg of KBr were ground and mixed with mortar and pestle. The mixture was pressed into disc for analysis. It is reported that the glutaraldehyde-crosslinked chitosan would show reduced transmittance at 1562 cm^{-1} [89] while the epichlorohydrin-crosslinked chitosan would show reduced transmittance at 1000-1300 cm^{-1} [17].

3.4.5. Visible reflectance spectroscopy

Band gap of semiconductor can be determined by the UV-VIS Spectroscopy. To calculate the band gap of spectral data, Tauc relation is the tool for that purpose. Optical absorption coefficient or absorbance is required for explicit use of the

relation. However, the catalyst composites are opaque and optical absorbance cannot be measured. Hence, only reflectance can be measured. Mathematical model was established to transform the reflectance data into the form that could be processed by Tauc relation like the absorption coefficient[90].Band gap of certain semiconductor provides useful information on the crystal size as increasing blue shift of absorption edge is observed with decreasing crystal size, which is caused by the quantum confinement effect.

Catalyst composites were analysed by the Konica Minolta CM-3500d spectrophotometer. Since the spectrophotometer was top-port thus, the catalyst composites were placed in the Petri Dish of the spectrophotometer tool kit during analysis. Measuring aperture mask with 3 mm diameter was used. The reflectance spectra between 400 nm and 700 nm were measured.

For a direct band gap material, the relation between the optical absorption coefficient, wavelength of light and band gap (E_g) was:

$$\alpha h\nu = A(h\nu - E_g)^{1/2} \quad (3\text{-}7)$$

where α = absorption coefficient, hν = light energy, A is a constant different for various transitions, E_g = band gap of material[90]. The plot of $(\alpha h\nu)^2$ vs hν yields a line. The X axis intercept of extrapolation of the straight line gives the hν, i.e. the energy, of band gap because $h\nu = E_g$ when $\alpha h\nu = 0$. That is the Tauc plot.

For opaque materials, it is difficult to measure the absorption coefficient and so mathematical model is established to utilize the reflectance data.

The established mathematical model that showed the below plot also gave E_g like the previously mentioned plot[90, 91].

$$\{h\nu\ln[(R_{max}-R_{min})/(R-R_{min})]\}^2 \text{ vs } h\nu \quad (3\text{-}8)$$

where R_{max} and R_{min} are maximum and minimum values of reflectance, and R is the reflectance at a given photon energy $h\nu$.

Chapter 4 Results and discussion

4.1. Adsorption and photodegradation of dyes

UV-visible absorption spectra of samples taken throughout the adsorption and photodegradation experiments may provide some information on the structural changes of dyes during experiments. Figure 4-1 depicts the change of UV-visible absorption spectra throughout adsorption including the air purging and photodegradation experiment carried out with 10 mg/kg of Methyl Orange (MO).

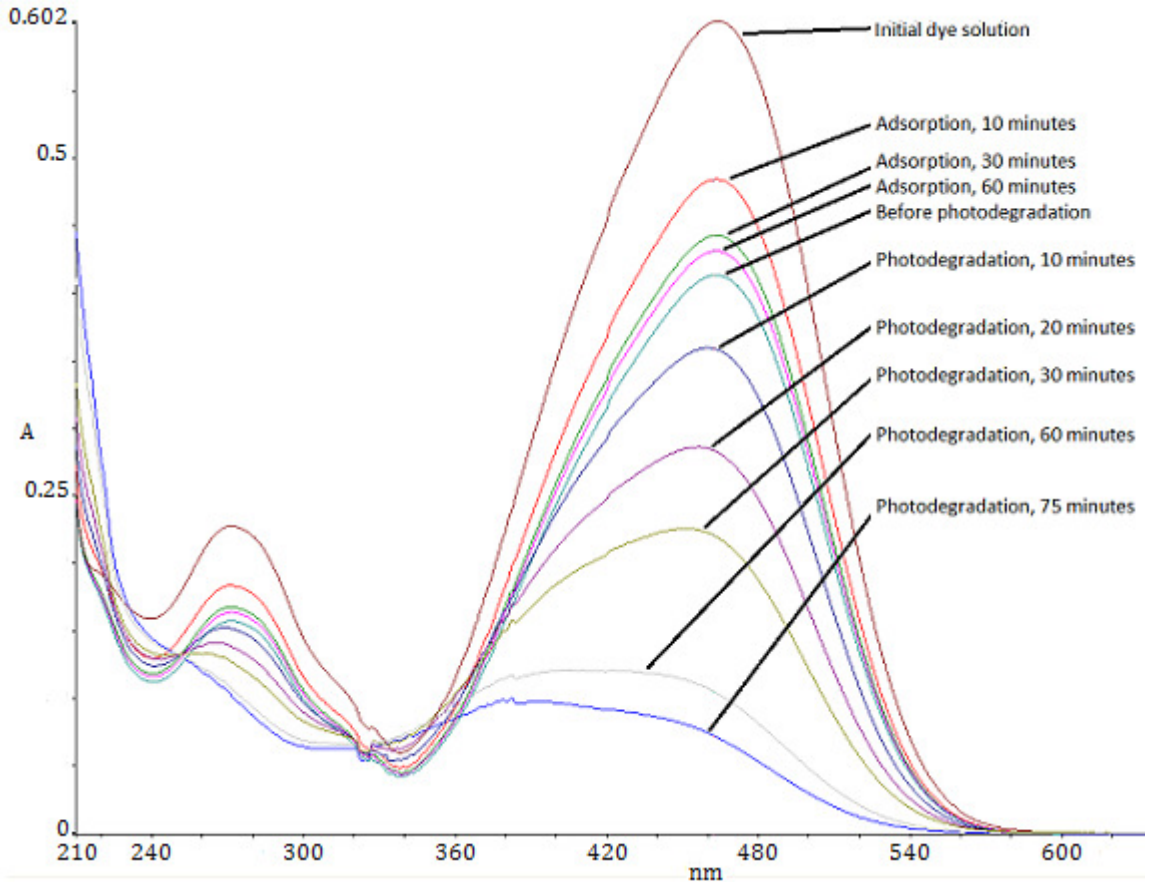

Figure 4-1 UV-visible spectra of samples taken during the experiment for the non-crosslinked OC composite with initial dye solution mass of MO = 0.28 kg, catalyst composite dosage = 0.3 g, Initial dye concentration = 10 mg/kg and initial pH not adjusted.

The characteristic of UV-visible absorption spectrum of MO solution is the two peaks. The main peak with the maximum located at 464 nm that demonstrates the colour arisen from the whole chromophore with an azo group. Another peak in the UV region with the maximum located at 271 nm is arisen from the 'benzene rings' structures of MO molecules. During adsorption and air purging, the absorbances and concentrations determined from the absorbances of the two peaks decreased with the same relative rate. After the 1 hour of adsorption, MO concentration reduced to 72 % of the original value. Obviously, the adsorption kinetics determined from both peaks were also fitted with the pseudo second order rate law with almost the same rate constants as shown in Table 4-1. During the 1 hour of air purging, another 3 % of dye adsorption was observed.

In photodegradation, the absorbances and concentrations determined from the absorbances of the two peaks no longer decreased with the same relative rate as shown in Table 4-2. The kinetic models of photodegradation were also different for the concentration data evaluated from various abscissas. At 464 nm, the results followed the commonly reported pseudo first order kinetics. At 271 nm, the pseudo second order kinetics was observed. After 1.25 hours of photodegradation, MO concentration reduced to 1.06 mg/kg as calculated from the absorbance at 464 nm. The corresponding value of concentration calculated from the absorbance at 271 nm was 4.50 mg/kg. This implied that the catalytic photodegradation process was more efficient to breaking the azo bond than the aromatic rings.

Apart from the decreasing absorbance, the peaks also shifted during photodegradation process. The peak originally located at 464 nm seemed to shift towards 380 nm throughout the degradation. Furthermore, the peak originally located at 271 nm seemed to shift towards a lower wavelength and eventually merged with the strong absorption edge located at the wavelength of less than 240 nm which grew gradually throughout the degradation. The shift of peak originally within the visible region would be caused by the periphery group modifications[57] while the shift of peak originally located at 271 nm would be caused by both destruction of the aromatic rings and overlapping with the growing absorption edge located at the wavelength of less than 240 nm. The growing absorption edge was likely to be caused by simple fragments resulted from photodegradation. The photodegradation of experiment carried out with 5 mg/kg MO dye solution showed a more complete degradation with no peak being observed after the 1.25 hour of reaction. It still exhibited (1) a weak absorption that gradually increased from 0 A to 0.04 A for the range of 540 nm to 300 nm, (2) a shoulder at around 250 nm and again (3) a relatively strong absorption edge located at the wavelength of less than 240 nm as shown in Figure 4-2.

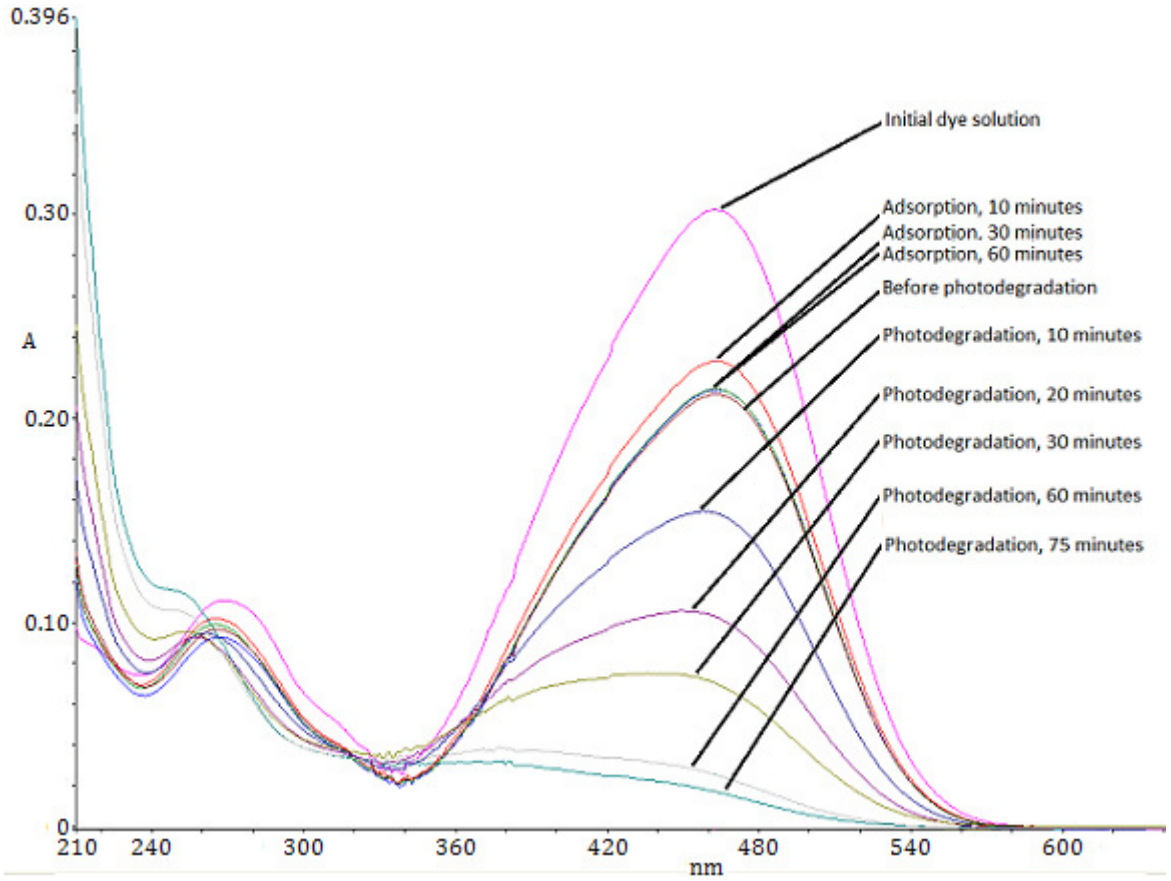

Figure 4-2 UV-visible spectra of samples taken during the experiment for the non-crosslinked OC composite with initial dye solution mass of MO = 0.28 kg, catalyst composite dosage = 0.3 g and initial dye concentration = 5 mg/kg, Initial pH not adjusted.

Figure 4-3 depicts the UV-visible absorption spectrum changing throughout adsorption including air purging and photodegradation experiment which were carried out with 30 mg/kg Acid Blue 25 (AB25). It was noticed that pH adjustments were done before adsorption and air purging by adding NaOH(aq). There were 3 characteristic spectroscopic absorption peaks for AB25 solution. The main peak with the maximum λ located at 600 nm demonstrated that colour was arisen from the whole chromophore. The other 2 peaks located at 256 and 230 nm in the UV region

should be arisen from aromatic rings or other fragments of AB25 molecules.

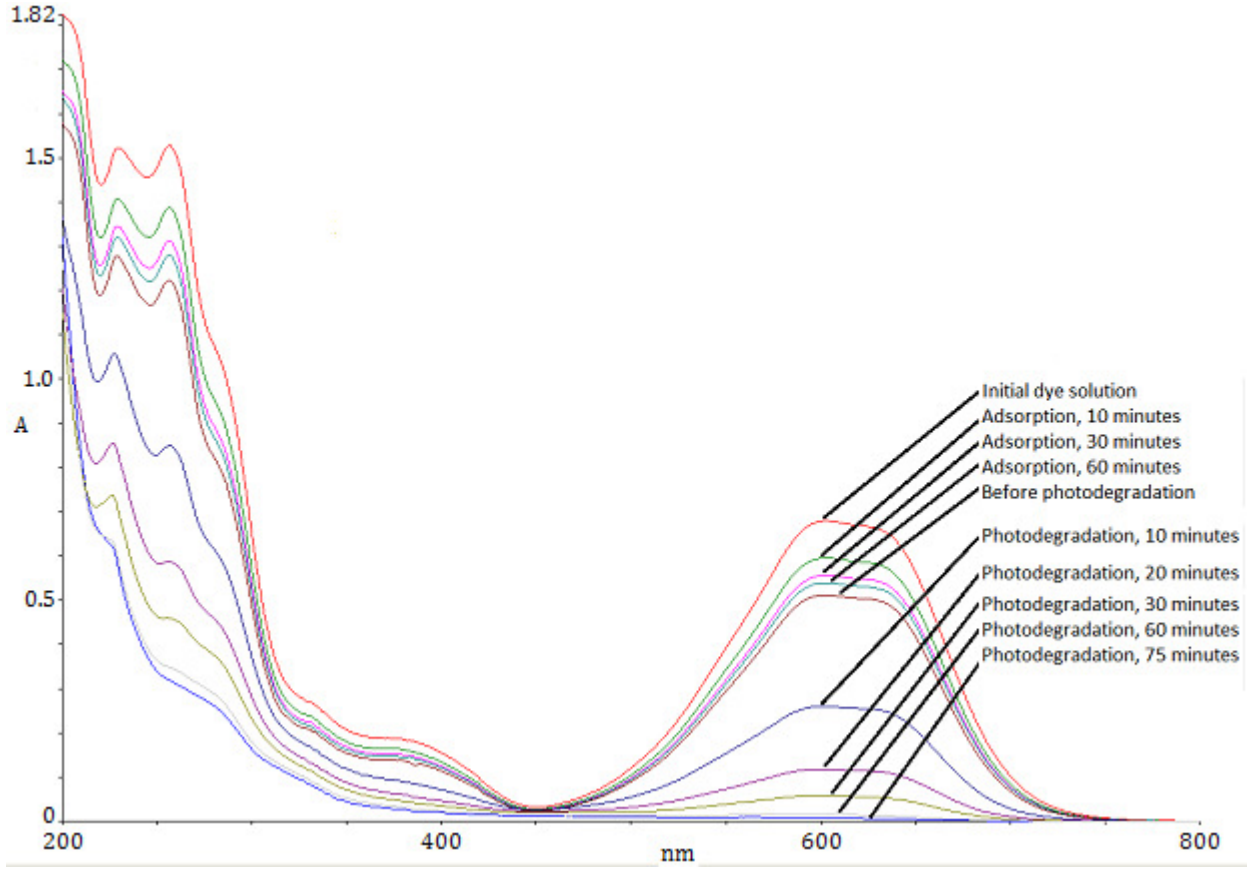

Figure 4-3 UV-visible spectra of samples taken during the experiment for the non-crosslinked OC composite with initial dye solution mass of AB25 = 0.28 kg, catalyst composite dosage = 0.3 g, Initial dye concentration = 30 mg/kg, Initial pH not adjusted.

During adsorption and air purging, the spectroscopic absorption indicated by three peaks decreased with almost the same relative rate. After the 1 hour of adsorption, the AB25 concentration reduced to 80 % of the original value. Obviously, the adsorption kinetic data determined from all three peaks fitted the pseudo second order rate law well as shown in Table 4-1.

The 3 spectroscopic peak absorbances no longer decreased with the same relative rate in photodegradation as shown in Table 4-2. After the 1.25 hour of

photodegradation, the AB25 concentration reduced to 0.33 mg/kg as calculated from the absorbance at 600 nm. The corresponding values of concentrations calculated from the absorbances at 256 and 230 nm are 5.15 and 9.62 mg/kg respectively. After 45 minutes of photodegradation, the absorbances of wavelengths less than 220 nm increased slightly from its minimum under further illumination. Moreover, the peak originally located at 230 nm shifted slightly just like the 271 nm peak in the MO photodegradation.

To conclude, the catalytic photodegradation process was more efficient in breaking part of the chromophore than the aromatic rings. During the course of photodegradation, accumulation of simple fragments that absorbed UV with shorter wavelength occurred. The system with MO or AB25 and without photocatalyst showed no photolysis after 75 minutes of illumination well as shown in Figure 4-4.

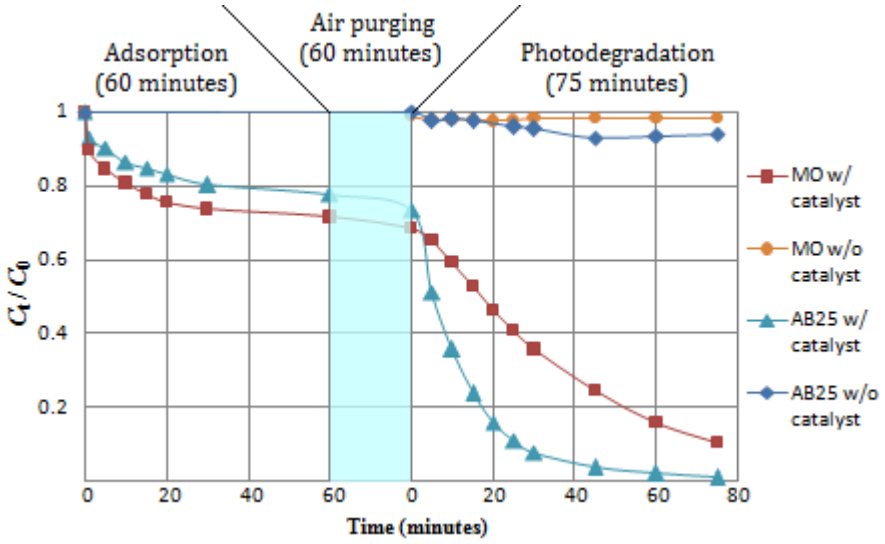

Figure 4-4 MO and AB25 adsorption - photodegradation curves, with and without catalyst. MO as well as AB denote Methyl Orange and Acid Blue 25 respectively. OC composite with various states of crosslinking, Initial dye solution mass = 0.28 kg, Initial dye concentration of MO = 10 mg/kg and AB25 = 30 mg/kg, Dosage of catalyst composite = 0.3 g, and initial pH not adjusted

Table 4-1 Kinetic models of adsorption and rate constants determined from the UV-Visible absorbance at various wavelengths of the experiments

Experiment	Wavelength (nm)	Adsorption model	Rate constant (g/mg min)	Q_e (mg/g)	R^2 of linearised plot
MO (C_0=10 mg/kg)	464	Pseudo second order	0.11±0.05	2.8±0.1	0.9987
MO (C_0=10 mg/kg)	271		0.09±0.02	2.81±0.08	0.9993
AB25	600		0.0155±0.0008	6.3±0.9	0.9937
AB25	256		0.016±0.001	5.7±0.9	0.9922
AB25	230		0.021±0.002	4.6±0.7	0.9921

Table 4-2 Kinetic models of photodegradation and rate constants determined from the UV-Visible absorbance at various wavelengths of the experiments

Experiment	Wavelength (nm)	Photodegradation kinetic model	Rate constant	R^2 of linearised plot
MO (C_0=10 mg/kg)	464	Pseudo first order	0.028±0.002 (min^{-1})	0.9982
MO (C_0=10 mg/kg)	271	Pseudo second order	0.00118±0.00004 (kg/mg min)	0.9902
AB25	600	Pseudo first order	0.062±0.007 (min^{-1})	0.9935
AB25	256	Pseudo second order	0.0025±0.0003 (kg/mg min)	0.9907
AB25	230	Pseudo second order	0.0012±0.0001 (kg/mg min)	0.9892

To conclude, the catalyst was able to degrade Methyl Orange and Acid Blue 25. The UV-visible absorption spectra of treated dye solutions indicated the destruction of chromophore and aromatic rings. The catalytic photodegradation process was more efficient in breaking part of the chromophore than the aromatic rings of dye. All the adsorption experiments followed the pseudo second order adsorption kinetics. For those data determined from the main UV/visible absorption peaks that demonstrated the colour of both dyes, the kinetic model for photodegradation was the pseudo first order kinetics. Nevertheless, the kinetic models for photodegradation could be different for the concentration data evaluated from other abscissas.

4.2. Effect of crosslinking on dye removal

Apart from using the original chitosan as catalyst carrier, researchers reported the use

of the crosslinked chitosan. Crosslinking could improve both mechanical strength and heat resistance[27]. In addition, the crosslinked chitosan will not dissolve at low pH. This property of the crosslinked chitosan allows the removal of pollutant in acidic solutions. Usually, crosslinking reactions are aimed at the amino or hydroxyl groups of chitosan. Two crosslinking agents namely glutaraldehyde[4, 27, 29, 56] and epichlorohydrin[17, 28] were frequently reported. Epichlorohydrin crosslinks the hydroxyl groups while glutaraldehyde crosslinks the amino groups. Nevertheless, the researchers reported the preparation of crosslinked chitosan; however, the effect of crosslinking was rarely mentioned. Hence, the effect of crosslinking on dye removal was analysed in this work by comparing adsorption – photodegradation characteristics of the non-crosslinked, glutaraldehyde crosslinked and epichlorohydrin crosslinked catalyst composites. The experiments were carried out with OC composites. It was found that crosslinking by glutaraldehyde caused the remarkable effects on both the dye adsorption and photodegradation while crosslinking by epichlorohydrin caused little or no effect as shown in Figure 4-5.

The results clearly showed that crosslinking by epichlorohydrin did not cause a significant change on both adsorption and photodegradation characteristics for both MO and AB25. However, the same was not true for glutaraldehyde. Glutaraldehyde crosslinking remarkably enhanced the adsorption rate and capacity. This implied that the amino groups present on chitosan were responsible for dye adsorption and converting it into Schiff base which enhanced the adsorption process. The target group used for adsorption should be sulfonic groups present on dye molecules. Schiff base was more attractive than the original amino groups used for these dye

molecules. From the UV-visible absorption measurement, it was interesting to observe that some adsorbed dye molecules were desorbed at the initial period of illumination. This phenomenon was believed to be a photodesorption of dye.

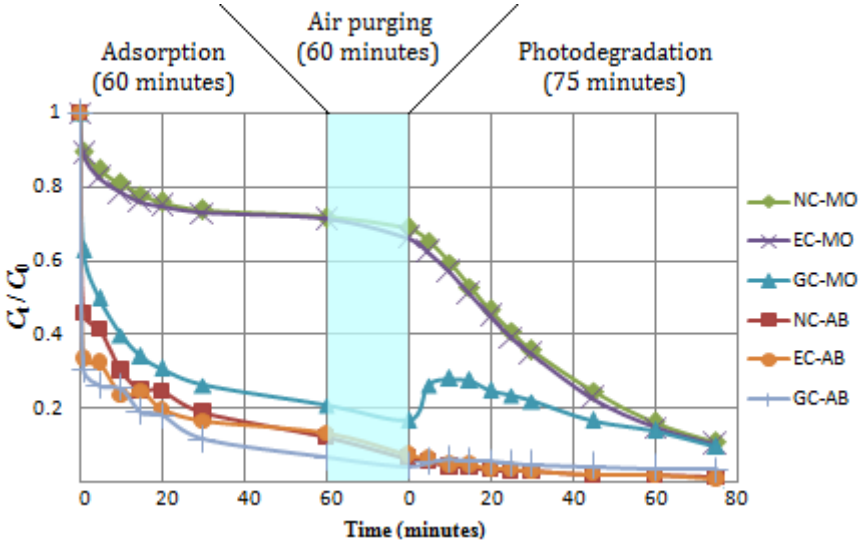

Figure 4-5 MO and AB25 adsorption - photodegradation curves where NC, EC and GC denote the non-crosslinked, epichlorohydrin-crosslinked and glutaraldehyde-crosslinked respectively. MO as well as AB denote Methyl Orange and Acid Blue 25 respectively. OC composite with various states of crosslinking, Initial dye solution mass = 0.28 kg, Initial dye concentration of MO = 10 mg/kg and AB25 = 30 mg/kg, Dosage of catalyst composite = 0.3 g, and initial pH not adjusted

Photodesorption was well studied for the cases where small adsorbate molecules and inorganic material adsorbents were involved[92]. Photodesorption involving large organic adsorbates and inorganic material adsorbents had been reported recently[92-96]. The reported photodesorption involving large organic adsorbates and biosorbents was not found. Another interesting observation was that similar desorption had also been found when pure chitosan with the adsorbed MO was illuminated. The final removal of AB25 removal by the glutaraldehyde-crosslinked

composite was relatively inferior to the non-crosslinked or epichlorohydrin crosslinked composite. Increased light absorption caused by the adsorbed dye molecules as well as the reduced semiconductor excitation could be the cause.

The results were analysed with the presented adsorption and photodegradation kinetic models. The determined order of reactions as well as the rate constants of adsorption and photodegradation were tabulated. The determined kinetic model of adsorption followed the very common pseudo second order kinetics as shown in Table 4-3.

Table 4-3 Determined kinetic models of adsorption and rate constants of various experiments. NC, EC and GC denote the non-crosslinked, epichlorohydrin-crosslinked and glutaraldehyde-crosslinked respectively. MO as well as AB denote Methyl Orange and Acid Blue 25 respectively.

Experiment	Adsorption model	Rate constant (g/mg min)	Q_e (mg/g)	R^2 of linearised plot
NC-MO	Pseudo second order	0.11±0.05	2.8±0.1	0.9987
EC- MO		0.07±0.02	3.0±0.1	0.9990
GC-MO		0.030±0.002	7.90±0.05	0.9993
NC-AB		$0.010733\pm8\times10^{-6}$	25.90±0.03	0.9982
EC-AB		0.0211±0.0007	25.3±0. 3	0.9987
GC-AB		0.0254±0.007	26.3±0. 4	0.9983

This meant that the rate determining steps of the adsorption of these experiments was chemical adsorption[97]. For the determined kinetic models of photodegradation as shown in Table 4-4, almost all the experiments associated with MO followed the pseudo first order kinetics except the experiment with the glutaraldehyde-crosslinked composite. For the glutaraldehyde-crosslinked composite, the experiment showed a

small change in MO concentration during photodegradation. The curved nature of non-zero-order degradation profile was so difficult to be observed for the situation due to the fact that there was only a small change in dye concentration and the experimental data quite fit with the zero-order kinetic equation. Unlike MO, all the experiments involving AB25 followed the second order kinetics.

Table 4-4: Determined kinetic models of photodegradation and rate constants of various experiments. NC, EC and GC denote non-crosslinked, epichlorohydrin-crosslinked and glutaraldehyde-crosslinked respectively. MO as well as AB denote Methyl Orange and Acid Blue 25 respectively.

Experiment	Photodegradation kinetic model	Rate constant	R^2 of linearised plot	Time interval complied with the rate law (minutes)
NC-MO	Pseudo first order	0.028±0.002 (min^{-1})	0.9982	5-75
EC- MO	Pseudo first order	0.026±0.001 (min^{-1})	0.9982	5-75
GC-MO	Pseudo zero order	0.029±0.001 (mg/kg min)	0.9941	20-75
NC-AB	Pseudo second	0.020±0.003 (kg/mg min)	0.9882	0-60
EC-AB	Pseudo second	0.0241±0.0007 (kg/mg min)	0.9781	0-60
GC-AB	Pseudo second	0.0072±0.0008 (kg/mg min)	0.9666	25-75

Epichlorohydrin crosslinking caused almost no change in dye removal characteristics. Glutaraldehyde crosslinking chitosan-loaded catalyst enhanced adsorption but not photodegradation. The adsorption kinetic model followed the pseudo second order.

For the MO photodegradation, the most common rate law of photodegradation was the pseudo first order kinetics. Unlike MO, the degradation profiles of AB25 followed the pseudo second order kinetics.

4.3. Effect of catalyst dosage on dye removal

The dosage of photocatalyst determines the rate of photodegradation and also the rate constant of photodegradation. . The experiments were carried out with three dosages of OC composite, and the adsorption and photodegradation characteristics were analysed.

The results showed that both the adsorption and photodegradation of dye increased with respect to the dosage of photocatalyst as shown in Figure 4-6.

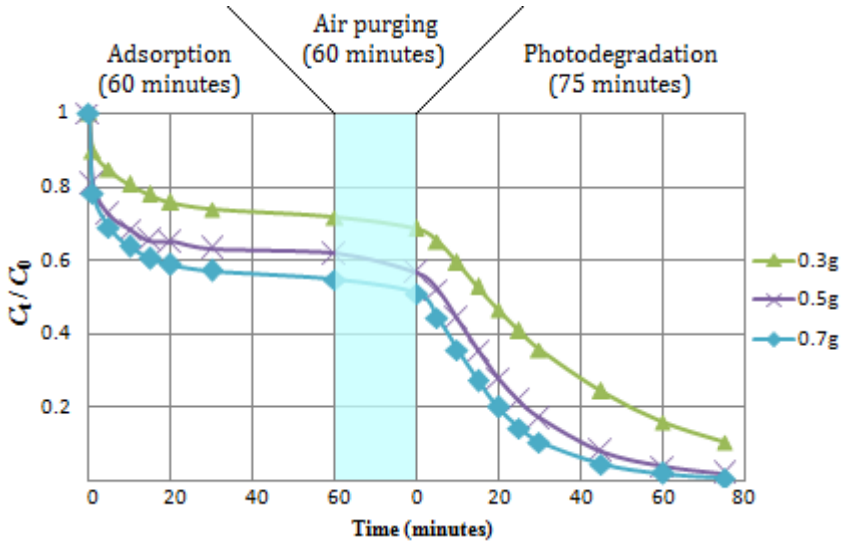

Figure 4-6 MO adsorption - photodegradation curves. OC composite, Non-crosslinked, Initial dye solution mass = 0.28 kg, Initial dye concentration = 10 mg/kg, Initial pH not adjusted

More obvious enhancement was observed on the photodegradation rate when

compared with adsorption. The three test dosages showed that the enhancements in the adsorption capacity and reaction rate of photodegradation were more remarkable when increasing the dosage from 0.3 g to 0.5 g rather than increasing the dosage from 0.5 g to 0.7 g. Diminishing the productive effect of increasing dosage on photodegradation when the dosage of catalyst had reached a certain level was reported by other researchers[10, 29, 69, 71]. They proposed that increasing the dosage could increase (1) the availability of active sites, (2) number of adsorbed dye molecules, and (3) illuminated area of semiconductor. Hence, the rate of photodegradation increased with dosage until a maximum level was reached. At higher dosage, the penetration of light could also be reduced by absorption, scattering and screening by catalyst itself.

The determined order of reactions and rate constants of adsorption and photodegradation were tabulated. The mostly fit kinetic model of adsorption was the common pseudo second order kinetics for the above tests as shown in Table 4-5.

Table 4-5 Determined kinetic models of adsorption and rate constants of experiments with various dosages

Dosage (g)	Adsorption model	Rate constant (g/mg min)	Q_e (mg/g)	R^2 of linearised plot
0.30	Pseudo second order	0.11±0.05	2.8±0.1	0.9987
0.50		0.19±0.03	2.3±0.1	0.9990
0.70		0.22±0.01	1.92±0.06	0.9992

For the determined kinetic models of photodegradation shown in Table 4-6, all the above experimental data followed the pseudo first order kinetics. Furthermore, the rate constant data showed that the enhancement in photodegradation by increasing

the dosage tapered off at higher dosages. The K_{1p} ratio between the experiments using 0.5 g of OC and that using 0.3 g of OC ($K_{1p\ 0.5}$/ $K_{1p\ 0.3}$) was higher than the actual weight ratio (0.5/0.3), and the same was no longer true for the ratios between the experiments using 0.7 g and 0.5 g.

Table 4-6: Determined kinetic models of photodegradation and rate constants of experiments with various dosages

Dosage (g)	Photodegradation kinetic model	Rate constant (min^{-1})	R^2 of linearised plot	Time interval complied with the rate law (minutes)
0.30	Pseudo first order	0.028±0.002	0.9982	5-75
0.50		0.0472±0.0003	0.9989	5-75
0.70		0.060±0.001	0.9992	5-75

Both the adsorption and photodegradation of dye increased with the dosage of photocatalyst. Effect of dosage on the rate of photodegradation was more significant when compared with adsorption. For higher dosages, the benefit of increasing dosage diminished.

4.4. Effect of initial pH on dye removal

Generally, the reviewed publications[4, 29] suggested that the pH significantly affected the performance of this class of catalysts. Usually, the lower the pH, the higher the removal efficiency would be. The dye removal performances of epichlorohydrin-crosslinked OC catalyst composite at initial pH = 4, 6, 8 and 10 were analysed. Both MO and AB25 dyes were tested. pH adjustments were done by using NaOH(aq) and HNO_3(aq) as shown in Figure 4-7.

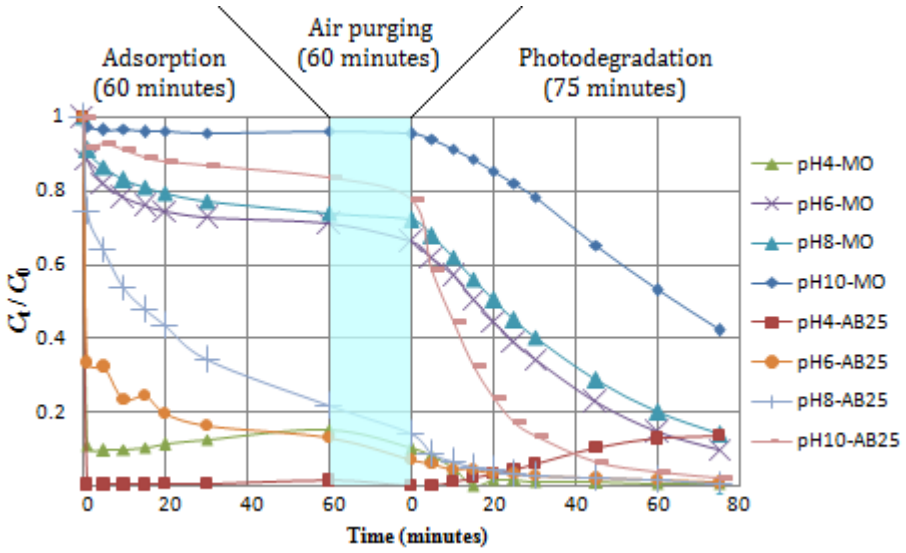

Figure 4-7 MO and AB25 adsorption - photodegradation curves. OC composite, Epichlorohydrin-crosslinked, Initial dye solution mass = 0.28 kg, Initial dye concentration = 10 mg/kg (MO) and = 30 mg/kg (AB25), Dosage of catalyst composite = 0.3 g

The results showed that rates and capacities of adsorption of both the MO and AB25 dyes were higher when the pH was low. MO adsorption at pH10 was almost completely quenched and AB25 adsorption at pH10 was largely suppressed. Photodegradation of MO was observed for all the tested pH values. The MO adsorption at pH4 was very high and the photodegradation at this pH was masked and hardly observed while 99 % removal of colour finally occurred. At the other pH values, photodegradation curves at various initial concentrations showed the dye degradation of 5-6 mg/kg in 75 minutes of illumination. At pH 6 and 8, photodegradation removal of over 80 % in 75 minutes of illumination except pH10 with photodegradation removal of over 50 % only. Photodegradation of AB25 was observed for all tested pH values except pH4. Photodesorption was observed at pH4

instead of the desirable photodegradation, and the final dye concentration was much higher than that of the experiments carried out at all other tested pH values. At pH4 only 86 % of colour was removed after the illumination while at pH6, pH8 and pH10 the removal of colour was more than 98 %. The AB25 adsorption was very high and the photodegradation was largely masked for the tested pH values other than 10. At pH10, the adsorption was weak and the starting concentration for the photodegradation was high. However, almost the complete removal of dye also occurred. At lower pH, a considerable amount of residual dye was adsorbed onto the photocatalyst composite after photodegradation. Hence, dye desorption test was carried out to investigate the actual pH dependency of dye degradation. Figure 4-8 depicts the percentage of total residual dye with respect to the initial amount of dye after photodegradation at various pH. By considering both the amount of latent dye desorbed as shown in Table 4-7 as well as dye concentration after photodegradation experiments, MO degradation was very efficient at pH4 while that of AB25 very most efficient at pH10. Low pH strongly enhances adsorption of the dye but not necessary the photodegradation as most efficient AB25 degradation observed at pH10 while at this pH, adsorption is largely suppressed. On the contrary, commonly reported that enhanced adsorption which occurs at low pH could also increase the photodegradation of the dye[4, 14, 21, 29, 82]. The reason may be due to the high localized dye concentration could block the light and the excitation of catalyst is precluded[19, 77].

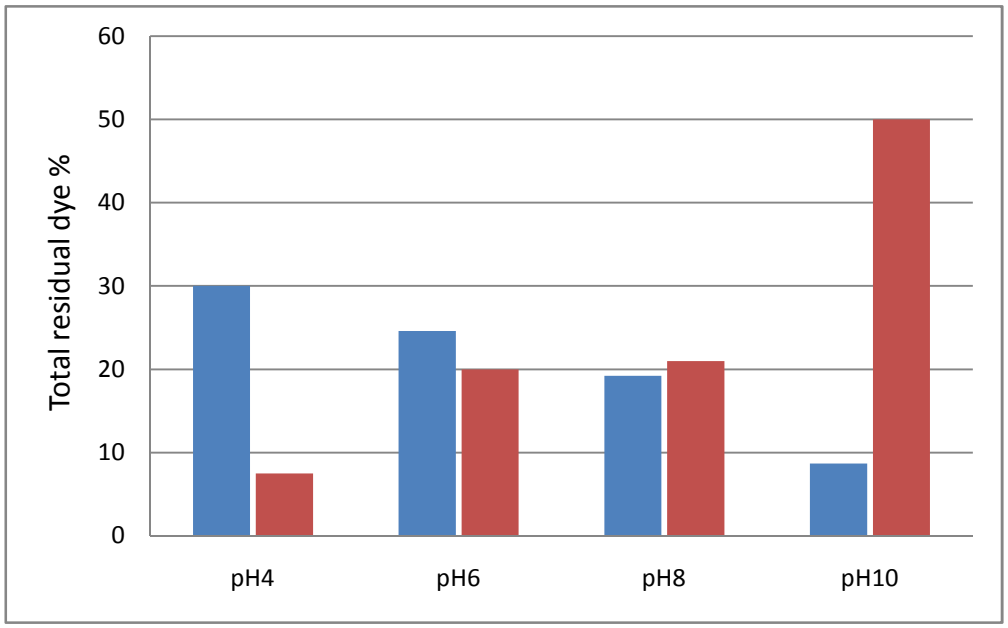

Figure 4-8 Percentage of total residual dye after photodegradation at various pH
Blue: Acid Blue 25, Red: Methyl Orange

Table 4-7: Final dye concentrations of desorption solutions, residual dye concentrations of reaction mixtures and total residual dye of different experiments at various initial pH

Dye	pH	Desorbed dye concentration (mg/kg) in desorption solution (40 ml)	Residual dye concentration (mg/kg) of reaction mixture (~240 ml)	Estimated total residual dye (mg)*
MO	4	5.1±0.2	0.03±0.03	0.21±0.02
	6	7.3±0.2	1.07±0.06	0.55±0.02
	8	6.2±0.5	1.45±0.04	0.60±0.03
	10	7.1±0.6	4.6±0.4	1.4±0.1
AB25	4	51±2	2±2	2.5±0.6
	6	50±1	0.276±0.009	2.07±0.04
	8	38.7±0.8	0.251±0.006	1.61±0.03
	10	15.2±0.5	0.5±0.2	0.728±0.07

* Residual dye content in both desorption solution and resultant reaction solution

For the determined kinetic models of adsorption as shown in Table 4-8, most of them

followed the very common pseudo second order kinetics. This meant that the rate determining steps of the adsorption of these experiments were chemical adsorption.

Table 4-8 Determined kinetic models of adsorption and rate constants of various experiments at different pH

Experiment	Adsorption model	Rate constant (g/mg min)	Q_e (mg/g)	R^2 of linearised plot
MO – pH4	Too fast to be calculated			
MO – pH6	Pseudo second order	0.07±0.02	3.0±0.1	0.9990
MO – pH8		0.049±0.002	2.61±0.07	0.9964
MO – pH10		1.3±0.2	0.38±0.02	0.9947
AB25 – pH4	Too fast to be calculated			
AB25 – pH6	Pseudo second order	0.0211±0.0007	25.3±0. 3	0.9987
AB25 – pH8		0.0042±0.0001	25.04±0.04	0.9932
AB25 – pH10		0.0155±0.0008	6.3±0.9	0.9937

For the determined kinetic models of photodegradation as shown in Table 4-9, the experiments used for testing MO at pH6 and pH8 followed the common first order kinetics while the experiments used for testing MO at pH10 was the pseudo zero order kinetics. The photodegradation of AB25 at pH6 and 8 followed the pseudo second order kinetics. At pH10, the common pseudo first order kinetics were shown. It was interesting to observe that desorption might occur for AB25 at pH4. Rauf et al. reported the photodegradation that had a high fitness with the pseudo second order kinetics[73] and suggested that it was due to the formation of dimmers by the dye at high concentration. AB25 adsorption onto the composite was very strong at all tested pH except pH10. In addition, high local concentration caused by high adsorption

might promote dimer formation.

Table 4-9 Determined kinetic models of photodegradation and rate constants of various experiments at different pH

Experiment	Photodegradation kinetic model	Rate constant	R^2 of linearised plot	Time interval complied with the rate law (minutes)
MO – pH4	Concentration too low to be calculated			
MO – pH6	Pseudo first order	0.026±0.001 (min^{-1})	0.9982	5-75
MO – pH8	Pseudo first order	0.0222±0.0004 (min^{-1})	0.9993	5-75
MO – pH10	Pseudo zero order	0.071±0.005 (mg/kg min)	0.9923	5-75
AB25 – pH4	Desorption			
AB25 – pH6	Pseudo second order	0.0241±0.0007 (kg/mg min)	0.9781	0-60
AB25 – pH8	Pseudo second order	0.039±0.009 (kg/mg min)	0.9976	0-30
AB25 – pH10	Pseudo first order	0.062±0.007 (min^{-1})	0.9935	0-45

Adsorption was enhanced at low pH for both dyes, particalarly within the tested range of pH. Reduced adsorption was also observed in alkaline condition. Low pH assisted photodegradation of MO but not AB25. Desorption was observed for AB25 at pH4. High pH facilitated photodegradation of AB25 and suppressed that of MO. Low pH strongly enhanced adsorption of the selected dyes but not necessary the photodegradation as most efficient AB25 degradation observed at pH that largely

suppressed adsorption despite the common belief that the adsorption could enhance photodegradation.

4.5. Effect of initial dye concentration on dye removal

In order to evaluate the effect of dye concentration on dye removal by the catalyst composite, some experiments were carried out with different concentrations varying from 5 to 20 mg/kg. Both the adsorption and photodegradation processes were found to be dye concentration dependent. The experiments were carried out with OC type composite. The adsorption capacity and rate increased with dye concentration. The dye removal by adsorption in the first hour of experiments with 5, 10 and 20 mg/kg of initial dye concentrations were 1.5 mg/kg, 2.8 mg/kg and 5 mg/kg respectively.

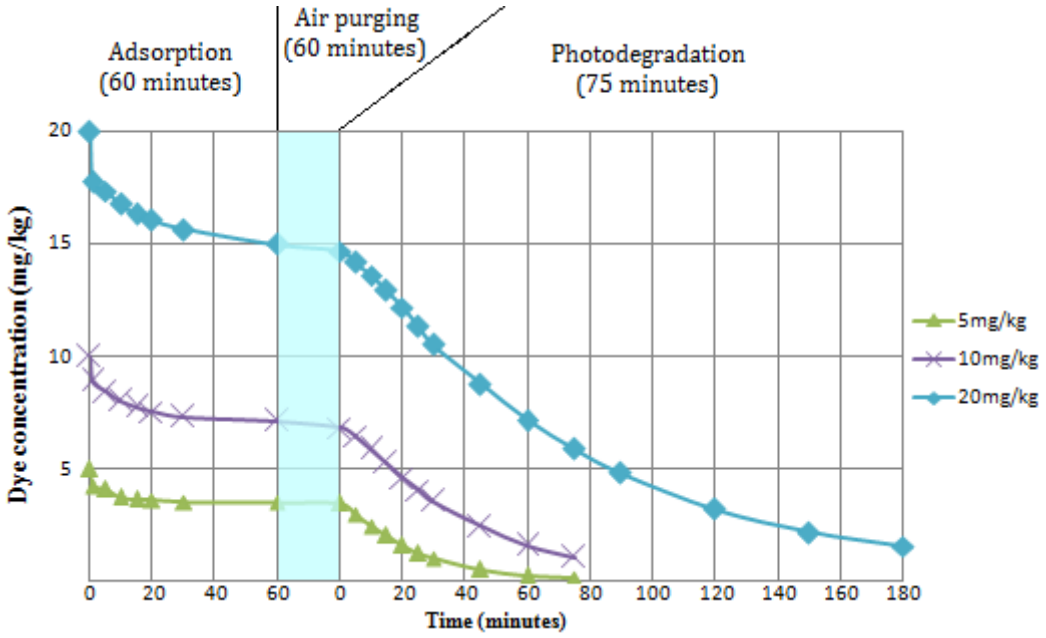

Figure 4-9 MO adsorption - photodegradation curves. OC composite, Non-crosslinked, Initial dye solution mass = 0.28 kg, catalyst composite dosage = 0.3 g, Initial pH not adjusted

As for photodegradation, it seemed that the higher the initial dye concentration, the lower the dye removal efficiency would be. By reducing the dye concentration from 3.4 to 1.5 mg/kg as shown in Figure 4-9, the experiments with 5, 10 and 20 mg/kg initial dye concentrations required 22 minutes, 31 minutes and 65 minutes respectively.

Nevertheless, the experiments started with a higher dye concentration showed a higher initial rate. The drop of dye concentration in the first 20 minutes for the experiments with 5, 10 and 20 mg/kg initial dye concentrations was confirmed to be 1.86, 2.23 and 2.51 respectively as shown in Figure 4-9. The results were analysed with the mentioned adsorption and photodegradation kinetic models. The determined order of reactions and rate constants of adsorption and photodegradation were tabulated. The pseudo second order adsorption kinetics was the best fit model for the adsorption as shown in Table 4-10.

Table 4-10 Determined kinetic models of adsorption and rate constants of various experiments with different initial dye concentrations

Initial dye concentration (mg/kg)	Adsorption model	Rate constant (g/mg min)	Q_e (mg/g)	R^2 of linearised plot
5	Pseudo second order	0.29±0.03	1.52±0.07	0.9979
10		0.11±0.05	2.8±0.1	0.9987
20		0.036±0.009	5.15±0.04	0.9986

Furthermore, the equilibrium capacity increased with initial dye concentration, and the determined photodegradation kinetic data shown in Table 4-11 was comparable with that reported by Zhu et al[4].

Table 4-11 Determined kinetic models of photodegradation and rate constants of various experiments with different initial dye concentrations

Initial dye concentration (mg/kg)	Photodegradation kinetic model	Rate constant (min^{-1})	R^2 of linearised plot	Time interval complied with the rate law (minutes)
5	Pseudo first order	0.052±0.009	0.9984	5-75
10		0.028±0.002	0.9982	5-75
20		0.0124±0.0006	0.9992	5-180

They used the similar catalyst and found out that the reaction followed the pseudo first order rate law. Their reported rate constants for the experiments with 10 and 20 mg/kg initial dye concentrations were 0.02927 min^{-1} and 0.01108 min^{-1} respectively. They proposed that the reasons were due to the increase in dye concentration that reduced the optical path length and the light that reached the photocatalyst. Additionally, adsorption of dye molecules on the photocatalyst surface increased with dye concentration. This prevented the adsorption of OH^- and O_2 which were the important part of the mechanism of degradation. The first reason was unlikely within the tested range of concentration as the experiments started with a higher dye concentration showed relatively higher initial degradation rates. Nevertheless, it had shown that the initial rate increasing with dye concentration only occurred at low concentration, and the rate eventually decreased at a higher dye concentration[29]. The reaction frequency between active sites and dye molecules could be increased with dye concentration, while the photon absorbed by dye became critical at the evaluated dye concentration. The light insensitive degradation residues could also reduce the rate since the slow degradation rate with a high initial dye load occurred

at the late stage of reaction where the extent of decolorisation was high. The mostly likely explanation was that the increased light insensitive degradation residues adsorbed onto the active sites reduced the adsorption of OH^- and O_2, which were the important species of degradation.

4.6. Effect of drying post treatment on dye removal

Drying of the catalyst composite is an important process for industrial application. First, it is easier to handle or test the dried catalyst as the actual amount of catalyst can be accurately measured easily without considering the moisture content. In addition, drying usually increases the mechanical strength and rigidity. This is essential for industrial applications as they can be easily packed, transported and stored[98]. However, the publications that reported the effects of various drying methods on photodegradation characteristics of the chitosan based catalyst composites were not found. In order to find out the most suitable drying process, the effect of freeze drying and oven drying on the dye removal characteristics of the catalyst composite were evaluated. Obviously, the composite that first freeze dried showed better results in both adsorption and photodegradation rates when compared with the composite that was only washed with methanol and then oven-dried as shown in Figure 4-10.

Porosity and permeability of the high density of oven-dried catalyst would be lower, thereby reducing the rates of adsorption as well as photodegradation. This is in close agreement with the SEM analysis. Chiou et al.[99] compared the kinetics of C.I. Reactive Red 189 adsorption with the size of wet and dried crosslinked chitosan

beads. There was a reduction of the diameter of the beads from 2.3-2.5 mm to about 0.67 mm after drying, and the dried beads showed a much lower initial adsorption rate. Chassary et al.[100] evaluated both the equilibrium and kinetic properties of Pd adsorption onto the grafted chitosan with and without drying-rehydration processes. The rehydrated beads needed more time to reach equilibrium and higher adsorbate concentration to reach the same metal uptake. Dried biopolymer beads did not re-swell well even though it was rehydrated and the compact structure might be kept permanently. The compromised isotherm and kinetic parameters were observed on the dried and rehydrated beads. Freeze drying is a well-known drying technique that can largely prevent shrinkage and preserve the porosity of the materials.

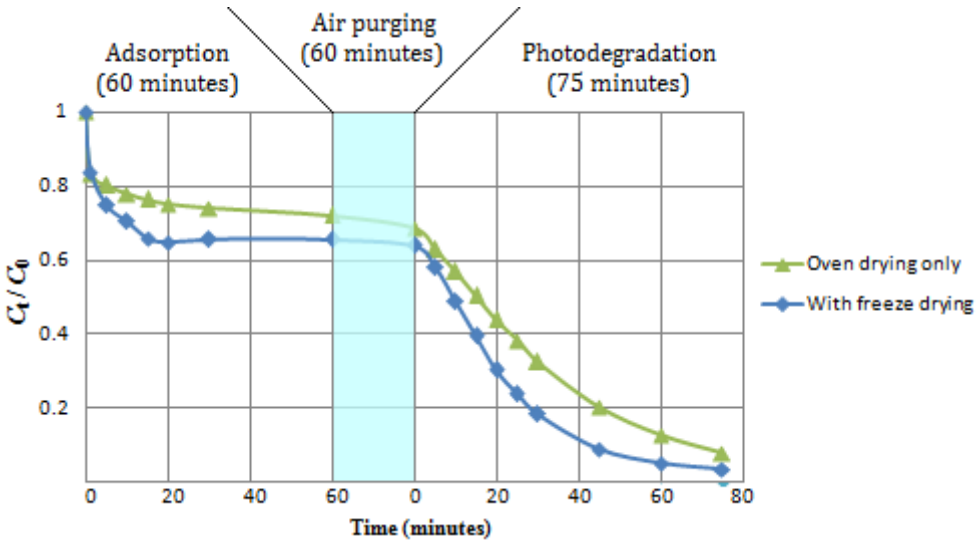

Figure 4-10 MO adsorption - photodegradation curves of composites with various post treatments. Non-crosslinked, Initial dye solution mass = 0.28 kg, Initial dye concentration = 10 mg/kg, Dosage of catalyst composite = 0.3 g, Initial pH not adjusted

The results were analysed with the mentioned adsorption and photodegradation

kinetic models. Adsorption rate constant and Q_e of OC composite were lower than those of FOC as shown in Table 4-12. As for photodegradation, the rate constant of experiment with the OC type composite was lower than that of FOC as shown in Table 4-13.

Table 4-12 Determined kinetic models of adsorption and rate constants of various experiments on composites with various post treatments

Catalyst composite used	Adsorption model	Rate constant (g/mg min)	Q_e (mg/g)	R^2 of linearised plot
OC	Pseudo second order	0.11±0.05	2.8±0.1	0.9987
FOC		0.18±0.03	3.2±0.2	0.9995

Table 4-13 Determined kinetic models of photodegradation and rate constants of various experiments on composites with various post treatments

Catalyst composite used	Photodegradation kinetic model	Rate constant (min^{-1})	R^2 of linearised plot	Time interval complied with the rate law (minutes)
OC	Pseudo first order	0.028±0.002	0.9982	5-75
FOC		0.044±0.003	0.9976	5-60

Higher adsorption and photocatalytic activity were observed on the freeze dried when composite compared with that without freeze drying before washing with methanol and oven drying. The beneficial effects of freeze drying were maintained in the process that the composite was washed with methanol and then oven dried.

4.7. Reuse the catalyst composites

Stability in the repeated use is necessary for practical implementation. Experiments

were carried out to demonstrate the influence of crosslinking and catalyst dosage on the dye removal performance of multiple cycle use of the catalyst composite. The effects of crosslinking on the dye removal by means of the reused catalyst composites were evaluated. Figure 4-11 shows the adsorption - photodegradation curves. All the experiments were carried out with the FOC catalyst composites using different types of crosslinking agents.

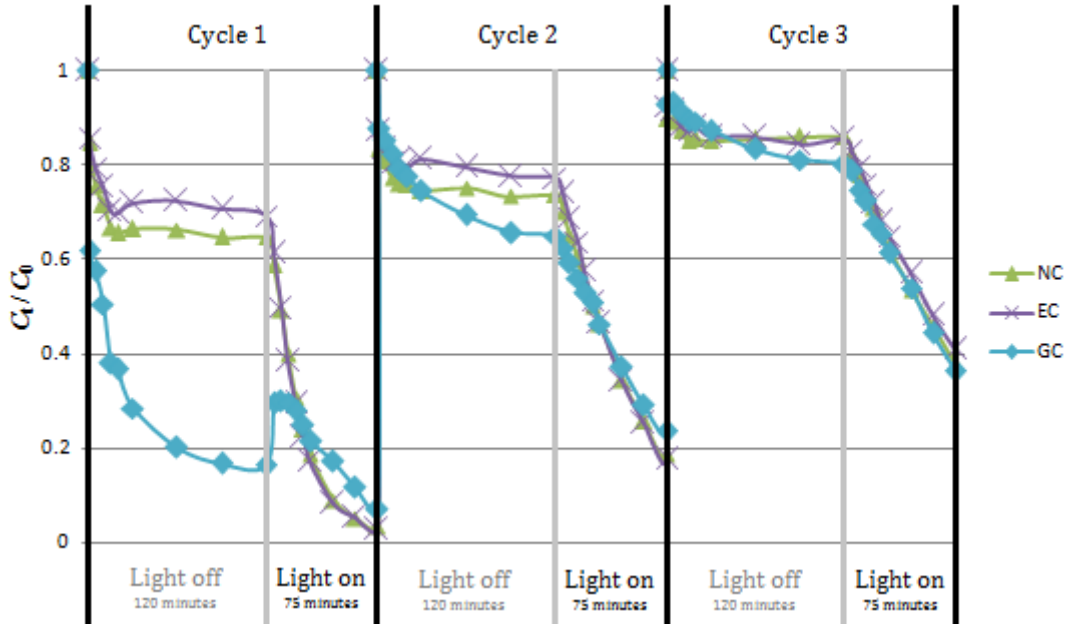

Figure 4-11 Multi-cycle MO adsorption - photodegradation curves of FOC composites with various states of crosslinking. NC, EC and GC denote the non-crosslinked, epichlorohydrin and glutaraldehyde-crosslinked composites, respectively while light off and light on denote adsorption in dark and photodegradation respectively. Initial dye solution mass = 0.28 kg, Initial dye concentration = 10 mg/kg, Dosage of catalyst composite = 0.3 g, Initial pH not adjusted

After the first cycle, the glutaraldehyde crosslinked catalyst composite showed the diminished special features. After the second cycle, the glutaraldehyde-crosslinked

catalyst composite showed no difference in activity when compared with other composites in terms of dye adsorption and photodegradation. This could be explained by the photodegradation of the Schiff bases and the reduced unoccupied adsorption sites caused by the residual species from the previous experiments. In the other words, both catalysts using different crosslinking agents demonstrated no significant difference on dye removal after the first cycle. For all the catalyst composites, both the rate and capacity of adsorption as well as the rate of photodegradation decreased with respect to the increasing cycle of uses. The decrease in catalytic activity was due to the reduced unoccupied adsorption sites caused by the residual dye molecules and insensitive species as referred to the pervious experiments. In addition photocorrosion of CdS was also the possible cause[22, 69].

The effects of catalyst dosage on the dye removal by reusing the catalyst composite were studied. Figure 4-12 shows the adsorption - photodegradation curves of the experiments. All the experiments were carried out with the OC catalyst composite using different dosages. Adsorption of dye increased with the dosage of photocatalyst regardless of the cycle of reuse. Moreover, the experiment with a higher dosage showed a relatively lower loss of photocatalytic activity after the use and recycling; with 0.7 g of the catalyst composite the dye decolorization just mildly decreased from 99 % (1st cycle) to 94 % in the 2nd cycle and 89 % in 3rd cycle and the catalyst remained sufficiently efficient after repeated use with this dosage. It was known that the productive effect of increasing dosage on photodegradation diminished when the dosage of catalyst had already reached a certain level. This

could explain why the experiments with higher dosages showed a less photocatalytic activity of drop after the use and recycling. Detrimental effect of fouling of part of catalyst on the photocatalytic activity also diminished for high dosage experiments. Moreover, the lower adsorbed residual dye or degradation product load per unit mass of composite also occurred in the experiments with higher dosage. This reduced the fouling of the photocatalytic composite. It was found that composites after the use released a remarkable yellow colour in dilute NaOH solution.

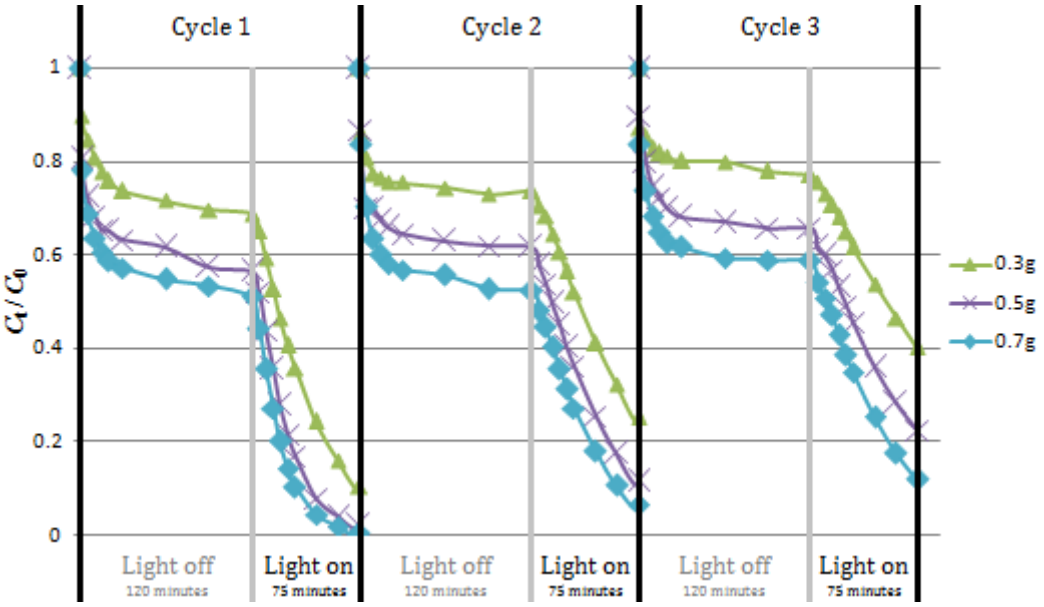

Figure 4-12 Multi-cycle MO adsorption - photodegradation curves of experiments with various dosages. Light off and light on denote adsorption in dark and photodegradation respectively. Initial mass of MO solution = 0.28 kg, Initial dye concentration = 10 mg/kg. OC were used and initial pH not adjusted

Zhu et al.[4, 29, 56] reported similar experiments with similar photocatalyst. Three dyes, namely Congo Red, C.I. Acid Red 66 and Methyl Orange were tested. Interestingly, photocatalytic activity loss in the repeated use of catalyst on the

experiments testing Methyl Orange removal was much severer than that of the experiments testing other dyes. The loss in 5 cycles of experiments testing Congo Red and C.I. Acid Red 66 were somewhat negligible. Destroying Methyl Orange would be a difficult task for this class of experiments. The reused catalyst composites showed the reduced adsorption and photodegradation. The reused catalyst composites also showed similar degradation profiles regardless of whether they were crosslinked or not. Both the tested crosslinking agents could not enhance the reusability of the catalyst composite. Photocatalytic activity drop using the recycled catalyst composite was relatively low for the experiments with higher dosages of catalyst; with 0.7 g of the catalyst composite the dye decolorization just mildly decreased after repeated use.

4.8. Development of catalyst composite

The adsorption and photodegradation characteristics of the two developed chitosan-based encapsulation systems with loaded CdS were analysed. Figure 4-13 shows the adsorption - photodegradation curves of the experiments.

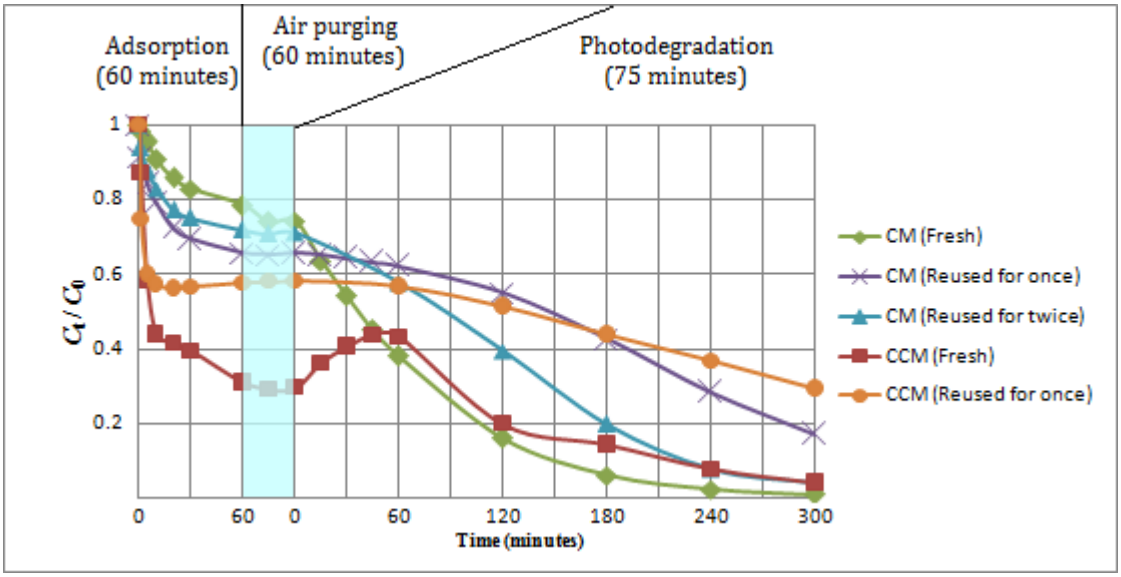

Figure 4-13 Adsorption - photodegradation curves of the developed novel catalyst composites. Initial dye solution mass = 0.25 kg, catalyst composite dosage = 0.25 g, Initial dye concentration = 10 mg/kg and initial pH not adjusted of MO

The rate of dye adsorption of the fresh CM was slower when compared with the fresh CCM. One reason of the high rate of CCM Schiff base could be due to the fact that Schiff base was more attractive than the original amino groups used for the dye molecules. Both the capacity and rate of adsorption were significantly reduced after the use which was similar to the case of the glutaraldehyde-crosslinked OC as discussed in section 4.7. The CCM composite showed an increase in the initial rate of adsorption after the first use. These could be the result of bead swelling during the first experiment cycle. The capacity and initial rate of adsorption of dye onto the CM composite were also slightly improved after the first use. This could be caused by the destruction of the originally compact structure of beads caused by the mechanical stirring. This exposed more sites for adsorption to solution. During photodegradation experiment, 1 hour of dye release was observed on the CCM after the start of illumination which was similar to the case of glutaraldehyde-crosslinked OC as

discussed in the section 4.2. Moreover, the reused catalyst composites demonstrated the reduced catalytic effect. A possible reason for the decline of the catalytic effect was the photocorrosion on CdS that destroyed sulfide and turned Cd into free Cd^{2+} ions[22] as well as release of loosely attached CdS particles. However, the third cycle of degradation using the CM composite was an exception and showed a better degradation than the second cycle. This could be caused by the bead disintegration as shown in Figure 4-14 which significantly occurred only in the third cycle that exposed more CdS to dye solution.

Figure 4-14 Bead disintegration of CM

The determined order of reaction and the rate constant of adsorption as shown in Table 4-14 and photodegradation as shown in Table 4-15 were tabulated:

Table 4-14 Determined kinetic models of adsorption and rate constants of various experiments - Development of catalyst composite

Experiment	Adsorption model	Rate constant	Q_e (mg/g)	R^2
CM (Fresh)	Pseudo second order	0.0195 (g/mg min)	2.83	0.995
CM (Reused for once)	Pseudo first order	0.0615 (min^{-1})	2.69	0.999
CM (Reused for twice)	Pseudo second order	0.0481 (g/mg min)	3.15	0.995
CCM (Fresh)	Pseudo second order	0.0179 (g/mg min)	9.60	0.997
CCM (Reused for once)	Pseudo second order	0.315 (g/mg min)	4.43	1.000

Table 4-15 Determined kinetic models of photodegradation and rate constants of various experiments - Development of catalyst composite

Experiment	Photodegradation kinetic model	Rate constant	R^2 of linearised plot	Time interval complied with the rate law (minutes)
CM (Fresh)	Pseudo first order	0.0144 (min^{-1})	0.998	0-300
CM (Reused for once)	Pseudo zero order	0.0216 (mg/kg min)	0.998	120-300
CM (Reused for twice)	Pseudo zero order	0.0290 (mg/kg min)	0.992	0-180
CCM (Fresh)	Pseudo first order	0.00971 (min^{-1})	0.998	60-300
CCM (Reused for once)	Pseudo zero order	0.0114 (mg/kg min)	0.998	120-360

Most of the photodegradation kinetic data of the fresh beads were highly fitted with the most commonly reported pseudo first order kinetics while that of the reused beads complied with the zero order kinetics apparently.

Judging from the adsorption rate and capacity, the CCM outperformed the CM made by the simple and traditional dropping. However, photodegradation performance of the fresh CCM as well as the both adsorption capacity and photocatalytic effect of the reused CCM were unsatisfactory. The laborious steps of preparation and the difficulties in cadmium loading of the emulsion beads precluded it from the practical application. Beads formed by dropping seemed more worthy to further study and investigate. Enhancement of mechanical strength and effective methods for regeneration should be developed to facilitate the practical application of the CM beads formed from both dropping and emulsion method.

4.9. Characterisation of catalyst composite

4.9.1. X-ray Diffraction (XRD)

Soltani et al.[101] reported the XRD patterns of cubic and hexagonal CdS nanocrystals. For cubic structure, peaks at 2θ values of 26.4 °, 43.8 °, 51.9 ° and 71.2 ° matched with the (111), (220), (311) and (331) crystalline planes of the face centered cubic structure. As for hexagonal structure, peaks at 2θ values of 24.8 °, 26.5 °, 28.2 °, 36.6 °, 43.7 °, 47.8 °, 51.8 °, 67.1 ° and 75.9 ° matched perfectly with the (100), (002), (101), (102), (110), (103), (112), (203) and (204) crystalline planes. Figure 4-15 shows the XRD analysis for the CdS crystal structures of the composites, and the result was similar to that reported by Zhu et al.[4] Peaks were observed in the XRD patterns at 2θ values of 25.3 °, 26.8 °, 28.0 °, 43.9 °, 48.0 °, 52.2 °, 67.0 ° and 74.8 °. The XRD pattern as shown possessed identical peak positions but it had different intensity patterns when compared with the hexagonal CdS as reported by Reyes et al.[102] and the standard CdS (ICSD #:067776).

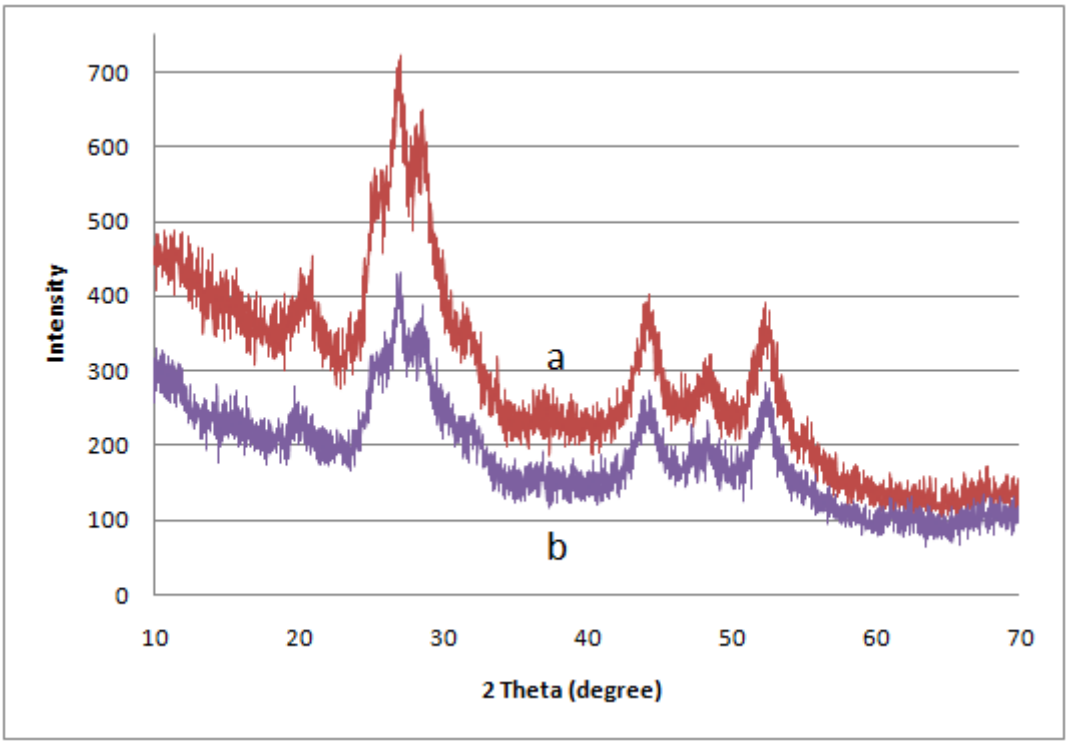

Figure 4-15 XRD spectra of FOC (a) and OC (b) composites.

Similar XRD pattern was reported by E. Maier et al.[103] who attributed the observation to the mixture of crystals of both forms. Overlapping the peaks with the Miller Indices of (111), (220) and (311) of the cubic CdS as well as the peaks with the Miller Indices of (002), (110) and (112) of the hexagonal CdS could be formed in the XRD pattern as shown. The peak present at $2\theta = 19.8$ ° was the crystalline peak of chitosan[104]. The broadness of XRD peaks indicated the existence of nanocrystals. The average sizes of the crystalline structures of CdS inside both the composites were calculated by analysing the XRD data of the peak at $2\theta = 43.9$ ° with the Scherrer's formula[103]. The sizes calculated were 46.0 Å for the composites.

Scherrer's formula:

$$D = \frac{0.89\lambda}{B\cos\theta} \quad (4\text{-}1)$$

where *D* is the average size of the crystal, λ is the wavelength of X-ray source, *B* is the full width at half maximum and, θ is the corresponding diffraction angle.

4.9.2. Transmission electron microscopy (TEM)

Figure 4-16a shows TEM image that exhibits the OC composite particles containing the CdS nanoparticles and the dark grains encapsulated in the relatively transparent chitosan. Figure 4-16b shows the observation of part of the above mentioned particles under a higher power magnification. The crystalline CdS nanoparticles were encapsulated in the amorphous chitosan. Extensive aggregation of CdS nanocrystals was observed. It seemed that the cubic or hexagonal crystals were observed in the TEM images as shown in Figure 4-16c. The sizes of CdS nanocrystal grains between 2.8 nm and 15.7 nm as shown in Figure 4-16d were comparable with the average size determined by the XRD data using the Scherrer's formula (4.6 nm).

(a) (b)

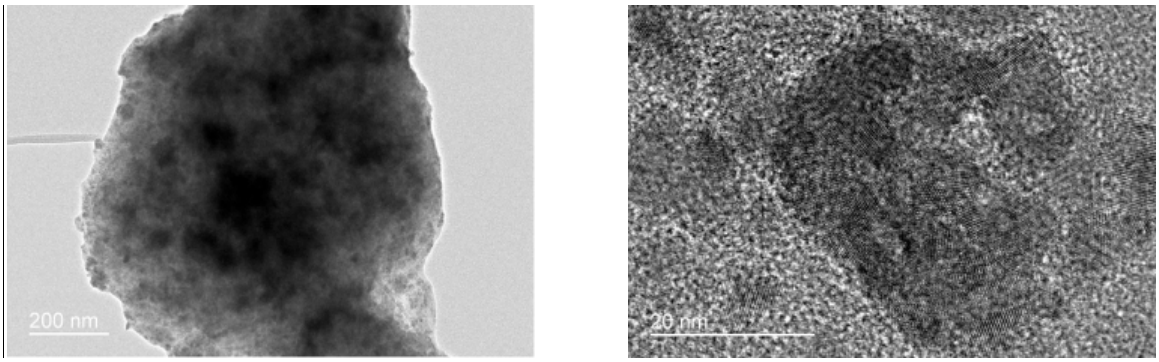

(c)

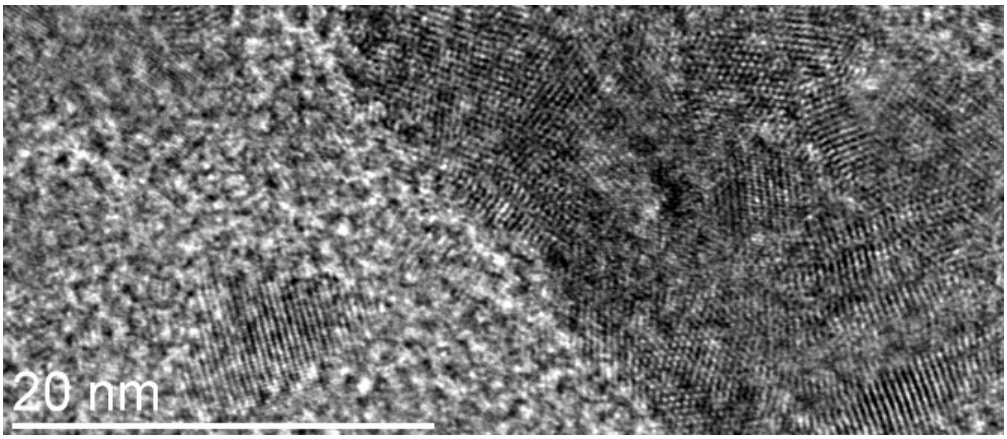

(d)

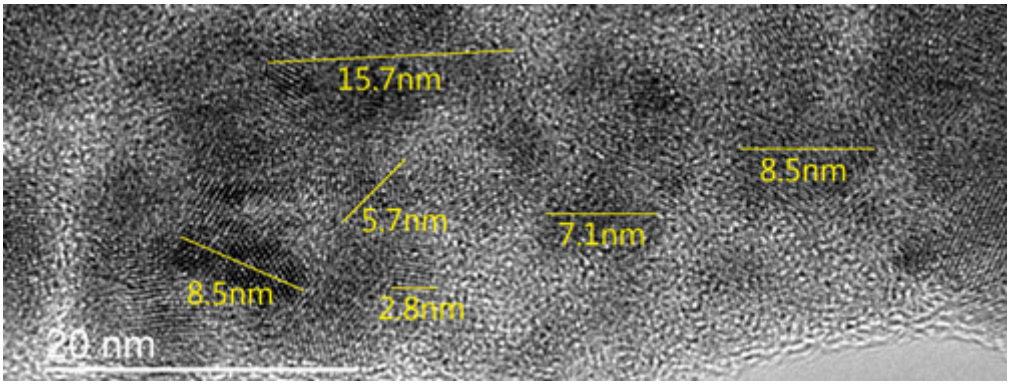

Figure 4-16 TEM images of OC catalyst composite: (a) crystals encapsulated into relatively transparent chitosan, (b) agglomerated grains, (c) CdS crystals and (d) another part of the sample showing the size of nanocrystal grains

4.9.3. Scanning electron microscopy (SEM)

Figure 4-17a and Figure 4-17b are the SEM images of FOC and OC composites.

Many pleats are observed on the surface of the OC composite. The same is not true for the FOC composite and much smoother surface is observed. Reflected by the result of dye adsorption and photodegradation experiments, the FOC composite was superior to the OC composite despite the intuition that rougher surfaces can provide a much larger surface area for photocatalytic reaction[4]. In this case, the pleats on the OC composite were possibly an evidence of excessive shrinkage of the originally porous composite. This compact structure could impede the mass transfer and the light penetration. Actually, the OC composite was apparently harder and denser that the FOC composite.

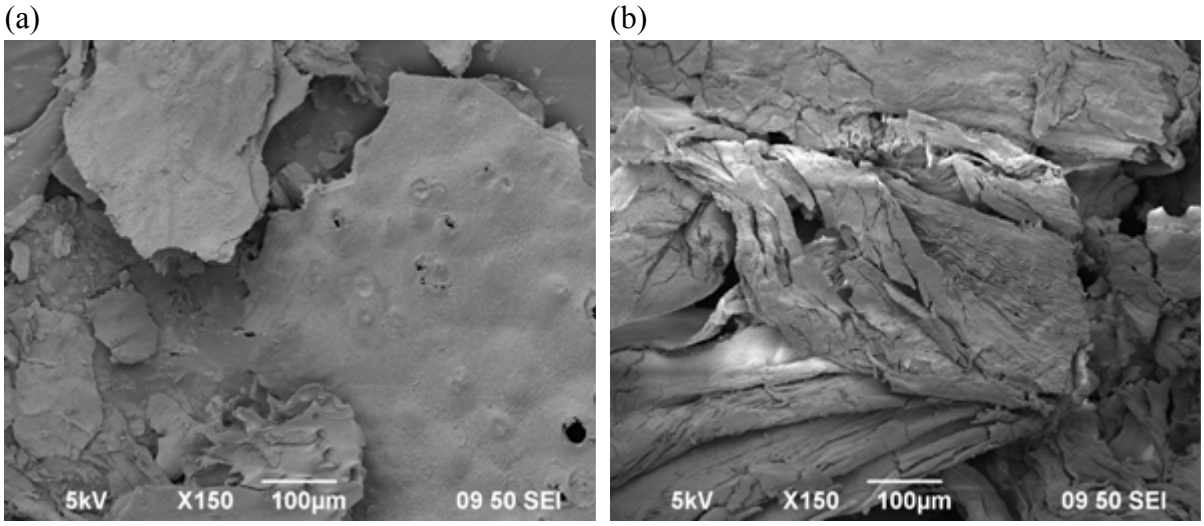

Figure 4-17 SEM images of (a) FOC and (b) OC catalyst composites.

4.9.4. Fourier transform infrared spectroscopy (FT-IR)

IR absorption measurements of various catalyst composites (OC, Glutaraldehyde-crosslinked OC, Epichlorohydrin-crosslinked OC and FOC) with different crosslinking treatments and the original chitosan were carried out to

investigate the information concerning the chemical functional groups as shown in Figure 4-18.

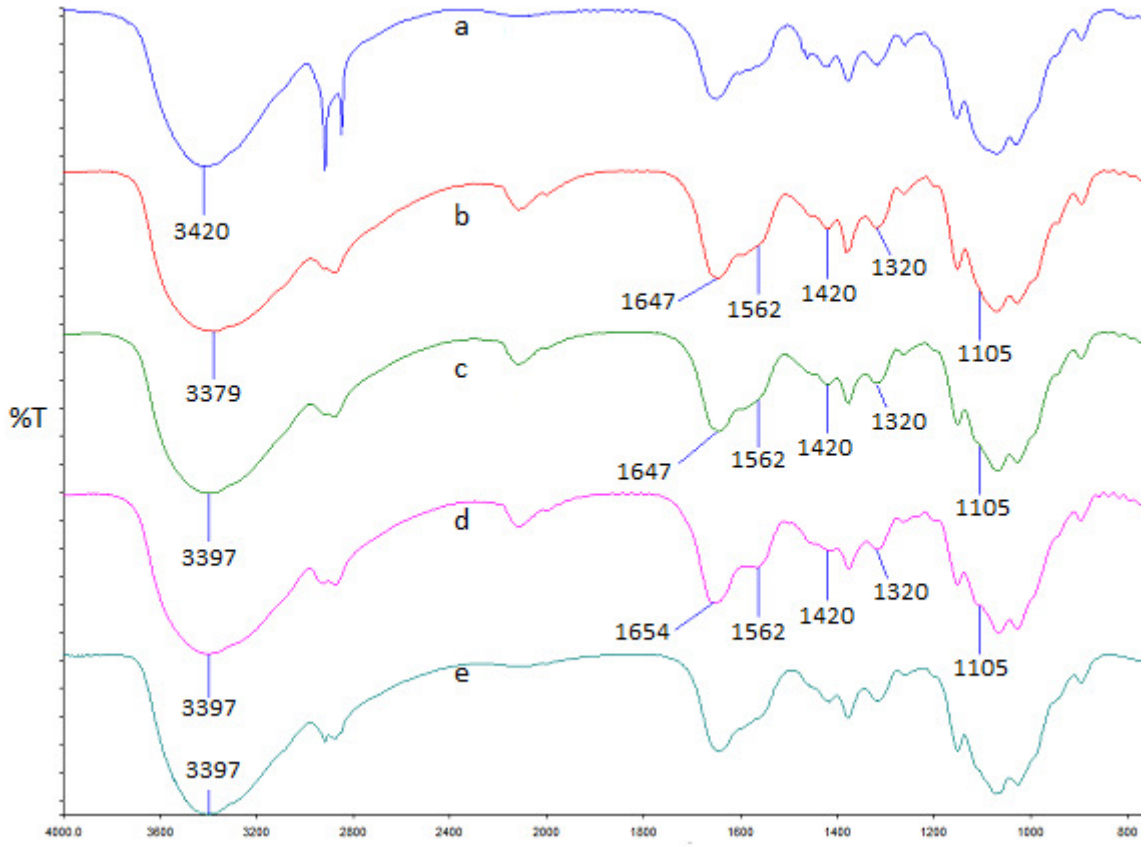

Figure 4-18 IR spectra of (a) the original chitosan, (b) OC, (c) epichlorohydrin-crosslinked OC, (d) glutaraldehyde-crosslinked OC and (e) FOC

The major difference between the original chitosan and the chitosan loaded with CdS was that the band related to the stretching vibrations of hydroxyl, amino and amide groups with the peak located at 3420 cm^{-1} for the original chitosan being shifted to 3397-3379 cm^{-1} after the introduction of CdS. Similar finding was reported by Zhu et al[4].

The spectrum of glutaraldehyde-crosslinked composite in the present work was similar to those reported by Zhu et al. As a comparison with the non-crosslinked composite, the peak originally located at 1647 cm^{-1} shifted slightly to 1654 cm^{-1} indicating that the $–NH_2$ bending was changed to the Schiff base (C=N). (Tasselli et al.[105] and Monteiro Jr. et al[89]). The absorption band around 1562 cm^{-1} was enhanced and formed a shoulder after crosslinking by glutaraldehyde as reported by Monteiro Jr. et al. This observation could be related to the long crosslinking time that allowed the glutaraldehyde to react themselves via Aldol condensation to form the unsaturated poly aldehydes[106]. Hu and coworkers[107] also suggested that the results might be due to the possibility that the chitosan was crosslinked by the unsaturated polyaldehydes. Another evidence showed that the crosslinking reaction could be reviewed by the weaken absorption peaks at 1420 and 1320 cm^{-1}, where the -NH deformation vibration and -CN stretching vibration of free intact chitosan could be observed. Ngah et al.[108] suggested that the consumed amino groups after crosslinking reaction was a good explanation for the two weaken infrared absorptions of chitosan. Further evidence showed that a small protrusion was found on the IR transmittance spectrum at 1105 cm^{-1} after the crosslinking. Beppu et al.[109] suggested that this observation might be due to the decrease in aliphatic amino groups.

Epichlorohydrin-crosslinked and non-crosslinked composite were identical in the IR absorption spectra in the present work. Epichlorohydrin crosslinking consumed part of the –OH groups present on the chitosan back bone to form new C–O and –OH groups as well as methylene groups. No special feature was generated for the crosslinking. Hence, it was not surprising to see that the IR absorption characteristics

remained unchanged although Beppu et al. reported the increased intensity within the 1300-1000 cm^{-1} region.

As a supplement for the FT-IR analysis, treating the non-crosslinked and crosslinked composites OC with 3 % HNO_3(aq) showed various results as shown in Figure 4-19. As for the non-crosslinked composite, the composite lumped together and the liquor became turbid. The same did not occur to both the crosslinked composites. This implied that the crosslinking reactions were successful as the crosslinked composites did not dissolve in acid like the original composite.

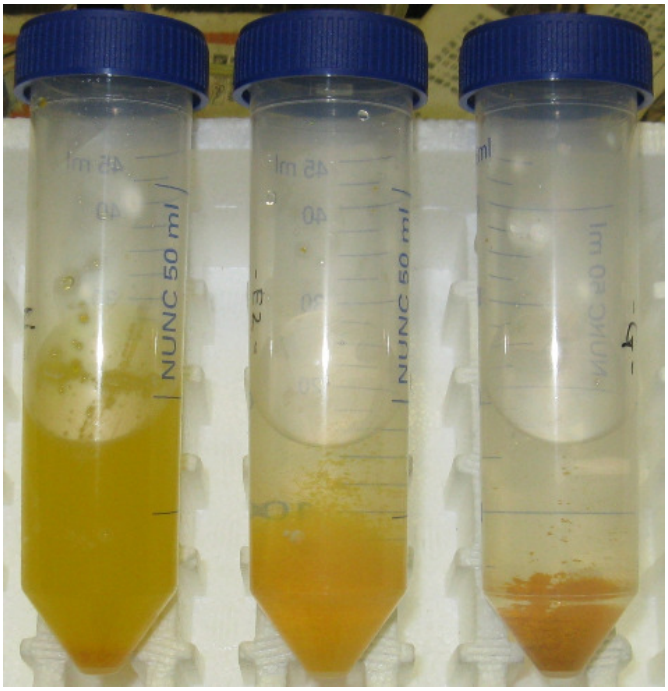

Figure 4-19 The chemical test: non-crosslinked OC (left), epichlorohydrin-crosslinked OC (middle) and glutaraldehyde-crosslinked OC (right)

4.9.5. Visible reflectance

The OC was subjected to the visible reflectance analysis. The measured

%Reflectance against wavelength plot is shown in Figure 4-20.

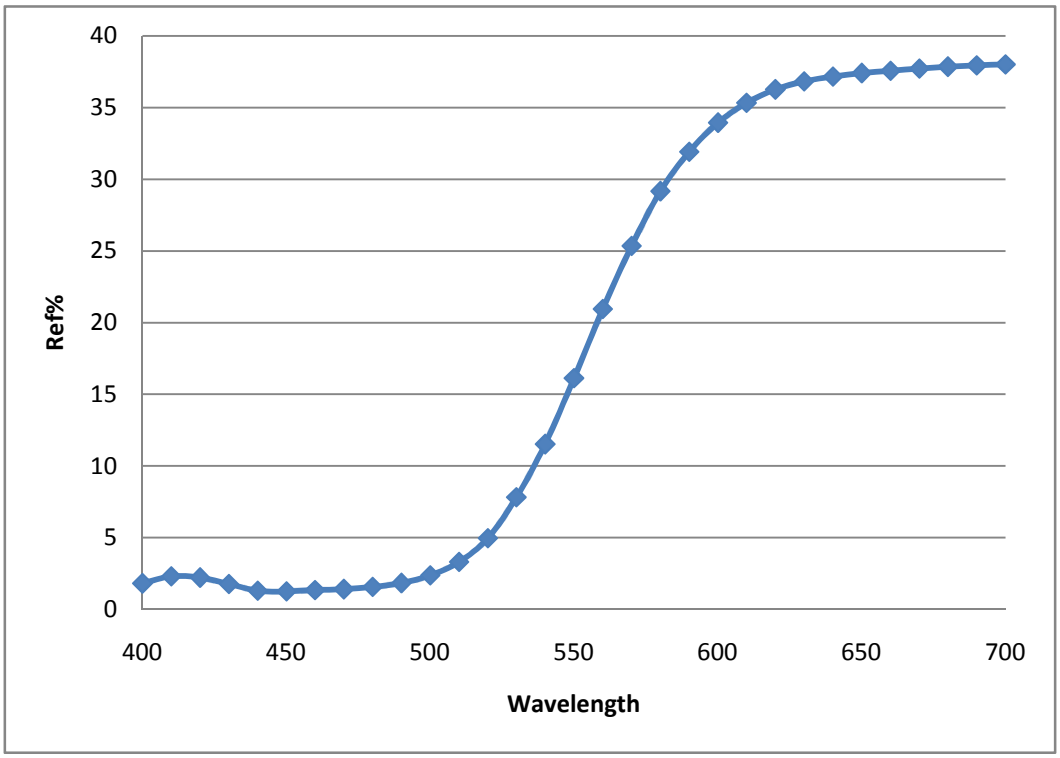

Figure 4-20 % Reflectance spectra

The X axis intercept of extrapolations of the $\{h\nu\ln[(R_{max}-R_{min})/(R-R_{min})]\}^2$ versus $h\nu$ plots (Figure 4-21) gave E_g. The determined E_g of OC was 2.40 ev. This meant that the band gap of CdS inside OC was almost equal to that of the bulk CdS material. Probably, the CdS nanocrystals present in the OC were aggregated to a certain extent that they did not exhibit blue shift. Vilius Poderys[110] and Chetan P. Shah[111] reported that the aggregation of the suspended CdTe or CdSe quantum dots could lead to the red shift of absorption spectrum.

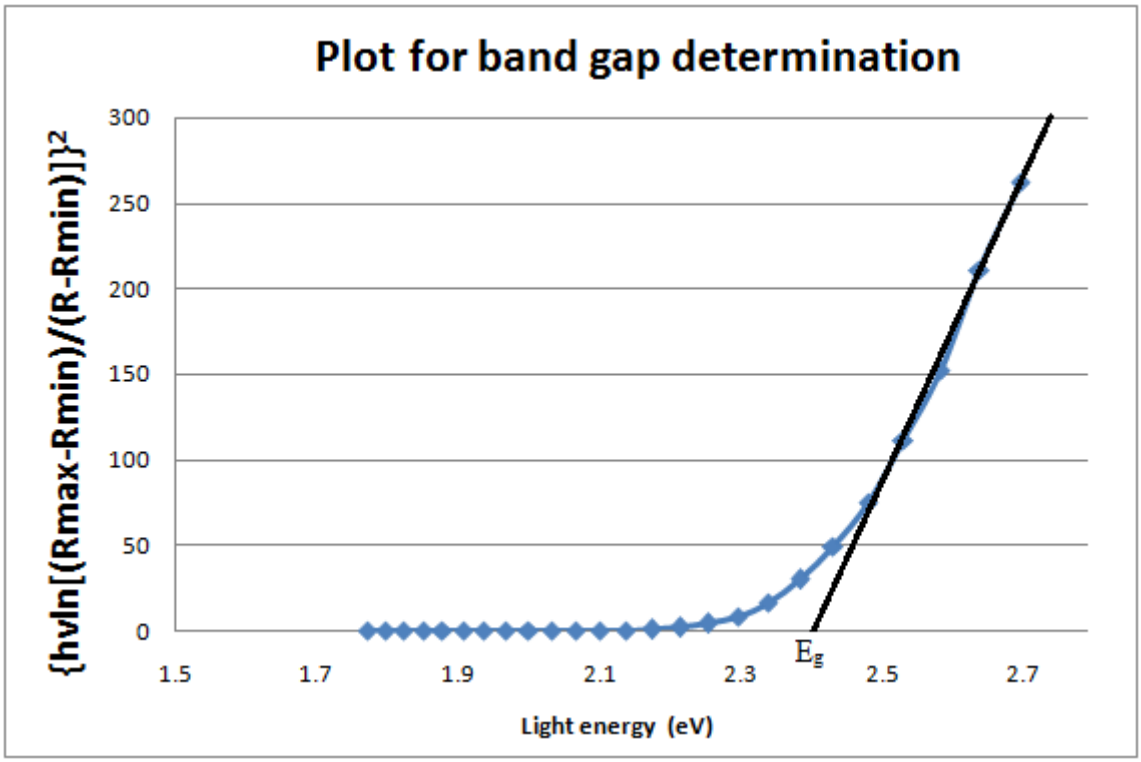

Figure 4-21 $\{h\nu\ln[(R_{max}-R_{min})/(R-R_{min})]\}^2$ versus $h\nu$ plots

Chapter 5 Conclusions and Suggestions for Future Research

5.1. Conclusions

Catalyst composite i.e. the chitosan with the encapsulated CdS, was prepared and tested. The catalyst was able to degrade Methyl Orange and Acid Blue 25. UV-visible absorption spectra of the treated dye solutions indicated the destruction of chromophore and aromatic rings. The catalytic photodegradation process was more efficient to break part of the chromophores than the aromatic rings of the dyes. Most of the adsorption experiments followed the pseudo second order adsorption kinetics. The most common kinetic model of Methyl Orange photodegradation was the pseudo first order kinetics. Unlike the Methyl Orange, the profiles of Acid Blue 25 photodegradation experiments followed the rare pseudo second order kinetics unless the experiment was started at pH10.

The effect of dosage, initial dye concentration, pH, drying post-treatment as well as crosslinking of catalyst composite on the dye removal and recycled use of catalyst composite were evaluated. Both the adsorption and photodegradation of dye increased with the dosage of photocatalyst. The enhancement was more significant for photodegradation when compared with adsorption. The benefit of increasing the dosage became diminished when the dosage already reached a certain level. The adsorption capacity and rate increased with dye concentration. Both the dye removal efficiency and K_{1p} decreased with increasing dye concentration although the experiments starting with higher dye concentrations showed a higher initial rate of photodegradation. The mostly likely explanation was that the increased adsorbed dye molecules onto active sites could reduce the adsorption of OH^- and O_2 which were

important species of degradation. It was believed that the adsorbed light insensitive degradation residues could also reduce the rate. High pH strongly suppressed the adsorption of dye but not necessary the photodegradation. The dye photodegradation efficiency was found highly pH sensitive and confirmed by the desorption test, the highest photodegradation efficiency of MO dye occurred in acidic condition while that of AB25 dyes occurred in basic environment. Much higher adsorption and photocatalytic activity were observed on the freeze-dried composite when compared with those that received only oven drying and no freeze drying. The beneficial effects of freeze drying were maintained in the process such that the composite were washed with methanol and then oven dried. The taken SEM images suggested that freeze drying can prevent excessive shrinkage of the composites and this may improve the catalytic activity by providing more active sites. Epichlorohydrin crosslinking caused almost no change to the dye removal characteristics. Glutaraldehyde crosslinking enhanced adsorption but not photodegradation. In Methyl Orange photodegradation, the most common rate law of photodegradation was the pseudo first order kinetics. However, the dye photodegradation profiles of the OC composite with glutaraldehyde crosslinking seemed to fit the zero order rate law.

The reused catalyst composites showed the reduced adsorption and photodegradation activities, and demonstrated the similar degradation profiles regardless of whether they were crosslinked or not. Both the tested crosslinking agents could not enhance the reusability of catalyst composite. Photocatalytic activity drop when using the recycled catalyst composites was relatively low for the experiments with higher

dosages of catalyst composite; with 0.7 g of the catalyst composite the dye decolorization just mildly decreased after repeated use.

The adsorption rate and capacity of the crosslinked chitosan micro-particles encapsulated with the CdS formed from the emulsion method outperformed the chitosan miniparticles encapsulated with the CdS made by the simple and traditional dropping method. However, photodegradation performance of the fresh crosslinked chitosan microparticles as well as the both adsorption capacity and photocatalytic effects of the reused CCM were unsatisfactory. The laborious steps of preparation and the difficulties in cadmium loading of the emulsion beads precluded it from the practical application. Chitosan mini-particles formed by the dropping method seemed to be more worthy of investigation.

5.2. Suggestions for future work

According to the result of the present research, the epichlorohydrin-crosslinked chitosan is a suitable material for the encapsulation of semiconductor photocatalysts because the chitosan can provide the immobilization while the epichlorohydrin crosslinking could improve the mechanical and chemical stabilities and allows the catalyst composites to be used in acidic environments without causing any detrimental effects on the vital photodegradation. Thus, the future works should be based on the epichlorohydrin-crosslinked chitosan with encapsulated semiconductor photocatalysts. Freeze drying should be the preferred drying method instead of the common oven drying when drying of catalyst composite is desired. The dye photodegradation efficiency was found highly pH sensitive and depending on the

dye involved. Hence, optimum pH for highest photodegradation efficiency of a certain dye should be determined and the subsequent tests on degrading that dye should be carried out on that pH. It has shown that 1. part of the removed dye was adsorbed onto the catalyst composite only rather than degraded under illumination and 2. at some pH, merely the adsorption of the dye onto the catalyst composite in dark could already remove almost all of the dissolved dye. These phenomenons could render the traditional methodology of assessing photodegradation efficiency only measuring the remaining dye concentration in the reaction liquid unreliable. Hence, the dye desorption test mentioned should be carried out in the future works to reveal the amount of residual dye present inside the catalyst composite after the photodegradation step and improve the reliability of the assessment of the photodegradation efficiency. Chitosan mini-particles should be adopted in the future works instead of the materials prepared without special shape forming technique in form of flakes because the particles could allow easier post-treatment retrival of the catalyst.

In addition, the following problems were identified through the present study. First, the photocatalytic activity of the reused catalyst composite in terms of rate constant of the pseudo first order photodegradation usually became half after a batch operation of photodegradation experiment. Second, the nanocrystals of CdS are easy to be produced with chitosan and are able to utilised visible light. However, Cd is not environmentally friendly. Third, the configurations of photoreactors reported in the publications changed differently. This means that the comparison of photocatalytic activity of the synthesised catalysts with that of the catalysts reported in the

literatures is virtually impossible. Fourth, it is known that the light intensity of electric light sources changes slowly with the total operation time.

In the future research, the solutions of the above-mentioned problems should be investigated. First, the reliable methods used for regeneration of the catalyst composite should be developed and the mentioned desorption of dye by alkaline solution should be a promising method. Second, the nanocrystals of other semiconductors, such as doped TiO_2 and coupled TiO_2 that are able to utilise visible light, should be studied. Last but not least, chemical actinometry-based method for the calibration of photoreactors should be developed to offer a method for equalisation of various photoreactors and light sources.

Reference

[1] O.Fatoki, O. Olujimi, J. Odendaal, B. Genthe, Health Risk Assessment of Plasticizer in Wastewater Effluents and Receiving Freshwater Systems, Recent Advances in Plasticizers, (2012) 191-212.

[2] P.B. Dorn, C.S. Chou, J.J. Gentempo, Degradation of Bisphenol A In Natural Waters, Chemosphere, 16 (1987) 1501-1507.

[3] G.M. Walker, L.R. Weatherley, Fixed bed adsorption of acid dyes onto activated carbon, Environmental Pollution, 99 (1998) 133-136.

[4] H.Y. Zhu, R. Jiang, L. Xiao, Y.H. Chang, Y.J. Guan, X.D. Li, G.M. Zeng, Photocatalytic decolorization and degradation of Congo Red on innovative crosslinked chitosan/nano-CdS composite catalyst under visible light irradiation, Journal of Hazardous Materials, 169 (2009) 933-940.

[5] Z. Zulkarnain Zainal, K.H. Lee, Z.H. Mohd, H.A. Abdul, R.H. Imad, Characterization of TiO_2–Chitosan/Glass photocatalyst for the removal of a monoazo dye via photodegradation–adsorption process, Journal of Hazardous Materials, 164 (2009) 138–145.

[6] S. Steffan, L. Bardi, M. Marzona, Azo dye biodegradation by microbial cultures immobilized in alginate beads, Environment International, 31 (2005) 201-205.

[7] G.M. Walker, L.R. Weatherley, Biodegradation and biosorption of acid anthraquinone dye, Environmental Pollution, 108 (2000) 219-223.

[8] B.W. Manning, C.E. Cerniglia, T.W. Federle, Metabolism of the Benzidine-Based Azo Dye Direct Black 38 by Human Intestinal Microbiota, Applied and environmental microbiology, 50 (1985) 10-15.

[9] C. Karunakaran, R. Dhanalakshmi, P. Gomathisankar, G. Manikandan, Enhanced phenol-photodegradation by particulate semiconductor mixtures: Interparticle electron-jump, Journal of Hazardous Materials, 176 (2010) 799-806.

[10] H. Yan, W. Pan, D.A. Ping, Y. Jing, H. Y. Ping, Y. Yong, Preparation of CdS Nanoparticles with Reverse Micelle Method and Photo-degradation of Malachite Green Dye, Journal of Inorganic Materials, 25 (2010) 1221–1227.

[11] D.I. Petkowicz, S.B.C. Pergher, C.D.S.D. Silva, Z.N.D. Rocha, J.H.Z.D. Santos, Catalytic photodegradation of dyes by in situ zeolite-supported titania, Chemical Engineering Journal, 158 (2010) 505-512.

[12] S.K. Papageorgiou, F.K. Katsaros, E.P. Favvas, G. Em. Romanos, C.P. Athanasekou, K.G. Beltsios, O.I. Tzialla, P. Falaras, Alginate fibers as photocatalyst immobilizing agents applied in hybrid photocatalytic/ultrafiltration water treatment processes, Water Research, 46 (2012) 1858-1872.

[13] A.G.S. Prado, E.A. Faria, J.R.S. De, J.D. Torres, Ammonium complex of niobium as a precursor for the hydrothermal preparation of cellulose acetate/Nb_2O_5 photocatalyst, Journal of Molecular Catalysis A: Chemical, 237 (2005) 115-119.

[14] H.Y. Zhu, R. Jiang, Y.Q. Fu, Y.J. Guan, J. Yao, L. Xiao, G.M. Zeng, Effective photocatalytic decolorization of methyl orange utilizing TiO_2/ZnO/chitosan nanocomposite films under simulated solar irradiation, Desalination, 286 (2012) 41-48.

[15] R. Afeesh, N.A.M. Barakat, S.S. Al-Deyab, A. Yousef, H.Y. Kim, Nematic shaped cadmium sulfide doped electrospun nanofiber mat: Highly efficient, reusable, solar light photocatalyst, Colloids and Surfaces A: Physicochemical and Engineering Aspects, 409 (2012) 21-29.

[16] A.R. Unnithan, N.A.M. Barakat, M.F. Abadir, A. Yousef, H. Y. Kim, Novel CdPdS/PVAc core–shell nanofibers as an effective photocatalyst for organic pollutants degradation, Journal of Molecular Catalysis A: Chemical, 363-364 (2012) 186-194.

[17] A.H. Jawad, M.A. Nawi, Oxidation of crosslinked chitosan-epichlorohydrine film and its application with TiO_2 for phenol removal, Carbohydrate Polymers, 90 (2012) 1987-1994.

[18] Y. Gao, H.T. Liu, Preparation and catalytic property study of a novel kind of suspended photocatalyst of TiO_2-activated carbon immobilized on silicone rubber film, Materials Chemistry and Physics, 92 (2005) 604-608.

[19] H.H. Tseng, W.L.W. Lee, M.C. Wei, B.S. Huang, M.C. Hsieh, P.Y. Cheng, Synthesis of TiO_2/SBA-15 photocatalyst for the azo dye decolorization through the polyol method, Chemical Engineering Journal, 210 (2012) 529-538.

[20] J.Y. Chen, P.J. Zhou, J.L. Li, Y. Wang, Studies on the photocatalytic performance of cuprous oxide/chitosan nanocomposites activated by visible light, Carbohydrate Polymers, 72 (2008) 128-132.

[21] C.H. Cao, L. Xiaoa, L. Liu, H.Y. Zhu, C.H. Chen, L. Gao, Visible-light photocatalytic decolorization of reactive brilliant red X-3B on Cu_2O/crosslinked-chitosan nanocomposites prepared via one step process, Applied Surface Science, 271 (2013) 105-112.

[22] Y.H. Yang, N. Ren, Y.H. Zhang, Y. Tang, Nanosized cadmium sulfide in polyelectrolyte protected mesoporous sphere: A stable and regeneratable photocatalyst for visible-light-induced removal of organic pollutants, Journal of Photochemistry and Photobiology A: Chemistry, 201 (2009) 111-120.

[23] X. Tao, J.M. Su, L.X. Wang, J.F. Chen, A new heterogeneous catalytic system

for wastewater treatment: Fe-immobilized polyelectrolyte microshells for accumulation and visible light-assisted photooxidative degradation of dye pollutants, Journal of Molecular Catalysis A: Chemical, 280 (2008) 186-193.

[24] Y.M. Lee, W.J. Lee, Degradation of trichloroethylene by Fe(II) chelated with cross-linked chitosan in a modified Fenton reaction, Journal of Hazardous Materials, 178 (2010) 187-193.

[25] R. Sulakova, R. Hrdina, G.M.B. Soares, Oxidation of azo textile soluble dyes with hydrogen peroxide in the presence of Cu(II)-chitosan heterogeneous catalysts, Dyes and Pigments, 73 (2007) 19-24.

[26] M.A. Nawi, S. Sabar, A.H. Jawad, Sheilatina, W.S. Wan Ngah, Adsorption of Reactive Red 4 by immobilized chitosan on glass plates: Towards the design of immobilized TiO_2–chitosan synergistic photocatalyst-adsorption bilayer system, Biochemical Engineering Journal, 49 (2010) 317–325.

[27] H.Y. Zhu, L. Xiaoa, R. Jiang, G.M. Zeng, L. Liu, Efficient decolorization of azo dye solution by visible light-induced photocatalytic process using SnO_2/ZnO heterojunction immobilized in chitosan matrix, Chemical Engineering Journal, 172 (2011) 746– 753.

[28] Q. Li, H.J. Su, T.W. Tan, Synthesis of ion-imprinted chitosan-TiO_2 adsorbent

and its multi-functional performances, Biochemical Engineering Journal, 38 (2008) 212-218.

[29] R. Jiang, H.Y. Zhu, X.D. Li, L. Xiao, Visible light photocatalytic decolourization of C. I. Acid Red 66 by chitosan capped CdS composite nanoparticles, Chemical Engineering Journal, 152 (2009) 537–542.

[30] M.S. Chiou, H.Y. Li, Equilibrium and kinetic modeling of adsorption of reactive dye on cross-linked chitosan beads, Journal of Hazardous Materials, B93 (2002) 233-248.

[31] S.T. Lee, F.L. Mi, Y.J. Shen, S.S. Shyu, Equilibrium and kinetic studies of copper(II) ion uptake by chitosan-tripolyphosphate chelating resin, Polymer, 42 (2001) 1879-1892.

[32] W.S. Wan Ngah, S. Ab Ghani, A. Kamari, Adsorption behavior of Fe(II) and Fe(III) ions in aqueous solution on chitosan and cross-linked chitosan beads, Bioresource Technology, 96 (2005) 443-450.

[33] W.S. Wan Ngah, S. Fatinathan, Adsorption of Cu(II) ions in aqueous solution using chitosan beads,chitosan–GLA beads and chitosan–alginate beads, Chemical Engineering Journal, 143 (2008) 62-72.

[34] H.L. Vasconcelos, T.P. Camargo, N.S. Goncalves, A. Neves, M.C.M. Laranjeira,

V.T. Favere, Chitosan crosslinked with a metal complexing agent: Synthesis, characterization and copper(II) ions adsorption, Reactive & Functional Polymers, 68 (2008) 572-579.

[35] R.S. Vieira, M.M. Beppu, Interaction of natural and crosslinked chitosan membranes with Hg(II) ions, Colloids and Surfaces A: Physicochem. Eng. Aspects, 279 (2006) 196-207.

[36] W.H. Cheung, Y.S. Szeto, G. McKay, Enhancing the adsorption capacities of acid dyes by chitosan nano particles, Bioresource Technology, 100 (2009) 1143-1148.

[37] P. Baroni, R.S. Vieira, E. Meneghetti, M.G.C. da Silva, M.M. Beppu, Evaluation of batch adsorption of chromium ions on natural and crosslinked chitosan membranes, Journal of Hazardous Materials, 152 (2008) 1155-1163.

[38] M.S. Chiou, P.Y. Ho, H.Y. Li, Adsorption of anionic dyes in acid solutions using chemically cross-linked chitosan beads, Dyes and Pigments, 60 (2004) 69-84.

[39] M.S.Chiou, G.S. Chuang, Competitive adsorption of dye metanil yellow and RB15 in acid solutions on chemically cross-linked chitosan beads, Chemosphere, 62 (2006) 731-740.

[40] W.S. Wan Ngah, S. Fatinathan, Chitosan flakes and chitosan–GLA beads for

adsorption of p-nitrophenol in aqueous solution, Colloids and Surfaces A: Physicochem. Eng. Aspects, 277 (2006) 214-222.

[41] N. Viswanathan, C.S. Sundaram, S. Meenakshi, Removal of fluoride from aqueous solution using protonated chitosan beads, Journal of Hazardous Materials, 161 (2009) 423-430.

[42] N. Viswanathan, C.S. Sundaram, S. Meenakshi, Development of multifunctional chitosan beads for fluoride removal, Journal of Hazardous Materials, 167 (2009) 325-331.

[43] Y.H. Gad, Preparation and characterization of poly(2-acrylamido-2-methylpropanesulfonic acid)/Chitosan hydrogel using gamma irradiation and its application in wastewater treatment, Radiation Physics and Chemistry, 77 (2008) 1101-1107.

[44] J.M. Li, X.G. Meng, C.W. Hu, J. Du, Adsorption of phenol, p-chlorophenol and p-nitrophenol onto functional chitosan, Bioresource Technology, 100 (2009) 1168-1173.

[45] G.Z. Kyzas, M.Kostoglou, N.K. Lazaridis, Copper and chromium(VI) removal by chitosan derivatives—Equilibrium and kinetic studies, Chemical Engineering Journal, 152 (2009) 440-448.

[46] P. Ding, K.L. Huang, G.Y. Li, Y.F. Liu, W.W. Zeng, Kinetics of adsorption of Zn(II) ion on chitosan derivatives, International Journal of Biological Macromolecules, 39 (2006) 222-227.

[47] K.C. Gavilana, A.V. Pestov, H. M. Garcia, Y. Yatluk, J. Roussy, E. Guibal, Mercury sorption on a thiocarbamoyl derivative of chitosan, Journal of Hazardous Materials, 165 (2009) 415-426.

[48] H.L. Vasconcelos, V.T. Favere , N.S. Goncalves, M.C.M. Laranjeira, Chitosan modified with Reactive Blue 2 dye on adsorption equilibrium of Cu(II) and Ni(II) ions, Reactive & Functional Polymers, 67 (2007) 1052–1060.

[49] C.Y. Chen, C.C. Chen, Y.C. Chung, Removal of phthalate esters by α-cyclodextrin-linked chitosan bead, Bioresource Technology, 98 (2007) 2578-2583.

[50] Y. Vijaya, S.R. Popuri, V.M. Boddu, A. Krishnaiah, Modified chitosan and calcium alginate biopolymer sorbents for removal of nickel (II) through adsorption, Carbohydrate Polymers, 72 (2008) 261-271.

[51] S. Haider, S.Y. Park, Preparation of the electrospun chitosan nanofibers and their applications to the adsorption of Cu(II) and Pb(II) ions from an aqueous solution, Journal of Membrane Science, 328 (2009) 90-96.

[52] C. Fel, L.G. Sheng, W.F.Yu and W.J. Yu, Adsorption and recovery of Cu(II) with

polysulphone (PSF) containing chitosan gel, Journal of Microencapsulation, 21 (2004) 513-523.

[53] R. Laus, R. Geremias, H.L. Vasconcelos, M.C.M. Laranjeira, V.T. Favere, Reduction of acidity and removal of metal ions from coal mining effluents using chitosan microspheres, Journal of Hazardous Materials, 149 (2007) 471-474.

[54] F.C. Wu, R.L. Tseng, R.S. Juang, Enhanced abilities of highly swollen chitosan beads for color removal and tyrosinase immobilization, Journal of Hazardous Materials, B81 (2001) 167-177.

[55] J.H. An, S. Dultz, Adsorption of tannic acid on chitosan-montmorillonite as a function of pH and surface charge properties, Applied Clay Science, 36 (2007) 256-264.

[56] R. Jiang, H.Y. Zhu, X.D. Li, Adsorption and Visible Light Photocatalytic Decolorization of Methyl Orange Using Innovative Chitosan Capped CdS Composite, 3rd International Conference on Bioinformatics and Biomedical Engineering, (2009) 1-4.

[57] T.W. Chen, Y.H. Zheng, J.M. Lin, G.N. Chen, Study on the Photocatalytic Degradation of Methyl Orange in Water Using Ag/ZnO as Catalyst by Liquid Chromatography Electrospray Ionization Ion-Trap Mass Spectrometry, Journal of the

American Society for Mass Spectrometry, 19 (2008) 997–1003.

[58] Y.M. He, Y. Wu, T.L. Sheng, X.T. Wu, Photodegradation of acetone over V-Gd-O composite catalysts under visible light, Journal of Hazardous Materials, 180 (2010) 675-682.

[59] L. Wu, J.C. Yu, X.Z. Fu, Characterization and photocatalytic mechanism of nanosized CdS coupled TiO_2 nanocrystals under visible light irradiation, Journal of Molecular Catalysis A: Chemical, 244 (2006) 25-32.

[60] L.M. Song, C. Chen, S.J. Zhang, Preparation and photocatalytic activity of visible light-sensitive selenium-doped bismuth sulfide, Powder Technology, 207 (2011) 170-174.

[61] M. M. Mohamed, M.M. Al-Esaimi, Characterization, adsorption and photocatalytic activity of vanadium-doped TiO_2 and sulfated TiO_2 (rutile) catalysts: Degradation of methylene blue dye, Journal of Molecular Catalysis A: Chemical, 255 (2006) 53-61.

[62] R. Solarska, A. Heel, J. Ropka, A. Braun, L. Holzer, J.H. Ye, T. Graul, Nanoscale calcium bismuth mixed oxide with enhanced photocatalytic performance under visible light, Applied Catalysis A: General, 382 (2010) 190-196.

[63] Y. Bessekhouad, D. Robert, J.V. Weber, Bi_2S_3/TiO_2 and CdS/TiO_2

heterojunctions as an available configuration for photocatalytic degradation of organic pollutant, Journal of Photochemistry and Photobiology A: Chemistry, 163 (2004) 569-580.

[64] C.A. Paez, D. Poelman, J.P. Pirard, B. Heinrichs, Unpredictable photocatalytic ability of H_2-reduced rutile-TiO_2 xerogel in the degradation of dye-pollutants under UV and visible light irradiation, Applied Catalysis B: Environmental, 94 (2010) 263-271.

[65] A.H. Zyoud, N. Zaatar, I. Saadeddin, C. Ali, D.H. Park, G. Campet, H.S. Hilal, CdS-sensitized TiO_2 in phenazopyridine photo-degradation: Catalyst efficiency, stability and feasibility assessment, Journal of Hazardous Materials, 173 (2010) 318-325.

[66] Y. Liu, X. Chen, J. Li, C. Burda, Photocatalytic degradation of azo dyes by nitrogen-doped TiO_2 nanocatalysts, Chemosphere, 61 (2005) 11-18.

[67] D.P. Subagio, M. Srinivasan, M. Lim, T.T. Lim, Photocatalytic degradation of bisphenol-A by nitrogen-doped TiO_2 hollow sphere in a vis-LED photoreactor, Applied Catalysis B: Environmental, 95 (2010) 414-422.

[68] X.P. Wang, T.T. Lim, Solvothermal synthesis of C-N codoped TiO_2 and photocatalytic evaluation for bisphenol A degradation using a visible-light irradiated

LED photoreactor Applied Catalysis B: Environmental, 100 (2010) 355-364.

[69] S.A. Song, L.J. Xu, Z.Q. He, H.P. Ying, J.M. Chen, X.Z. Xiao, B. Yan, Photocatalytic degradation of C.I. Direct Red 23 in aqueous solutions under UV irradiation using $SrTiO_3/CeO_2$ composite as the catalyst, Journal of Hazardous Materials, 152 (2008) 1301-1308.

[70] J. Bandara, K. Tennakone, P.P.B. Jayatilaka, Composite Tin and Zinc oxide nanocrystalline particles for enhanced charge separation in sensitized degradation of dyes, Chemosphere, 49 (2002) 439–445.

[71] K. Hayat, M.A. Gondal, M.M. Khaled, Z.H. Yamani, S. Ahmed, Laser induced photocatalytic degradation of hazardous dye (Safranin-O) using self synthesized nanocrystalline WO_3, Journal of Hazardous Materials, 186 (2011) 1226–1233.

[72] W.Z. Yin, W.Z. Wang, L. Zhou, S.M. Sun, L. Zhang, CTAB-assisted synthesis of monoclinic $BiVO_4$ photocatalyst and its highly efficient degradation of organic dye under visible-light irradiation, Journal of Hazardous Materials, 173 (2010) 194–199.

[73] M.A. Rauf, M.A. Meetani, A. Khaleel, A. Ahmed, Photocatalytic degradation of Methylene Blue using a mixed catalyst and product analysis by LC/MS, Chemical Engineering Journal, 157 (2010) 373–378.

[74] S.J. Yang, H. Tian, H.M. Xiao, Z.H. Shang, X.D. Gong, S. Yao, K.C. Chen, Photodegradation of cyanine and merocyanine dyes, Dyes and Pigments, 49 (2001) 93-101.

[75] N. A. Jamalluddin, A. Z. Abdullah, Reactive dye degradation by combined Fe(III)/TiO_2 catalyst and ultrasonic irradiation: Effect of Fe(III) loading and calcination temperature, Ultrasonics Sonochemistry, 18 (2011) 669-678.

[76] B.B. Kale, J.O. Baeg, J.S. Yoo, S.M. Lee, C.W. Lee, S.J. Moon, H.J. Chang, Synthesis of a novel photocatalyst, $ZnBiVO_4$, for the photodecomposition of H_2S, Canadian Journal of Chemistry, 83 (2005) 527-532.

[77] A.F. Caliman, C. Cojocaru, A. Antoniadis, I. Poulios, Optimized photocatalytic degradation of Alcian Blue 8 GX in the presence of TiO_2 suspensions, Journal of Hazardous Materials, 144 (2007) 265-273.

[78] S. Qourzal, N. Barka, M. Tamimi, A. Assabbane, Y. Ait-Ichou, Photodegradation of 2-naphthol in water by artificial light illumination using TiO_2 photocatalyst: Identification of intermediates and the reaction pathway, Applied Catalysis A: General, 334 (2008) 386-393.

[79] H.R. Pouretedal, A. Kadkhodaie, Synthetic CeO_2 Nanoparticle Catalysis of Methylene Blue Photodegradation: Kinetics and Mechanism, Chinese Journal of

Catalysis, 31 (2010) 1328-1334.

[80] M. Pelaez, A.A. de la Cruz, K. O'Shea, P. Falaras, D.D. Dionysiou, Effects of water parameters on the degradation of microcystin-LR under visible light-activated TiO_2 photocatalyst, Water Research, 45 (2011) 3787-3796.

[81] F. Shahrezaei, Yadollah Mansouri, Ali Akbar Lorestani Zinatizadeh, Aazam Akhbari, Process modeling and kinetic evaluation of petroleum refinery wastewater treatment in a photocatalytic reactor using TiO_2 nanoparticles, Powder Technology, 221 (2012) 203-212.

[82] M.A. Nawi, S. Sabar, Sheilatina, Photocatalytic decolourisation of Reactive Red 4 dye by an immobilised TiO_2/chitosan layer by layer system, Journal of Colloid and Interface Science, 372 (2012) 80-87.

[83] S.F. Chen, Y.Z. Liu, Study on the photocatalytic degradation of glyphosate by TiO_2 photocatalyst, Chemosphere, 67 (2007) 1010-1017.

[84] N.M. Mahmoodi, M. Arami, J. Zhang, Preparation and photocatalytic activity of immobilized composite photocatalyst (titania nanoparticle/activated carbon), Journal of Alloys and Compounds, 509 (2011) 4754–4764.

[85] W.S. Nam, K.C. Woo, G.Y. Han, Photooxidation of anionic surfactant (sodium lauryl sulfate) in a three-phase fluidized bed reactor using TiO_2/SiO_2 photocatalyst,

Journal of Industrial and Engineering Chemistry, 15 (2009) 348-353.

[86] M.N. Chong, B. Jin, C.W.K. Chow, C.P. Saint, A new approach to optimise an annular slurry photoreactor system for the degradation of Congo Red: Statistical analysis and modelling, Chemical Engineering Journal, 152 (2009) 158-166.

[87] S. Chowdhury, P. Das, Linear and Nonlinear Regression Analyses for Binary Sorption Kinetics of Methylene Blue and Safranin onto Pretreated Rice Husk, Bioremediation Journal, 15 (2011) 99-108.

[88] M.I. El-Khaiary, G.F. Malash, Y.S. Ho, On the use of linearized pseudo-second-order kinetic equations for modeling adsorption systems, Desalination, 257 (2010) 93-101.

[89] O.A.C. Monteiro Jr. , C. Airoldi, Some studies of crosslinking chitosan-glutaraldehyde interaction in a homogeneous system, International Journal of Biological Macromolecules, 26 (1999) 119-128.

[90] V. Kumar, S. Kr. Sharma, T.P. Sharma, V. Singh, Band gap determination in thick films from reflectance measurements, Optical Materials, 12 (1999) 115-119.

[91] G.P. Joshl, N.S. Saxena, R. Mangal, A. Mishra, T.P. Sharma, Band gap determination of Ni–Zn ferrites, Bulletin of Material Science, 26 (2003) 387–389.

[92] I.E. Saliby, M. Shahid, A. McDonagh, H.K. Shon, J.H. Kim, Photodesorption of

organic matter from titanium dioxide particles in aqueous media, Journal of Industrial and Engineering Chemistry, 18 (2012) 1774–1780.

[93] R.B. Bjorklund, S. Karlsson, H. Boren, B. Allard, I. Lundstrom, Photodesorption of fulvic acid from iron oxide surfaces into aqueous solutions, Applied Surface Science, 174 (2001) 166-175.

[94] H.K. Shon, S. Vigneswaran, H.H. Ngo, J.H. Kim, Chemical coupling of photocatalysis with flocculation and adsorption in the removal of organic matter, Water Research, 39 (2005) 2549-2558.

[95] L. Erdei, N. Arecrachakul, S. Vigneswaran, A combined photocatalytic slurry reactor–immersed membrane module system for advanced wastewater treatment, Separation and Purification Technology, 62 (2008) 382-388.

[96] Z. Ambrus, K. Mogyorosi, A. Szalai, T. Alapi, K. Demeter, A. Dombi, P. Sipos, Low temperature synthesis, characterization and substrate-dependent photocatalytic activity of nanocrystalline TiO_2 with tailor-made rutile to anatase ratio, Applied Catalysis A: General, 340 (2008) 153-161.

[97] H. Qiu, L. Lv, B.C. Pan, Q.J Zhang, W.M. Zhang, Q. X. Zhang, Critical review in adsorption kinetic models, Journal of Zhejiang University Science A, 10 (2009) 716-724.

[98] J.P. Ibanez, Y. Umetsu, Potential of protonated alginate beads for heavy metals uptake, Hydrometallurgy, 64 (2002) 89-99.

[99] M.S. Chiou, H.Y. Li, Adsorption behavior of reactive dye in aqueous solution on chemical cross-linked chitosan beads, Chemosphere, 50 (2003) 1095–1105.

[100] P. Chassary, T. Vincent, E. Guibal, Metal anion sorption on chitosan and derivative materials: a strategy for polymer modification and optimum use, Reactive & Functional Polymers, 60 (2004) 137-149.

[101] N. Soltani, E. Gharibshahi, E. Saion, Band gap of cubic and hexagonal CdS quantum dots - Experimental and theoretical studies, Chalcogenide Letters, 9 (2012) 321-328.

[102] P. Reyes, S. Velumani, Structural and optical characterization of mechanochemically synthesized copper doped CdS nanopowders, Materials Science and Engineering B, 177 (2012) 1452- 1459.

[103] E. Maier, A. Fischereder, W. Haas, G. Mauthner, J. Albering, T. Rath, F. Hofer, E.J.W. List, G. Trimmel, Metal sulfide–polymer nanocomposite thin films prepared by a direct formation route for photovoltaic applications, Thin Solid Films, 519 (2011) 4201-4206.

[104] R. Jiang, H.Y. Zhu, J. Yao, Y.Q. Fu, Y.J. Guan, Chitosan hydrogel films as a

template for mild biosynthesis of CdS quantum dots with highly efficient photocatalytic activity, Applied Surface Science, 258 (2012) 3513-3518.

[105] F. Tasselli, A. Mirmohseni, M.S. S. Dorraji, A. Figoli, Mechanical, swelling and adsorptive properties of dry–wet spun chitosan hollow fibers crosslinked with glutaraldehyde, Reactive & Functional Polymers, 73 (2013) 218-223.

[106] S. Margel, A. Rembaum, Synthesis and Characterization of Poly(glutaraldehyde). A Potential Reagent for Protein Immobilization and Cell Separation, Macromolecules, 13 (1980) 19-24.

[107] H.W. Hu, J.H. Xin, H. Hu, A. Chan, L. He, Glutaraldehyde–chitosan and poly (vinyl alcohol) blends, and fluorescence of their nano-silica composite films, Carbohydrate Polymers, 91 (2013) 305-313.

[108] W. S. Wan Ngah, S. Fatinathan, Pb(II) biosorption using chitosan and chitosan derivatives beads: Equilibrium, ion exchange and mechanism studies, Journal of Environmental Sciences, 22 (2010) 338-346.

[109] M.M. Beppu, R.S. Vieira, C.G. Aimoli, C.C. Santana, Crosslinking of chitosan membranes using glutaraldehyde: Effect on ion permeability and water absorption, Journal of Membrane Science, 301 (2007) 126-130.

[110] V. Poderys, M. Matulionyte, A. Selskis, R. Rotomskis, Interaction of

Water-Soluble CdTe Quantum Dots with Bovine Serum Albumin, Nanoscale Research Letter, 6 (2011) 9.

[111] C.P. Shah, M. Rath, M. Kumar and P. N. Bajaj, Precursor concentration and temperature controlled formation of polyvinyl alcohol-capped CdSe-quantum dots, Beilstein Journal of Nanotechnology, 1 (2010) 119-127.